

Characterisation and selective modification of semiconductor nanowires for electrical applications

Dissertation

zur Erlangung des akademischen Grades

doctor rerum naturalium (Dr. rer. nat.)

vorgelegt dem Rat der Physikalisch-Astronomischen Fakultät der
Friedrich-Schiller-Universität Jena

von

Diplom-Physiker Raphael Niepelt
geboren am 3. März 1982 in Hildesheim

Gutachter

Prof. Dr. Carsten Ronning, FSU Jena
Prof. Dr. Marius Grundmann, Uni Leipzig
Ass.-Prof. Dr. Alois Lugstein, TU Wien

Tag der Disputation: 05.06.2012

Contents

1	Introduction	5
1.1	Semiconductor nanowires: Chances and challenges	6
1.2	Goal of this thesis	9
2	Background, simulations and experimental details	11
2.1	Semiconductor nanowires	11
2.1.1	Synthesis of Semiconductor nanowires	15
2.1.2	Contacting of semiconductor nanowires	16
2.1.3	Electrical characterisation	18
2.1.4	Persistent photoconductivity	19
2.1.5	Electron beam induced current measurement	20
2.1.6	Cathodoluminescence	25
2.1.7	Photoluminescence	28
2.2	Ion-solid interactions	29
2.2.1	Ion implantation	29
2.2.2	Simulation of implantation profiles	30
2.2.3	Ion implanters	32
2.3	Techniques and terms used for the biofunctionalisation experiments	34
2.3.1	DNA	34
2.3.2	Surface engineering	35
2.3.3	Fluorescence microscopy	35
3	Carrier diffusion lengths in semiconductor nanowires	37
3.1	Minority carrier diffusion lengths	37
3.2	EBIC investigations on axial GaAs nanowire pn-junctions	38
3.3	Surface passivation with ammonium sulfide	42
3.4	Carrier diffusion lengths in ZnO nanowires	43
3.5	CL investigations on ZnO nanowire Schottky junctions	44
3.6	Conclusions	51
4	Ion implantation in ZnO nanowires	53
4.1	Motivation	53
4.2	Hydrogen implantation in ZnO nanowires	55
4.2.1	Optical properties of hydrogen implanted nanowires	56
4.2.2	Electrical properties of hydrogen implanted nanowires	59

Contents

4.3	Persistent ion beam induced conductivity	66
4.4	Countable ion implantation in ZnO nanowires	71
4.5	Conclusion	77
5	Biofunctionalisation of ZnO nanowires	79
5.1	Nanowire biosensors	79
5.2	Nanowire preparation and functionalisation	81
5.3	Characterisation of functionalised nanowires	82
5.4	Conclusions	91
6	Summary and outlook	93
	Bibliography	97
A	List of publications	121

1 Introduction

The prefix "nano", which is derived from *νανος*, the ancient Greek word for dwarf, is omnipresent in today's technology. Nano stands for the use of nanoscale structured materials, which means that at least one dimension of the structure is in the nanometer range. On this scale, the properties of the material are not only governed by the composition but also the form and shape, which opens up a wide field of possible new applications. Nano has become quite a trendy prefix, it is used to advertise a broad range of products, from furniture polish to razor blades, from antifouling paint to functional clothing. Nanotechnology in the sense of science denotes the interdisciplinary research on processes and objects on the nanoscale. The beginning of nanotechnology is often traced back to the famous talk by Richard Feynman in 1959 "There's plenty of room at the bottom" [Fey60]. Today, we know that Feynman's talk had hardly any influence on the development of the modern nanotechnology [Tou05]. However, his visions on the possibilities that evolve due to miniaturised devices on an atomic scale are still impressive.

The term nanotechnology was first used by Norio Taniguchi in 1974 to describe thin film semiconductor techniques with thickness ranges in the order of a nanometer [T⁺74]. Finally, the invention of the scanning tunneling microscope by Binnig and Rohrer in 1981 [BR83] brought the possibility of imaging and manipulating single atoms. Other milestones in the history of nanotechnology have been the discovery of the buckminsterfullerenes [KHO⁺85] and carbon nanotubes [I⁺91].

The electronic properties of nanoscaled materials can differ extremely from bulk due to the increased surface-to-volume ratio of the nanostructures. The ongoing miniaturisation of electronic devices down to pitch sizes of only 20 nm in 2012, that will be even reduced by a factor of two by 2020 [ITR11], requires a deep understanding of the properties of semiconductors at the nanoscale. Thus, nanotechnology and nanoelectronics have gained major interest in the last decades. The integration of bottom-up synthesised nanostructures into integrated circuits could contribute to cost reduction and material savings during

1 Introduction

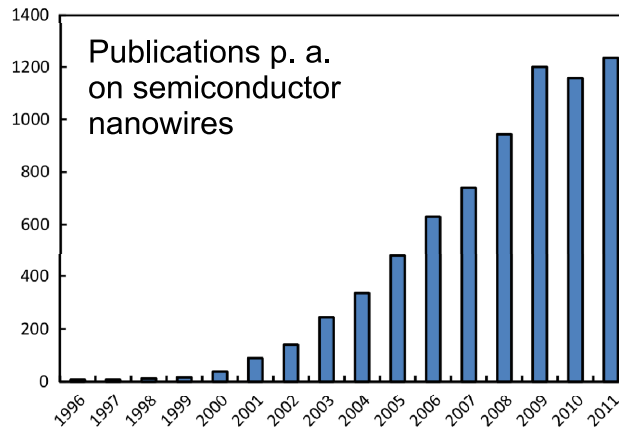


Figure 1.1: Publications per year on semiconductor nanowires determined with the ISI Web of Knowledge in January 2012 [isi12]. The used search term was `semiconduct AND nanowir*` and revealed a total of 7,296 results. The query might not include all publications on this field, but the massively increased interest in semiconductor nanowires during the past years is clearly visible.*

fabrication. Furthermore, complex device structures in all three dimensions are imaginable due to the integration of selectively arranged bottom-up nanostructures.

Quasi one-dimensional nanostructures, which are confined in two dimensions down to the nanometer scale, are commonly named nanowires. The maximum diameter of a nanowire is not clearly defined. Generally, the term is used for the description of wire-like structures with diameters from one to a few hundred nanometers in diameter [LGY04,LL06,RGBN10]. The successful implementation of semiconductor nanowires into electric circuits roughly ten years ago was categorised as a major breakthrough in science [Ser01, App02] and lead to a massive boost on the research in such structures since then. The increased interest in semiconductor nanowires can also be seen from the total number in publications on semiconductor nanowires within the past 15 years, as displayed in Figure 1.1.

1.1 Semiconductor nanowires: Chances and challenges

Semiconductor nanowires are particularly distinguished by their unique transport properties governed by the extreme surface-to-volume and nanowire aspect ratio. They can be easily grown up to length of micrometers and therefore be integrated into larger device structures. On the other hand, the confinement in the other two dimensions leads to the

1.1 Semiconductor nanowires: Chances and challenges

formation of novel properties that can be used for applications. Nanowires with diameters below the wavelength of light can act as photonic waveguides [VSM⁺07]. Furthermore, they can even act as cavities for nanolasers [YYF10]. Electrically driven nanowire light emitting diodes (LEDs) act as light sources that are smaller than the wavelength of the emitted light [ZSR⁺08]. The small footprint of the nanowires reduces the lattice strain and allows the combination of formerly incompatible materials via epitaxial growth [YYF10, WB11]. Thus, the integration of photonic materials like gallium nitride into a silicon based device platform becomes imaginable despite large lattice mismatches.

Large-scale assembly methods have been developed for the integration of nanowires into electrical circuits [WG09]. Moreover, advances in doping of semiconductor nanowires have been made during the past few years [RBGN10, WB11]. New possibilities for the creation of innovative memory devices with semiconductor nanowires are accompanied by new challenges regarding nanowire growth and assembly methods [LL07]. Due to the surface influence on the transport properties, nanowires are excellently adapted for the application in sensing devices; optical [ZGH⁺09], chemical [CHC⁺08], and biological [CKJL10] sensors have been demonstrated. Furthermore, nanowires can also be used as probes for single cell endoscopy [LL07] or label-free DNA sensing [PTZL07].

Finally, the nanowire geometry provides potential advantages for energy production. Silicon nanowire solar cells [GBCM11] show a massive reduction in reflectance. Additionally, nanowires arranged in periodic arrays provide excellent light trapping possibilities. Both effects lead to improved absorption and a higher energy conversion efficiency. If the pn-junction is placed along the nanowire surface, the active area, where charge separation can take place, is multiplied compared to thin film devices. Thermoelectric applications might benefit from the concurrence of high electrical conductivity and poor heat transfer in semiconductor nanowires [LGY04]. With the use of piezoelectronic materials, nanowire-based nanogenerators have been shown [Wan07].

Highly doped ZnO is often used in photovoltaics as a transparent conducting layer to transport the carriers generated inside the active layer to the front electrodes of the solar cell. ZnO nanowires have gained additional interest with the use as basic building blocks in dye-sensitized solar cells (DSSC) [BA05, WCY⁺07]. In a DSSC the incoming light is adsorbed by a dye attached to a wide bandgap semiconductor nanoparticle, originally made of TiO₂ [OG91]. The motivation of using nanowires instead of nanoparticles lies in the provision of direct conduction paths for the electrons from the dye to the collecting

1 Introduction

electrode of the cell. With a band gap and electron affinity comparable to TiO_2 [BA05] ZnO nanowires are well-suited for the use in nanowire-based DSSC. In a similar approach, ZnO nanowire solar cells have been realised by replacing the dye layer by extremely thin absorber layers like CdSe [MB10]. Via functionalisation of the nanowire surface with organic semiconducting layers it is possible to build organic/inorganic hybrid nanowire solar cells [BHB⁺09]. All-oxide nanowire solar cells have been shown by covering ZnO nanowires with p-type Cu_2O nanoparticles [YY09]. Besides the field of photovoltaics, ZnO nanowires have been applied to a huge variety of devices so far, including LEDs, nanolasers, UV sensors, gas sensors, and nanogenerators [Wan09]. ZnO nanowires can be produced cheaply and easily in a wide range of sizes and forms, adaptable to many different sample geometries.

Due to the electronic properties of GaAs and the widespread use of this material in semiconductor industry, GaAs nanowires are promising candidates for future use in nanoscale optoelectronic devices. LEDs [CSC⁺10] as well as Solar cells [MWK⁺11, TPKL11] have both been presented based on GaAs nanowires. The application in photovoltaic devices is encouraged by enhanced optical absorption [GPLN11]. The possibility of doping during growth facilitates the synthesis of nanowire pn-diodes, either in radial [MWK⁺11] or axial [RGL⁺10] geometry.

For the use of semiconductor nanowires in devices, it is essential to know and understand the nature of the nanowires. Thus, advanced characterisation methods have to be developed to investigate the electrical and optical properties of nanoscaled objects. Especially the influence of the reduced size and the surface configuration on the nanostructure properties has to be determined. Novel, functional elements for semiconductor devices can be achieved by the selective modification of the nanowires, what can be done by either modifying the wire composition or the surface conditions. Standard techniques used for the modification of bulk material might not work in the case of nanowires, owing to the reduced size. Therefore, altered or new techniques have to be developed in order to selectively modify the properties of semiconductor nanowires.

1.2 Goal of this thesis

This thesis reports on different approaches to the characterisation and the modification of the properties of semiconductor nanowires; in particular, the SEM based characterisation of the transport properties of semiconductor nanowires, the manipulation of the optical and electrical properties of ZnO nanowires by ion implantation and the functionalisation of ZnO nanowires via DNA attachment.

Chapter 3 deals with the characterisation of semiconductor nanowires. On GaAs and ZnO nanowire devices, measurements of the carrier diffusion length are conducted, which is a key parameter for the application of nanowires in any electro-optical device. In the case of GaAs nanowires, it is shown how surface passivation can enhance the carrier diffusion length and thus improve the usability of the nanowires for device application.

The targeted manipulation of the nanowire properties helps to extend the field of possible applications. Ion implantation, a standard doping technique in semiconductor industry, can be used for enhancing the properties of semiconductor nanowires. Apart from doping, ion implantation induced effects causing changes of the electrical properties of nanowire devices are found. The unique interaction between ZnO nanowire devices and impinging ions allows the detection of single ion impacts spatially confined to a small area of the nanowire device. Ion implantation experiments on ZnO nanowires are conducted in order to investigate these phenomena in chapter 4.

The surface has a large influence on the nanowire properties. Selectively modifying the surface is another possibility for the targeted manipulation of nanowire properties for the use in devices. An example of this is the biofunctionalisation of ZnO nanowires with DNA. This treatment gives way to the development of a electrically driven, label-free DNA sensing device. The biofunctionalisation of ZnO nanowires is investigated in chapter 5.

Detailed motivations for the individual approaches can be found at the beginnings of the respective chapters.

1 Introduction

2 Background, simulations and experimental details

2.1 Semiconductor nanowires

Semiconductors are defined as materials with a conductivity intermediate between insulators and conductors, where the specific resistance of the material is in the range between $10^{-2} \Omega\text{cm}$ (GaAs, InAs) and $10^6 \Omega\text{cm}$ (selenium) [Inf04]. The electrical properties of a semiconductor can be modified by the systematic incorporation of impurities into the crystal, called doping. This opened the door to the development of the variety of semiconductor devices, including transistors, microchips, LEDs, and solar cells; components without our modern world could not exist [Sch00]. The physics of semiconductors are well explained in several textbooks [SN06, Ham10], that can provide further insight into the field of semiconductor physics. Here, only some relevant terms addressed in this thesis will be discussed very briefly.

In the scope this work, experiments have been conducted with semiconductor nanowires made from GaAs and ZnO. Both materials belong to the group of compound semiconductors, where, further classified with respect to the main groups in the periodic system, GaAs represents a III-V material and ZnO a II-VI material.

GaAs is a direct semiconductor with a bandgap of 1.42 eV at room temperature. It is widely used for the application in optoelectronic devices like LEDs, lasers and solar cells [BP07]. The material has some electronic properties, like the direct bandgap and a higher electron mobility, which are superior to those of Si, especially for the use in high speed microelectronics and photovoltaic devices. Thus, GaAs nanowires, that can be synthesised in a bottom-up process from the vapour phase [GRB⁺09], have attracted great research interest during the past few years.

2 Background, simulations and experimental details

ZnO is a direct wide bandgap semiconductor with a wide range of applications in several fields of technology, including optics, optoelectronics, and biomedical sciences [ÖHM10]. The versatility of ZnO nanostructures and the availability of easy-to-handle nanostructure synthesis methods have made ZnO one of the three most popular material systems in the nano-material research [Wan09]. ZnO grows usually in a wurtzite crystal structure. The high excitonic binding energy of 60 meV entails potential for optoelectronic devices using excitonic transitions. ZnO emits light in the ultraviolet range due to the bandgap of ≈ 3.4 eV. Thus, ZnO has shown to be attractive for the development of light-emitting devices in the ultraviolet region. Nanoscaled ZnO devices and their integration with the mainstream semiconductor materials are of interest due to the large number of possible geometries owing to the variety of available ZnO nanostructures [ÖHM10].

pn- and Schottky junction

The maximum of the available electron energy levels inside a solid at low temperatures is called Fermi level. The Fermi level of an intrinsic semiconductor usually lies in the center of the bandgap. Doping shifts the Fermi level upwards (n-type) or downwards (p-type). On the junction between a p-type and a n-type region of semiconductor, free electrons from the conduction band in the n-region will diffuse across the junction and combine with holes. Filling a hole produces a negative ion on the p-side and leaves behind a positive ion on the n-side. A space charge is induced, countervailing the diffusion process and leading to an equilibrium state. The space charge creates a depletion region which inhibits any further electron transfer over the junction unless an extra forward bias is applied. At the pn-junction in equilibrium, the Fermi levels match on both sides of the junction, resulting in a band bending in the energy band diagram.

An applied bias voltage will either drive the charge carriers towards the junction, reducing the depletion zone and enabling current transport across the junction (forward direction), or drive the carriers away from the junction, preventing any conduction (reverse direction). This rectifying diode behaviour of the p-n junction is the key element of the enormous variety of solid-state electronic devices.

The junction between a semiconductor and a metal can also show rectifying behaviour. Such a junction is called a Schottky diode. When the semiconductor and the metal form an electrical contact, carriers from the semiconductor diffuse into energetically lower states in the metal. Analogous to the pn-junction, a space charge region and a depletion zone

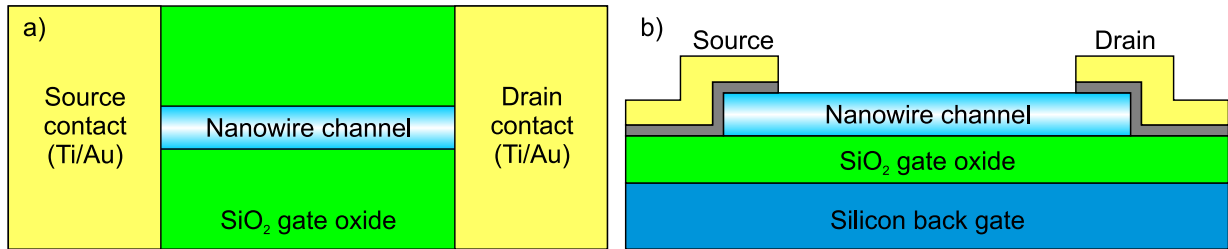


Figure 2.1: Top view a) and side view b) scheme of a simple back-gate FET assembled on a Si-SiO₂ substrate and contacted on both sides with Ti-Au metal contact pads. The carrier concentration inside the nanowire channel and therefore the current between drain and source contact can be adjusted by applying a voltage to the Si back gate.

build up in the semiconductor and cause a rectifying behaviour. Likewise existing metal-semiconductor junctions without rectifying behaviour are referred to as "ohmic". Ohmic contacts require a highly doped semiconductor in order to reduce the width of the depletion layer to allow tunnelling and a uniform, extended contact area. Electrical contacts to nanowires often show Schottky-behaviour due to the nature and limited size of the contact region.

Semiconductor nanowire transistors

While methods for the large scale integration of nanowires into conventional integrated circuits are still to be developed, field effect transistors (FETs) with nanowires as active channels can be configured easily for research purposes [CZW⁺03, CFC⁺06]. A typical setup is displayed in Figure 2.1. The nanowire is placed on an insulating substrate surface, where source and drain contacts are defined to the nanowire ends. The substrate beneath the insulating layer can be used as the gate electrode to control the current flow in the nanowire channel. FETs manufactured in this simple construction type are usually referred to as back gate FETs. In a more advanced setup, the gate electrode can also be placed on top of the nanowire channel, separated by an insulating layer. This alternative design is commonly termed top gate architecture [CL08].

Within this thesis, only nanowire devices contacted in back gate geometry have been used.

Semiconductor detectors

In a semiconductor particle detector, the semiconductor material is used for the detection of ionising radiation [SW09]. The principle is based on the detection of charge carriers that are generated inside the semiconductor crystal by the incoming radiation and migrate to the detector electrodes. The resulting current signal is then amplified and analysed, giving access to the nature and/or energy of the detected radiation. The detector consists in principle of a reverse-biased semiconductor pn-diode (see previous sections of this chapter). The particle detection takes place inside the depletion layer of the diode junction. Electron-hole pairs generated by the incoming radiation are separated by the internal electrical field and a current pulse can be detected. The current signal is proportional to the energy transferred to the electron-hole pair excitation process. Thus, it is possible to draw a conclusion on the energy of the detected radiation particles from the current signal.

In order to build a detector with a wide energy detection range, a detector geometry with an extended depletion zone that fully absorbs the incoming radiation is useful. For this purpose often PIN (p-type-intrinsic-n-type) diodes are deployed. Here, an extended, depleted, intrinsic region between a n-type and a p-type layer is used for the detection of the incoming radiation. In order to achieve a reliable separation of the generated carriers, PIN diodes have to be operated heavily biased, what is making high demands on the purity of the used semiconductor material, as leakage currents have to be avoided. Commonly used materials are high-purity silicon or germanium. Semiconductor detectors are widely used in spectroscopy and in particle physics.

Nanowires could be used in principle as the active elements of nanosized particle detectors. A high-energy particle detector based on an array of TiO₂ nanowires has been developed by Angelucci et al. [ACC⁺06, ACD⁺06]. The nanowires act as nanosized, separated, and independent particle detectors and allow the spatially resolved detection of incoming particles. Superconducting nanowires made from niobium or niobium nitride can be used for the detection of single photons or other accelerated neutral particles [SHH⁺09, ASC⁺09, MDS⁺09]. However, those detectors need low temperature ($\approx 1-10$ K) conditions to work. In chapter 4, the suitability of ZnO nanowires to be applied as extremely locally confined semiconductor detectors will be investigated.

2.1.1 Synthesis of Semiconductor nanowires

Different wet-chemical or vapour phase deposition techniques can be used for the bottom-up production of nanostructures and especially semiconductor nanowires [BDC02, Wan09]. Nanowires used for experiments in this thesis have been produced using the so-called vapour-liquid-solid (VLS) process, first described by Wagner and Ellis in 1964 [WE64]. Here, a metal seed particle, typically gold, is placed on the growth substrate. The substrate is heated up beyond the melting point of the particle. Then, the particle is enriched with the desired nanowire growth material from the vapour phase and forms an eutectic. Keeping up the supply from the gas phase, the particle will finally be supersaturated and the supplied material will begin to precipitate and recrystallise. In most cases, this happens at the interface between the seed droplet and the substrate. The process will continue as long as material from the vapour phase is provided. The material precipitated from the eutectic lifts up the droplet, forming the nanowire. The nanowire diameter is governed by the diameter of the seed droplet.

Although the VLS model has to be expanded to be capable of explaining the growth of compound semiconductor wires [BMS⁺06], it is widely adopted as a standard growth model for vapour phase deposition techniques of semiconductor nanowires. Recently, there have been some attempts to further generalise and expand the model [Moh08, WDJ⁺09].

Zinc oxide nanowires used in this work have been synthesised in a horizontal tube furnace following [BMS⁺06]. A thin Au layer of ≈ 5 nm thickness was applied to the substrates prior to the growth process. As source material, 2 g high-purity ZnO powder was placed in the middle of the furnace and heated up to 1350 °C in order to evaporate the material. The growth substrates were placed somewhat towards the end of the furnace where a temperature between 1100 °C and 900 °C is present, causing the Au layer to melt and form nanowire seed droplets. The growth pressure was between 15 and 150 mbar. A gas flow of 50 sccm argon was used to transport the ZnO vapour to the growth substrates. Typical growth times for the synthesis of nanowires with some tens of μm are between 15 and 30 min.

Gallium arsenide nanowires were synthesised at the University of Duisburg with a commercial low-pressure (50 mbar) AIX200 RF molecular vapour phase epitaxy (MOVPE) reactor [GRB⁺09, GLR⁺10, RGL⁺10]. Polydisperse metal seeds were formed by evaporation and subsequent annealing of a thin Au layer of nominally 2.5 nm thickness, resulting in seed particles with diameters from 80 nm to some 100 nm. Trimethylgallium (TMGa) and

2 Background, simulations and experimental details

Tertiarybutylarsine (TBAs) were used as group-III and group-V precursors. The wires were doped during growth in order to receive axial pn-junctions by applying Diethylzinc (DEZn) or Tetraethyltin (TESn) as dopant precursors for the p-type (lower) and n-type (upper) part of the nanowire. The doping procedure led to carrier concentrations of $N_A = 1.6 \cdot 10^{19} \text{ cm}^{-3}$ in the lower, and $N_D = 1 \cdot 10^{18} \text{ cm}^{-3}$ in the upper nanowire part [RGL⁺10].

2.1.2 Contacting of semiconductor nanowires

Electrical contacts have to be applied to the nanowires in order to conduct electrical measurements on them. ZnO nanowires were contacted at the IFK in Jena via photolithography, a well known and widely used method to prepare electrical contacts on a micrometer scale. Hereby, an UV-sensitive photoresist is exposed to light through a microstructured mask and developed afterwards. The remaining resist has adopted the masks structure and can be used as a mask itself for the evaporation of metallic contacts. The minimum feature size available depends on the light wavelength used for exposure as well as the performance of the lithography apparatus. The resolution limit of the system used in this thesis is about 1-2 μm , where fully developed structures smaller than 5 μm are very difficult to achieve. Thus, nanowires that are to be contacted via photolithography should feature a minimum length of a few μm , which however can be attained easily in the VLS process.

The sequence of work steps used for the contacting of ZnO nanowires is outlined in Figure 2.2. First, the nanowires are transferred from the growth substrate to a clean SiO_2 -Si substrate via contact imprint. One is capable of adjusting the density of nanowires dispersed on the substrate by varying the force applied during the imprint. Directional sliding of the growth substrate further helps to align the nanowires with a specific orientation [FHJ⁺08]. Second, the later contact structures are predefined via photolithography using the negative photoresist TI 35ES from Microchemicals [mic12]. In this work, a lithography mask with 15 pairs of contact pads with a 5 μm wide gap between the counterparting pads was used. The underlying nanowires were hit just by chance, depending on the density of the dispersed nanowires on the substrate. Third, Ti and Au were evaporated onto the pre-patterned sample. After the lift-off of the developed resist, only the predefined contact structures and the imprinted nanowires remain. Fourth, the sample is fixed on a chip carrier and the contacts are bonded to the carrier pins enabling electrical measurements in the lab environment. An SEM image of contacted nanowires between the evaporated contact pads is shown in Figure 2.2e).

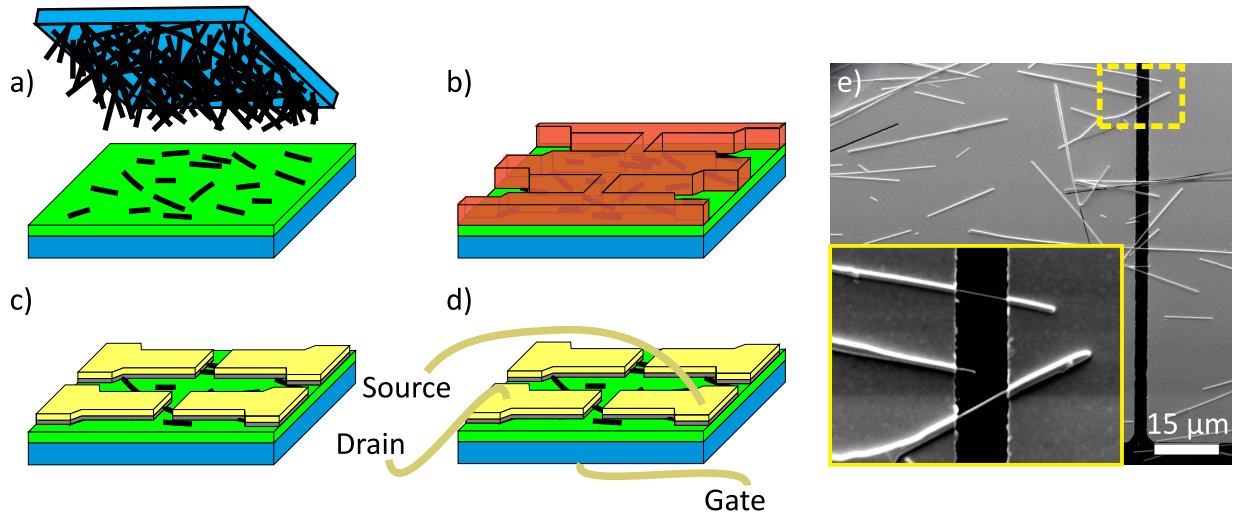


Figure 2.2: Nanowire contacting sequence used for ZnO nanowires throughout this thesis: a) Nanowire transfer by imprint. b) Contact contour predefinition by photolithography. c) After evaporation of Ti/Au and lift-off, predefined contact structures remain. d) Bonding for electrical connection of FET terminals. e) SEM image of contacted nanowires.

The contact composition of Ti and Au was chosen in order to get both durable and conductive contacts. Ti is known to act as an adhesive agent, countervailing undesired contact cracking or peeling during the bonding process [Uen92,JXW10]. The Ti-Au system has been reported to form ohmic contacts on ZnO nanowires [YNPR05]. However, the same material system was found to form Schottky contacts in other studies [ITY⁺06]. In an overview study on the electrical properties of ZnO nanowires Schlenker et al. [SBW⁺08] point out that the transport properties of ZnO nanowires can be influenced by so many factors that a reliable transfer of results from one lab to another is quite impossible. Thus, optimisation of the evaporated contacts, e.g. by replacing Ti-Au with a more complex system like Ti-Al-Pt-Au [ITY⁺06], has played a less important role in the scope of this work, as the experimental conditions in the lab do not meet the high demands that are necessary to come to a reliable statement in this field.

The contacted ZnO nanowires usually showed s-shaped IV-characteristics that imply a Schottky contact on both sides of the nanowire. However, as the contacting is done by a random success process, the Schottky barriers on both sides of the nanowire might differ significantly in height and therefore the IV-characteristics often remain asymmetric. Multi-wire devices are typically found to provide more symmetric characteristics, as their curves represent an average of the characteristics of several wires. By applying a voltage

2 Background, simulations and experimental details

to the silicon substrate, the device can be used as a simple FET. Hereby, the nanowire represents the transistor channel between the source and the drain contact. The substrate below the oxide layer serves as back gate electrode.

In order to produce single nanowire transistors, it is possible to cut unwanted bridging wires between the contact pads with a focused ion beam (FIB) system. By cutting all but one nanowires, a single nanowire device can be produced easily by this rather simple contacting approach.

The contacting of GaAs nanowires investigated in this work was carried out with electron beam lithography at the University of Duisburg-Essen. The process is described in detail in [GLR⁺11]. Ohmic contacts on the p-doped nanowire part were formed by evaporation of Pt (5 nm)/Ti (10 nm)/Pt (100 nm)/Au (300 nm), and subsequent rapid thermal annealing for 30 s at 360 °C, while Pd (50 nm)/Ge (170 nm)/Au (80 nm) contacts followed by annealing for 30 s at 280 °C were used for the n-doped part.

2.1.3 Electrical characterisation

Electrical characterisation of nanowire devices within this work was conducted in an EP6 probe station by Süss MicroTec [sus12]. The probe station can be darkened to avoid photo induced side effects on the measurement. A Keithley 237 [kei12] source measurement unit (SMU) was used for current-voltage measurements. The SMU allows accurate current measurements down to ≈ 1 pA and is optimised for current measurements at a set bias voltage. A custom LabView™ software written by Steffen Milz [Mil10] allows computerised electrical measurements. Current-voltage (IV) as well as transfer characteristics of the devices can be measured.

The transfer characteristic of a FET describes the current flow between the source and the drain electrode at constant bias while the voltage applied to the gate electrode is varied [SN06]. Thus, it is describing the switching and amplification behaviour of the transistor. From the transfer characteristic, it is possible to determine the type of dopant of the semiconductor material in the channel and the working mode of the transistor. Depletion mode transistors provide a conductive channel that can be depleted when a gate voltage is applied. On the contrary, enhancement mode transistors own a usually depleted channel that can be populated by an applied gate voltage.

2.1.4 Persistent photoconductivity

ZnO devices, especially thin films and nanodevices, often show persistent photoconductivity (PPC), which denotes a photo induced excess conductivity with a rather slow drop in conductivity after stopping the excitation [WLS⁺11]. In a semiconductor, illumination with light of an energy higher than the bandgap leads to charge carrier generation due to the excitation of electron-hole pairs. Thus, semiconductors always show an enhanced photoconductivity. However, the time scale for the recombination of photoinduced charge carriers lies usually in the region below one second. For ZnO nanowires, recombination times as short as 100 ps have been estimated [RGW⁺10]. However, much longer timespans on the order of minutes have been observed for the conductivity to drop down to pre-illumination level due to PPC [PHRJD⁺08, WLS⁺11, BSS⁺11].

Investigations on the PPC of coated and uncoated ZnO nanowires in different atmospheres point to a surface related effect [PHRJD⁺08, SHL⁺09]. In [PHRJD⁺08], Prades et al. attribute the PPC to the separation of the photogenerated carriers due to a surface built-in potential. Owing to band-bending towards the surface, generated holes will accumulate near the surface, while the electrons remain in the middle of the nanowire, causing the increased conductivity. The delayed decline towards the initial value after terminating the illumination is attributed to a comparably slow oxygen-assisted surface recombination mechanism. Here, oxygen adsorbed on the surface traps electrons from the nanowire conduction band. Those electrons are able to recombine with the holes accumulated near the surface, whereupon the oxygen molecule is desorbed. In principle, photo induced desorption of oxygen from the nanowires should be observable, as was reported from ZnO bulk [CFS74]. There have not been any reports on the desorption of oxygen from ZnO nanowires under illumination so far. The model described above could also work with oxygen-containing molecules like water or CO₂, where the desorption of the latter indeed has been reported [BSS⁺11].

Some ideas exist to take advantage of the PPC for the development of non-volatile memory or optical switches and integrators [WCLK11]. A negative consequence of this phenomenon is the need of a reset process in order to do reproducible measurements. This issue becomes important for the application of such structures as sensing elements or switches. Some possible reset processes have already been investigated. Prades et al. reported a faster conductivity drop for an increased current flow through the wire, caused by thermally enhanced recombination of the separated carriers [PHRJD⁺08]. White et al.

2 Background, simulations and experimental details

applied a high gate voltage pulse to ZnO FETs in order to reset the devices [WCLK11]. Wang et al. achieved a significantly shortened decay time of the PPC by illuminating the nanowires with a 980 nm infrared laser [WLS⁺11]. ZnO nanowire devices should always be measured very carefully and just under defined lighting environment if no well defined reset process is available.

2.1.5 Electron beam induced current measurement

The analysis of the electron beam induced current (EBIC) within a SEM is a powerful tool for the characterisation of semiconductor samples, enabling the determination of material properties like carrier lifetime, diffusion length, defect energy levels and surface recombination velocities [PBPR07, Lea82]. In early experiments, this technique was mostly used to visualize sites of enhanced recombination, like dislocations or stacking faults, inside semiconductor crystals [WK64, Hol74]. However, by scanning the beam in a direction normal to the plane of a pn-junction, the decrease of the current with increasing distance from the junction permits the determination of the minority carrier diffusion length, as already described in 1965 by Higuchi et al. [HT65].

Working principle

In this work EBIC was used to investigate axial pn-junctions in GaAs semiconductor nanowires with the focus on the investigation of the minority carrier diffusion length. The working principle of such an EBIC measurement is displayed in Figure 2.3 a). An electron hitting a semiconductor sample like the nanowire in the figure will dissipate its kinetic energy through the sample and therefore generate charge carriers at its impact point. If those charge carriers reach a pn-junction, they will be separated and can be detected by an external current measurement setup. The majority carriers will be repelled at the internal electrical potential, as displayed in Figure 2.3 b). Only the minority carriers will contribute to the current signal. If the electron beam is moved off the junction, the induced minority carriers will only be detected if they are able to diffuse to the space charge region of the junction, where the internal electrical field is present. Measuring the induced current with respect to the electron beam position allows the determination of the diffusion characteristics of the respective minority carriers. The method does not necessarily require an axial pn-junction; any region with an internal electrical field can be used to separate

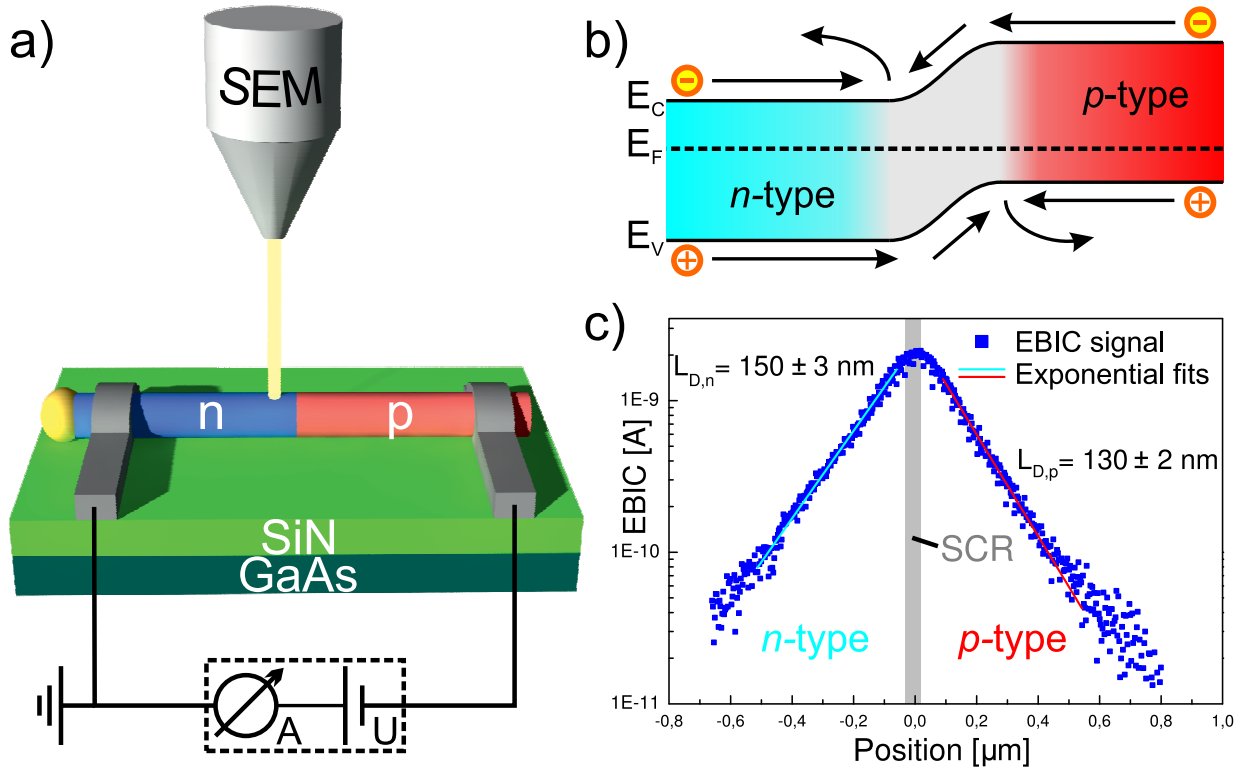


Figure 2.3: EBIC working principle: a) EBIC measurement setup scheme. b) During the measurement, both majority and minority carriers can diffuse to the junction. Only the respective minority carriers are collected, whereas the majority carriers of both sides are repulsed. c) From the EBIC signal along the wire axis, minority carrier diffusion lengths of both p-type and n-type region can be extracted.

the induced carriers. An example of the EBIC based determination of the minority carrier diffusion length on a silicon-nanowire-gold Schottky contact can be found in [AHP⁺08].

Minority carrier diffusion length

The minority carrier diffusion lengths can be extracted by analysing the reduction of the EBIC signal, recorded along the axis of the nanowire away from the junction. The signal strength is given as

$$I = I_0 \cdot e^{-\frac{x}{L}} \quad (2.1)$$

2 Background, simulations and experimental details

where I_0 is the intensity at the edge of the junction, x is the distance from the junction and L_p and L_n are the minority carrier diffusion lengths for holes and electrons following

$$L_i = \sqrt{D_i \cdot \tau_i} \quad (2.2)$$

with D_i and τ_i as the respective diffusion coefficient and carrier recombination lifetime. It is important that the device is investigated under low injection conditions (LIC), which means that the amount of excess carriers excited in the sample has to be small compared to the doping level [CC94]. If LIC does not apply, one might measure a diffusion length of both minority and excess carriers. The injection conditions can be checked with computer simulations and will be discussed in more detail in a following paragraph. Scanning a nanowire with an axial pn-junction allows the extraction of both electron and hole diffusion lengths on the respective p- and n-type site of the junction simultaneously, as shown in Figure 2.3 c). Very similar to such an experiment, the minority carrier diffusion length can also be determined by photocurrent measurements within a micro-photoluminescence (μ -PL) setup. However, the use of an electron beam results in a far better spatial resolution.

Surface recombination velocity

It is possible to extract the surface recombination velocities from the relation of the measured minority carrier diffusion lengths of nanowires of different diameters. The diameter of our samples is way below the bulk diffusion lengths [Hwa69,WOPS81]. Thus, a determined value L_i has to be interpreted as an effective diffusion length

$$L_i^* = \sqrt{D_i \cdot \tau_i^*} \quad (2.3)$$

with an effective lifetime τ_i^* that is governed by the surface recombination velocity S of the nanowires [AHP+08]. This parameter τ_i^* is connected with the surface recombination velocity S and the bulk lifetime τ_b via

$$\frac{1}{\tau_i^*} = \frac{1}{\tau_b} + \frac{4S}{d} \quad (2.4)$$

where d denotes the nanowire diameter [DST⁺11]. This relation is only valid to certain values of S , as it is based on an approximation. The exact relation between τ_i^* and τ_b resulting from the continuity equation of the carrier concentration profile is

$$\frac{1}{\tau_i^*} = \frac{1}{\tau_b} + \frac{4\beta^2 D}{d^2} \quad (2.5)$$

where D is the diffusion constant, d is the nanowire diameter and β is defined by

$$\beta J_1(\beta) - \Lambda J_0(\beta) = 0 \quad (2.6)$$

where Λ is

$$\Lambda = \frac{d \cdot S}{2D} \quad (2.7)$$

with J_1 and J_0 as the 1st and 0th order of Bessel function of the first kind. If $\Lambda < 1$, the approximation $\beta = \sqrt{2\Lambda}$ leads to an error in β of less than 10% [DST⁺11]. This leads to an upper limit for S for the validity of the approximation. The limit for a 300 nm diameter GaAs nanowire with an electron diffusion coefficient of 200 cm²/s in the p-type region [JG89] can be estimated to:

$$\frac{d \cdot S}{2D} \leq 1 \implies S \leq \frac{2D}{d} = \frac{2 \cdot 200 \text{ cm}^2/\text{s}}{300 \text{ nm}} = 1,33 \cdot 10^7 \text{ cm/s} \quad (2.8)$$

For the holes in the n-type region the respective upper limit can be estimated using values from the same reference to $S \leq 6 \cdot 10^5$ cm/s. For both holes and electrons in our nanowires S is below the upper limit and therefore the error caused by the approximation is less than 10%.

Using the relations between L , τ , and S enables one to extract the surface recombination velocity from the diameter dependence of the observed minority carrier diffusion lengths.

Injection conditions

As mentioned above, a conclusive determination of L_i is only feasible when the measurement is carried out in the so-called low injection regime [CC94]. Within LIC, the resulting values of L_i and τ_i are independent of the amount of excess carriers produced in the sample Δp . LIC is only fulfilled when Δp is comparatively small in reference to the doping level. To verify this, one has to determine Δp and compare it to the doping level. The value of

2 Background, simulations and experimental details

Δp can be analytically derived for bulk material by comparing the activation volume and the deposited energy E_0 . In the case of nanostructures the distribution of energy inside the sample is strongly dependant on the sample structure and dimension. Therefore, the Monte Carlo code Casino v3.2 [DPDC⁺11] was used to determine the energy distribution inside an irradiated GaAs nanowire lying on a SiN substrate. With E_0 distributed inside a volume V , it is possible to calculate the excess carrier generation rate G_0 following [Kle68]

$$G_0 \approx \frac{E_0}{3E_g} \cdot \frac{1}{V} \quad (2.9)$$

expressing the amount of carriers excited per volume by a single electron. The energy distribution E_0/V provided by the Monte Carlo code depends on the choice of spatial resolution during the simulation. Here, the simulation was conducted for volume cells of $4 \cdot 4 \cdot 4 \text{ nm}^3$ size. Larger simulation cell sizes would lead to a more uniform energy distribution. However, if the cell size is not small enough compared to the carrier diffusion length, the distribution will be smeared out too much and a reasonable conclusion on the injection regime following G_0 is not possible. For a certain electron beam current I_B and a known excess carrier lifetime τ_{exc} the value of Δp can be estimated with

$$\Delta p \approx \frac{G_0}{e} I_B \tau_{exc} \quad (2.10)$$

where e is the elementary charge. Within GaAs bulk samples, the existence of LIC is often very unlikely due to the relatively high excess carrier lifetime and the μm -ranging of the carrier diffusion lengths [CC94]. However, within GaAs nanowires, excess carrier lifetimes and diffusion lengths are strongly reduced due to surface influence. In Figure 2.4, Δp is displayed for a nanowire with 200 nm diameter and typical electron current density (40 pA) and acceleration voltage (10 kV) values used in this thesis. With the carrier lifetimes estimated for the minority carriers from the EBIC profiles, Δp is always more than one order of magnitude below the typical doping level.

The EBIC measurements in chapter 3 have been conducted with a JEOL JSM-6490 scanning electron microscope equipped with a LaB₆ cathode and a Gatan SmartEBIC analysing system. The electron beam current used was always below 40 pA, ensuring low injection conditions at 10 kV accelerating voltage.

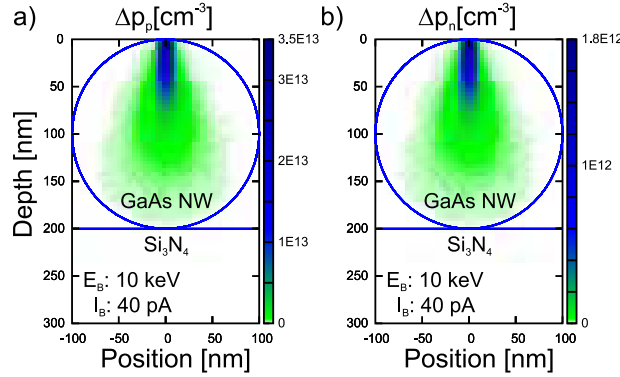


Figure 2.4: Distribution of Δp in a nanowire with 200 nm diameter for an electron current of 40 pA and acceleration voltage of 10 kV determined using Casino v3.2 and the carrier lifetimes estimated for the minority carriers from the EBIC profiles. The concentration of excess carriers Δp is always more than one order of magnitude below the doping level, which is $1.6 \cdot 10^{19} \text{ cm}^{-3}$ in the nanowire p-type region (left side) and $1 \cdot 10^{18} \text{ cm}^{-3}$ in the n-type region (right side).

2.1.6 Cathodoluminescence

Cathodoluminescence (CL) denotes the phenomenon of light emission from a semiconductor impinged by an energetic electron beam [MG74], caused by radiative recombination of the excited charge carriers. The observation of such luminescence inside a cathode ray tube led originally to the discovery of "cathode rays" or electrons. CL emission characteristics give access to the electronic properties of the investigated semiconductor material. If applied within a SEM, CL allows the investigation of luminescence properties and therefore recombination dynamics of a sample with spatial resolution [YH86, PR07].

Electron-hole pairs generated inside a sample by an incoming electron beam can recombine either radiatively or non-radiatively. The probability of the one or the other case to happen depends on the local environment of the charge carriers. Therefore, CL measurements offer access to the local carrier dynamics of selected nanostructures, gaining information of the influence of the shape of the nanostructures on the carrier transport and recombination mechanisms. Non-radiative recombination is often induced by defects in the semiconductor crystal. Thus, CL can give information on the crystal quality of a nanoobject [PPAD06]. As an example, information about the uniformity of the optical and electrical properties of bottom-up grown ZnO nanowires can be ob-

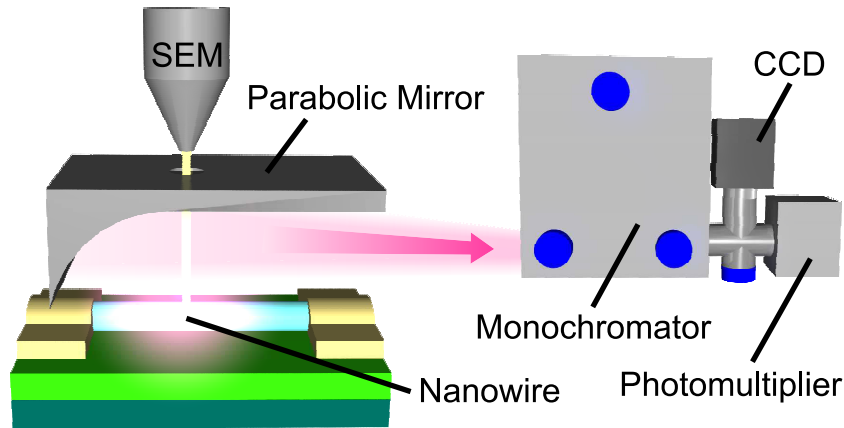


Figure 2.5: CL working principle. The electron beam induced luminescence is colimated by a parabolic mirror and coupled into an optical spectroscopy system. With the monochromator, the incoming light can be spectrally decomposed and analysed as a function of wavelength. A photomultiplier or a CCD camera can be used for signal detection.

tained [NKR⁺04, PYE⁺07, CAM⁺11]. Furthermore, CL can be used for studying carrier dynamics in single quantum dot devices [MSC⁺05].

In the presence of an internal electrical field, generated electron-hole pairs must not necessarily recombine but might get separated before the recombination takes place. Detecting such separated carriers is the principle of the EBIC measurement explained in section 2.1.5. However, it is also possible to measure the electron beam induced CL signal instead of the induced current to obtain information on the diffusion dynamics of the excited carriers. While with EBIC the separated carriers are monitored, CL counts the non-separated, radiatively recombining carriers. In addition, also non-radiative recombination dynamics can be monitored in principle when it is possible to measure the EBIC and CL signal simultaneously on the same sample [Hol89].

The working scheme of the CL setup used in this work is displayed in Figure 2.5. A parabolic mirror is used to collimate the emitted luminescence and couple the light into a chamber-mounted monochromator with attached optical sensors, enabling spectroscopic analysis of the CL emission. The signal is detected by either a CCD or a photomultiplier attached to the monochromator exit slit. Besides the monochromatic imaging, it is also possible to drive the machine in panchromatic mode and detect the overall light emission independent of the wavelength of the emitted light. Regardless of the working mode, the CL setup always collects the emission of the whole sample, caused by a local excitation

from the confined electron beam. Thus, the excitation is spatially resolved, and not the CL signal.

Analogous to the EBIC technique, CL measurements can be used for the extraction of carrier diffusion lengths by monitoring the decay of the signal towards a pn- or Schottky junction. In chapter 3, CL was used in this manner to determine the carrier diffusion dynamics inside ZnO nanowires. According to equation 2.1 in the previous section, the probability that electron beam induced carriers will be separated in the internal field of the junction and contribute to EBIC drops exponentially with increasing distance between the position of carrier generation and the junction. In the same way, it becomes more likely for the carriers to recombine with their counterparts. Therefore, in the case of a negligible or constant ratio of non-radiative to radiative recombination, the CL intensity towards the junction will decrease by [IY08]

$$I_{CL} \propto A \cdot (1 - e^{-\frac{x}{L_D}}) \quad (2.11)$$

where I_{CL} is the CL intensity, x is the distance from the junction and L_D is the carrier diffusion length. Thus, the carrier diffusion length can be extracted by measuring the CL intensity along the nanowire, as shown in Figure 2.6 a) and b). The fit of equation 2.11 to the intensity characteristics directly gives the diffusion length of the recombining carriers, which is in this case (ZnO nanowire) the exciton diffusion length.

The CL measurements in chapter 3 have been conducted with a Gatan MonoCL3 system on a JEOL JSM-6490 scanning electron microscope with a LaB₆ cathode. The system is equipped with a helium cooling stage for temperatures between 6 K and 300 K. Further details on the CL system can be found in [Bul09].

The electron beam current used was always about 100 pA. The applied acceleration voltage was 10 kV. In parallel to section 2.1.5, Casino simulations give the number of electron beam induced excess carriers Δp . Under the applied conditions, Δp is always lower than $1 \cdot 10^{12} \text{ cm}^{-3}$ and thus more than one order of magnitude below the doping level of intrinsic ZnO which is in the range of 10^{17} cm^{-3} [GSLY05], ensuring low injection conditions. All diffusion length measurements have been performed at 12 K temperature.

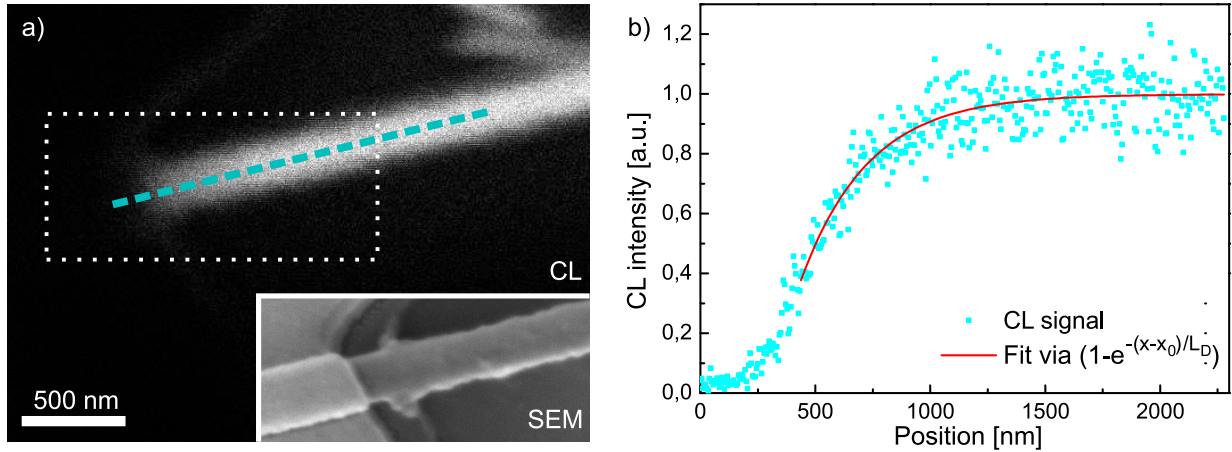


Figure 2.6: Example for the estimation of the exciton diffusion length in ZnO via CL. In a), the CL image of a ZnO nanowire contacted by an Au-Ti contact pad is shown. Only the uncovered part of the nanowire is exhibiting a significant luminescence signal. The inset shows the SEM image from the white dotted rectangular area. In b), that CL intensity along the dashed cyan line in a) is plotted. The exponential fit of the intensity drop along the nanowire towards the contact region allows the determination of the exciton diffusion length.

2.1.7 Photoluminescence

Photoluminescence (PL) denotes the light emission from a semiconductor excited by absorbed photons. In principle, PL and CL are relying on the same mechanisms, distinguished just by the nature of the excitation. An advantage of PL over CL is avoiding carbon deposition on the surface of the investigated sample, a phenomenon that is often observed inside a SEM, which makes PL the favoured method for the investigation of surface related effects. Additionally, the PL intensity depends on the excitation wavelength, a detail that can provide further information on the excitation mechanisms in the sample [YH86]. It is also possible to visualise the depletion zone in electrical devices [HZAL07]. PL spectra in the scope of this work have been recorded by Apurba Dev, University of Bremen. Details on the setup can be found in [Ric10]. The Photoluminescence (PL) measurements were carried out in a liquid-helium-cooled cryostat at 10 K. A He-Cd laser was used for excitation at a wavelength of 325 nm. The emission signal was detected either with an Ocean Optics HR4000 spectrometer or a Jobin Yvon HR320 monochromator with an attached CCD camera.

2.2 Ion-solid interactions

The irradiation of material with energetic ions is the basis for a variety of methods for the analysis and processing of materials. An ion that is impinging on a solid material will be slowed down by flying through the surrounding matter and transferring its energy to the local environment. The energy dissipated inside the target can result in the breakup of existing crystal structures, rearrangement of the target atoms and the creation of voids inside the target material. By selectively controlling these effects, ion beam irradiation can be applied to the processing of materials. On the other hand, the same effects have to be considered for ion implantation processes, where the ion beam is used to implant a distinct amount of atom species into a target material.

The energy loss or stopping power of an energetic ion in matter can be divided into two processes [ZI80]: First, the interaction of the ion with the target electrons, and second, the interaction with the target nuclei by collision. Thus, the terms "electronic energy loss" and "nuclear energy loss" are used. The stopping powers are dependent on the ion charge and energy as well as on the ion mass and the target composition. Although the fundamental processes can be treated independently, it is important to know the ratio between electronic and nuclear energy loss in order to determine the impact of the ion energy on the electronic system of the target.

2.2.1 Ion implantation

Ion implantation is widely used in the semiconductor industry [Wil98]. As already mentioned, the incorporation of dopants into a semiconductor is essential for tuning the electrical properties of the material. With ion implantation, it is possible to modify the dopant concentration in a semiconductor device subsequent to the device fabrication. Implanting through a mask gives lateral control. Furthermore, the depth distribution of the dopants can be adjusted by varying the ion energy. The amount of implanted ions per area is called ion fluence and given in ions/cm^2 . Common ion energies for implantation are between 1 and 500 keV, where the latter energy corresponds to an ion range of about 600 nm of ^{31}P in Si. Due to the statistical nature of the ion energy loss, the depth distribution of implanted ions is always widened, a phenomenon referred also as longitudinal straggling; analogously, radial straggling also occurs.

2 Background, simulations and experimental details

An important advantage of ion implantation is that it can be used for every element of the periodic table without restriction to any solubility limits. Especially in the case of bottom-up grown nanostructures, where doping during growth is quite challenging, ion implantation is often the only method that can provide a homogenous, well defined doping profile. The main disadvantage of ion implantation is the production of defects concurrent to the implantation process [RBGN10]. Therefore, usually a thermal annealing treatment has to be applied subsequently to ion implantation. In the case of nanowires this can be quite difficult as they often show a lower thermal stability compared to bulk material. On the other hand, under certain conditions so called dynamic annealing can be observed [DDW⁺03, CFR⁺08, BMB⁺11]: The confined geometry of the nanowires might hamper the dissipation of the impact energy of the implanted ion and lead to a local heating of the nanowire, whereby a part of the implantation induced defects is annihilated immediately. This effect is already known from the implantation in bulk structures [Wil98], however, it was found to be enhanced in semiconductor nanowires [BMB⁺11]. Nevertheless, in most of the material systems investigated so far, an additional annealing step has proven to be mandatory for the successful doping of ion implanted nanostructures [RBGN10, RBG⁺10].

2.2.2 Simulation of implantation profiles

The expected trajectories of the ions inside the implantation target are usually calculated in advance in order to prepare an implantation experiment. A well established and often used code for this purpose is the Monte-Carlo package SRIM [ZBL85, ZZB10]. Based on the simulation of binary collisions between the incoming ion and the target atoms, the program is capable of calculating the distribution of implanted ions and implantation induced defects for any ion species in any material. Monte-Carlo codes like SRIM have been proven to provide a sufficiently accurate result for the implantation in bulk samples or thin films within an acceptable time. However, SRIM and similar programs are only taking laterally homogeneous samples into account, as implantation targets can only be defined as layered and flat structures. The determination of implantation profiles in nanostructures with sizes in the order of the ion range will not work using SRIM, as the program does not take into account the possibility of an incoming ion being scattered sideways and leaving the nanostructure to the side. For this purpose, the Monte Carlo code "iradina" has been developed [BR11], partially based on SRIM and the similar but faster code CORTEO [Sch08]. Iradina supports 3d-geometries, allowing the consideration of all peculiarities

that arise during the implantation of nanostructures. Iradina was found to determine the amount and distribution of implanted ions in nanowires in good agreement to TEM and EDX measurements, while SRIM is overestimating the atom number by a factor of about two, depending on the size of the nanowire [BR11].

SRIM and iradina are both based on the simulation of binary collisions in order to simulate the nuclear energy transfer between the incoming ion and the target atoms. A decisive factor for this value is determined by the choice of the interatomic potential during the collision. A realistic choice is the screened Coulomb potential

$$V(r) = \left(\frac{Z_1 Z_2 e^2}{r} \right) \chi(x) \quad (2.12)$$

with $x = r \cdot a_S$ and

$$a_S = \frac{0.8853 a_B}{Z_1^{0.23} + Z_2^{0.23}} \quad (2.13)$$

where a_S denotes the so called screening length, Z_1 and Z_2 the charge of the nuclei of projectile and target atom, a_B the Bohr radius and $\chi(x)$ a screening function, that is explained in detail in [ZBL85]. With this potential, the scattering angle and thus the transfer of momentum between the projectile and the target atom can be calculated for a given impact parameter.

The simulation calculates the path of an ion through the crystal based on binary collisions with the target atoms, using random numbers for the variation of the impact parameter and the mean free path, until the projectile is either stopped or leaving the target. Recoiled target atoms are also taken in account. By repeating the calculation many times, a realistic distribution of the implanted atoms and the damage induced inside the target is obtained. While the nuclear energy loss is calculated for each collision of the ion with a target atom, the electronic energy loss is assumed to be a continuous process and independently subtracted from the ion energy between the nuclear collisions, only depending on the path the ion has travelled. Well known experimentally obtained values for the electronic stopping of lighter elements are included in the simulation code; electronic stopping of heavy ions is calculated from the data of protons and helium ions by the so called heavy-ion-scaling [ZBL85].

2 Background, simulations and experimental details

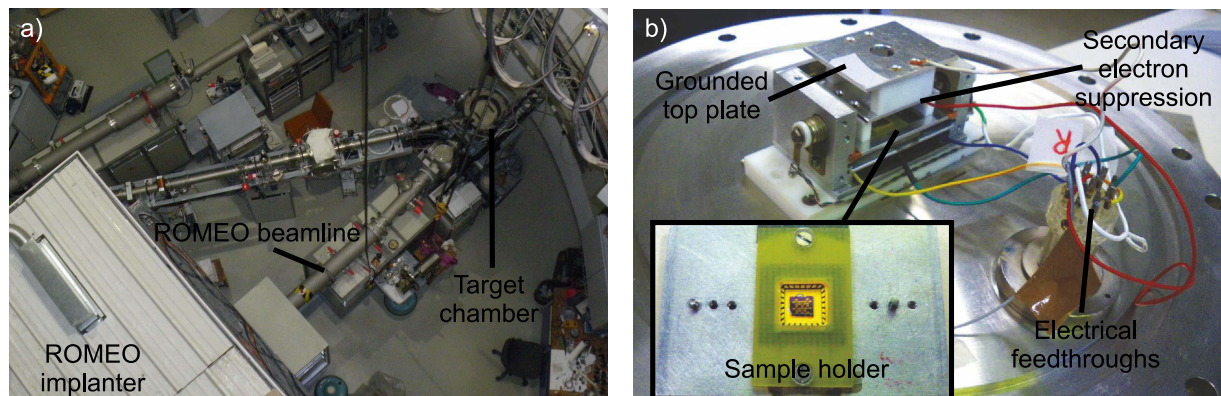


Figure 2.7: a) ROMEO beam line at the IFK Jena, top view. b) Sample holder design for electrical in-situ measurements on ion implanted nanowire devices. The picture shows the high-vacuum flange with the sample holder mount on top. The inset shows the sample holder itself. The sample is clamped to the holder with an epoxy plate. The electrical connections are placed on the back side of the sample holder.

Both SRIM and iradina were used within this thesis in order to determine ion ranges and defect profiles for the respective experiments.

2.2.3 Ion implanters

An ion implanter consists of the following parts: An ion source, where the ion species are generated, an accelerating, mass separating, and focussing system, where the ion beam is defined, and an implantation chamber, where the target is mounted. Ion source, beam line and target chamber are usually held under high vacuum conditions. Besides this, there are a lot of varying designs with different strengths and shortcomings. Thus, in this section a brief description of the implanters where ion implantation has been carried out during this work will be given, namely the implanter ROMEO for ion energies larger than 10 keV and the implanter LEILA for ion energies between 300 eV and 10 keV, both located at the IFK in Jena.

ROMEO

The implanter ROMEO is an air insulated Cockroft-Walton accelerator for acceleration voltages up to 400 kV, build by High Voltage Engineering Europa [hve12]. The positively

charged ions are extracted out of the ion source by a 30 keV DC voltage. Mass separation is provided by a 90° sector magnet right behind the ion source extraction lens. A voltage multiplier cascade (Cockroft-Walton principle [CW30]) is used to apply an adjustable, positive potential on the ion source and mass separation unit, while the target chamber stays at ground level. By regulating this voltage, the overall ion energy can be varied between 30 keV and 400 keV for singly charged ions. The ions are then guided into the beamline (see Figure 2.7 a)) where the beam is confined by a quadrupole lens and additional horizontally and vertically aligned deflection plates. The beam is further deflected by 5° before entering the target chamber, ensuring that only charged ions enter the chamber and neutral species are filtered out. A beam sweep unit is used to scan the beam homogeneously over the sample according to a Lissajous figure with both frequencies close to 1 kHz. The actual beam sweep position can be tapped from an external voltage signal. Symmetrically aligned Faraday cups at the entrance of the target chamber allow a continuous assessment of the beam current, which can be attenuated down to around 10 pA.

In order to measure implantation induced changes of the characteristics of nanowire devices in-situ, a sample holder was constructed, which is displayed in Figure 2.7 b). The holder sits on a high-vacuum flange that can be mounted on the implantation chamber. A metal plate above the sample is insulated against the rest of the sample, Thus, a negative potential can be applied in order to suppress the emission of secondary electrons from the implanted device, which would falsify the current measurement.

LEILA

The low energy implanter LEILA is based on a model G-2 ion gun manufactured by Colutron [col12]. The ion gun is able to work with acceleration voltages between 100 V and 10 kV. The Colutron unit consists of an ion source assembly, a beam confining and focusing sytem, and a velocity filter for mass separation. The ion source is able to provide ions of any gaseous source. Beam confinement is obtained by an einzel lens as focusing element and vertical deflection plates. The velocity filter (Wien-Filter principle [Wie02]) works with perpendicular electric and magnetic fields, that can be adjusted in such a way that only the desired ion species advance into the target chamber at a given acceleration voltage.

A beam sweep unit with user-definable frequency and amplitude allows for homogeneous irradiation of the sample. The ion current is measured with a Faraday cup that is placed

2 Background, simulations and experimental details

at the end of the beam path. During implantation, the sample holder is plugged-in into the path and therefore the cup is covered. This arrangement is a major disadvantage of this accelerator setup, as it is not possible to monitor the total ion flux during the implantation process. In connection with ion current variations over the implantation timespan, this can lead to a large deviation of the implanted fluence. Therefore, the ion current was checked by plugging the sample out of the beam path for a short time every few minutes during the implantation experiments, resulting in a reasonably accurate estimation of the current history and the overall fluence. A second major disadvantage of the design of LEILA, which became apparent during implantation with 10 kV acceleration voltage, is that when setting up the accelerator, special emphasis was placed to the ion energy range below 1 keV. Hence, some of the parts are not working properly at higher acceleration voltages. In the absence of alternatives, LEILA was used for implantation experiments with acceleration voltages up to 10 kV anyway.

2.3 Techniques and terms used for the biofunctionalisation experiments

2.3.1 DNA

A DNA (deoxyribonucleic acid) molecule is containing the complete genome of an organism and thus carrying the genetic instructions for the development and the functioning of the species. As such, DNA sensors can be used for the unambiguous identification of living organisms, including bacteria and viruses. The DNA molecule is organised in a double helix structure, consisting of two complementary, long polymers of simple units called nucleotides. DNA sensors are made by using one of the polymers or a part of it, called oligonucleotide, as a capture molecule, looking out for the complementary target molecule. As the DNA backbone is negatively charged, an electrical working DNA sensor can be realised that is sensitive to the electrical field induced by the attachment of the target molecule.

2.3.2 Surface engineering

Surface science is referred to as the interdisciplinary study of the effects and processes taking place at the interface of two different phases. The research field includes and connects methods and techniques from physics, chemistry, and biology. The intended modification of surfaces and surface properties with surface science techniques is called surface engineering. Surface engineering has made significant contributions to a wide field of technology, like the development of catalytic processes for fuel production, the functionalisation of surfaces for chemical or biological sensing purposes, or the optimisation of semiconductor devices by tailoring the surface related properties of semiconductor devices [Som96].

A connotative sub-category of surface science is the biological surface science, where interfaces between synthetic materials and biological environments are investigated. Here, the major emphasis in research is placed on biofunctional or biomimetic surfaces for the development of medical implants, artificial leaves, or biosensors, for example [Kas02].

In chapter 5, the biofunctionalisation of ZnO nanowires with DNA capture molecules is shown. This is an example of biofunctionalisation, a term that is used for surface engineering with biological molecules. Most biomolecules can not covalently bind to inorganic materials. Thus, so-called linker molecules are applied, that bind covalently to the inorganic surface as well as to the biomolecule. In this work, the linker molecule Glycidylpropyltrimethoxysilane (GOPS) is used to bind DNA molecules covalently to the ZnO nanowires surface. The reaction scheme and the applied parameters are discussed in detail in chapter 5.

2.3.3 Fluorescence microscopy

Fluorescence microscopy is a method combining the phenomena of fluorescence and phosphorescence with optical microscopy. The method is often used in biological surface science for studying the formation of biomolecule layers on thin film surfaces as well as on nanostructures [CDH08, BHS⁺09]. The biomolecules of interest are marked with a fluorescent dye in advance. During layer formation the specimen is illuminated with light at a wavelength where the dye is excited and fluorescence occurs. With the help of a filter cube in the optical path the marker specific fluorescence is guided to the microscope ocular. As different dyes emit on different wavelengths, a special filter cube for every dye is needed.

2 Background, simulations and experimental details

Fluorescence studies in this work have been conducted with the Zeiss Axio Imager 2 fluorescence microscopy setup at the IPHT Jena.

3 Carrier diffusion lengths in semiconductor nanowires

This chapter deals with carrier diffusion length measurements at axial GaAs nanowire pn-junctions and ZnO nanowire Schottky junctions. Detailed knowledge on the carrier diffusion is essential for the design of nanowire based photovoltaic devices, since the absorption length inside a solar cell is comprised of the depletion region at the pn-junction and the mentioned diffusion lengths. The GaAs wires have been investigated with EBIC. The EBIC signal obtained on the GaAs nanowires was used to determine the minority carrier diffusion lengths of both holes and electrons on the respective sides of the junction. The experiment was conducted in collaboration with Chrisoph Gutsche from the University of Duisburg-Essen, where the GaAs devices were produced. Martin Gnauck assisted with the measurements. Parts of the results are going to be published in [GNG⁺12]. The ZnO nanowires were investigated using CL. Here, the diffusion length of electron beam induced excitons was determined on ZnO nanowire Schottky devices.

3.1 Minority carrier diffusion lengths

Nanowire transport properties often differ from bulk properties owing to the enhanced surface-to-volume ratio of the wires leading to a higher influence of surface related effects. In semiconducting nanowires, surface enhanced recombination of charge carriers can lead to a drastical reduction of minority carrier diffusion lengths and lifetimes [PJG⁺09, DST⁺11]. Investigations on the diameter dependant behaviour of the diffusion lengths help understand and quantify the surface recombination mechanisms. There are several methods that have been used to investigate minority carrier diffusion lengths in semiconductor nanostructures: Scanning photocurrent microscopy (SPCM) with a focused laser spot [GMOY11], SPCM combined with near field optical microscopy (NSOM) [GRD⁺06,

3 Carrier diffusion lengths in semiconductor nanowires

KTEK⁺⁰⁸, DST⁺¹¹], cathodoluminescence [GBSS10, BMSG10], cathodoluminescence combined with NSOM [BAL⁺⁰⁹, BOC⁺¹¹], and EBIC [GBS07, AHP⁺⁰⁸].

In almost all the studies on minority carrier diffusion lengths in semiconductor nanowires so far the respective lengths were significantly shortened compared to bulk material. In the case of Si, Allen et al. found a 100- to 1000-fold decrease for uncapped nanowires with diameters between 30 and 100 nm. If the wire surface is passivated by a thin layer of SiO₂, surface recombination is reduced by two orders of magnitude and the diffusion length is almost comparable to bulk level [DST⁺¹¹]. For thicker nanowires with 900 nm diameter, Kelzenberg et al. found bulk-like diffusion lengths [KTEK⁺⁰⁸]. In the case of III-V-semiconductors, diffusion lengths were found to be reduced strongly for uncapped GaN nanowires [BAL⁺⁰⁹] as well as uncapped GaAs nanowires [GBSS10].

3.2 EBIC investigations on axial GaAs nanowire pn-junctions

EBIC measurements were carried out on four different nanowire pn-diodes with diameters ranging from ≈ 100 to 300 nm. IV-characteristics have been recorded before and after the measurements in order to exclude side effects caused by the analysing electron beam. Apart from the choice of the right electron beam parameters, it is necessary to check if the collected current is really driven by diffusion and not by electrical drift along the nanowire. Thus, the same nanowire diode was repeatedly measured under varying applied bias voltages. From Figure 3.1 it is evident, that the EBIC signal strength depends on the applied voltage. However, the estimated diffusion lengths did not show any bias dependence for a bias between 0 V and 0.5 V, which implies that drift currents are negligible in this voltage range [DST⁺¹¹]. In contrast, the diffusion lengths change when applying a reverse bias of 1 V or higher.

The determined effective minority carrier diffusion lengths $L_{n,p}$ of both, electrons and holes, which were determined from various nanowires, are plotted in Figure 3.2. They show a monotonically increasing behaviour with increasing nanowire diameter. The nanowire diffusion lengths are significantly small (about 10-fold decreased) compared to minority carrier diffusion lengths of a few μm in GaAs bulk crystals or thin layers [Hwa69, CMP73, WOPS81], in accordance to the results from literature discussed in the precedent section.

3.2 EBIC investigations on axial GaAs nanowire pn-junctions

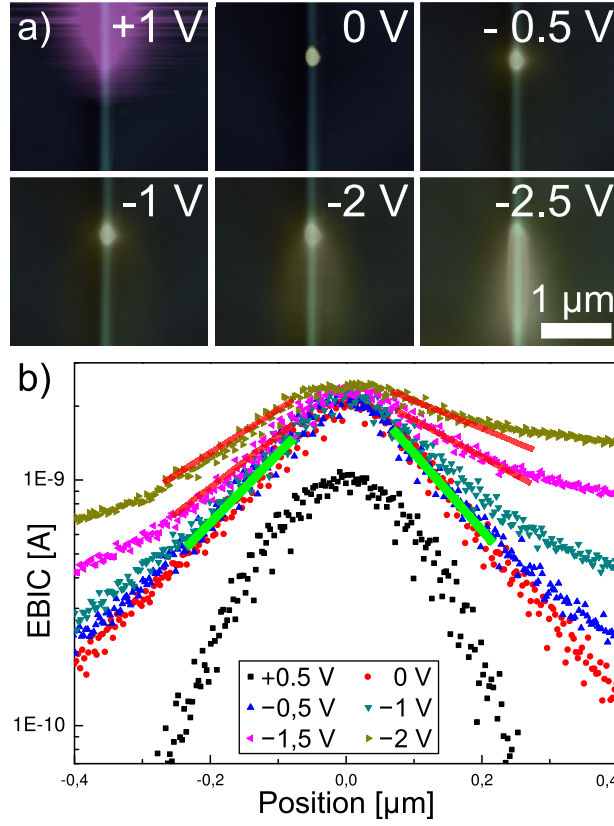


Figure 3.1: (a) EBIC signal images measured under varying applied bias voltages. The signal strength depends on the applied voltage. (b) EBIC signal line scans along the nanowire axis in the EBIC image. The pn-junction lies at position zero on the x-axis. The ascending slope of the EBIC signal does not show any bias dependence for reverse bias voltages up to 0.5 V (green bars) but seems flattened for higher voltages (red bars). Forward bias also changes the slope significantly (black curve).

The observed diameter dependence points to a strong influence of the nanowire surface. Investigating the diameter dependency of the determined diffusion lengths, it has to be taken into account that not the whole nanowire diameter is actually contributing to the carrier transport. In uncapped GaAs nanowires, usually a doping level dependent surface depletion layer occurs. This is caused by deep level Fermi energy pinning on the nanowire surface that leads to band bending. The width of the depletion layer d_{spc} can be calculated as [GRB⁺09]

$$d_{spc,i} = \sqrt{\frac{2 \cdot \epsilon_o \epsilon_r \phi_{s,i}}{q \cdot N_i}} \quad (3.1)$$

3 Carrier diffusion lengths in semiconductor nanowires

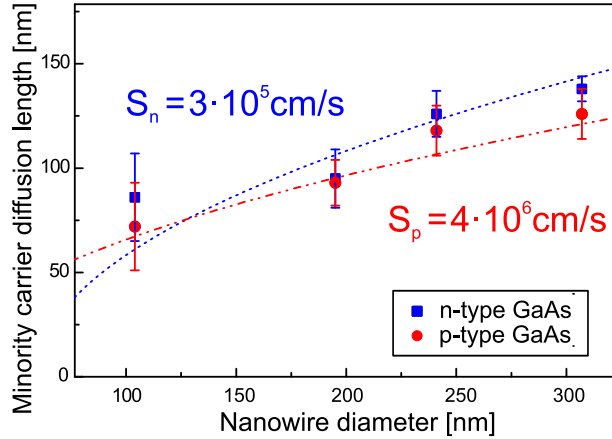


Figure 3.2: Measured minority carrier diffusion lengths for *pn*-GaAs nanowires of different diameter. The dashed lines are showing the theoretical progression of the diameter dependence for the stated surface recombination velocities. Depletion layers with 29.6 nm (*n*-type) and 6.8 nm (*p*-type) width have been taken in account for the calculation.

where ϵ_0 is the vacuum permittivity, ϵ_r the dielectric constant of GaAs, $\phi_{s,i}$ the surface potential of *i*-type GaAs and N_i the respective carrier concentration. Carriers generated inside or diffusing into the surface depletion layer will immediately be extracted to the surface and do not contribute to the EBIC signal. Hence, for the diameter dependency evaluation of the EBIC measurements an effective nanowire diameter $d_i^* = (d - 2 \cdot d_{spc,i})$ has to be taken into account. Trend lines of the diffusion lengths calculated for these effective nanowire diameters are also displayed in Figure 3.2. The curves have been fitted to the measured values by adjusting the surface recombination velocity S . The resulting surface recombination velocities ($S_p = 4 \cdot 10^6 \text{ cm/s}$, $S_n = 3 \cdot 10^5 \text{ cm/s}$) are comparable to values measured in GaAs bulk samples [JLG75, II94]. While S_p is almost identical to the bulk value [II94], the value of S_n is one order of magnitude smaller than expected for a carrier concentration of $N_D = 1 \cdot 10^{18} \text{ cm}^{-3}$.

The lower value of S_n indicates a lower doping level than expected [JLG75]. In the region near the junction, where the EBIC measurements were conducted, this can be the case due to the fabrication method. During VLS nanowire growth, the Au seed particle acts as a delaying element for the dopant atoms. Although the type of dopant precursor is switched from *p* to *n* rapidly, it still takes some time to reach a high doping level on the *n*-doped part, which finally leads to an axially graded dopant profile. This result is in agreement to other studies on the same nanowire structures, where the doping concentration profile was

3.3 Surface passivation with ammonium sulfide

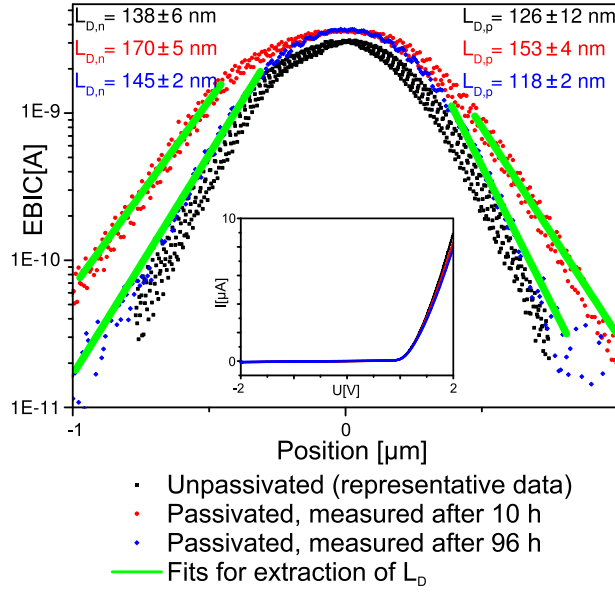


Figure 3.3: EBIC scans at a single nanowire pn-junction before and after the passivation treatment using ammonium sulfide. Directly after the treatment the EBIC signal shows a more gentle slope, indicating an increased minority carrier diffusion length. After 4 days, slope and diffusion length have dropped down to their initial values. Inset: The I-V-curve of the device remains unchanged.

analyzed with μ -photoluminescence [LOG⁺11] or Kelvin probe force microscopy [LVO⁺11] and therefore fits to the actual model of dopant incorporation in catalyst assisted VLS nanowire growth.

As the EBIC signal might also depend on the carrier generation volume inside the nanowire [AHP⁺08], measurements at different acceleration voltages were conducted in order to vary the extent of the excited volume. No effect on the diffusion length was visible, showing that the observed diameter dependence of the diffusion length is not an effect related to the dimensions of the excitation volume. The same conclusion has been obtained for Si nanowires before [AHP⁺08].

3.3 Surface passivation with ammonium sulfide

The reduction of minority carrier diffusion lengths in GaAs nanowires compared to GaAs bulk material is not supportive for photovoltaic applications. An effective surface passivation treatment could help to increase L_n and L_p again, as the observed reduction is strongly related to recombination over the nanowire surface. The positive influence of passivation has already been shown in the case of Si [DST⁺11] and GaN [BOC⁺11] nanowires before. A standard procedure for GaAs and InGaAs surfaces is the passivation with ammonium sulphide [BMH⁺11]. Applied to GaAs nanowire solar cells, this sulfur passivation step was shown to result in an increased photovoltaic efficiency [TPKL11]. In this thesis, rather conservative reaction conditions have been chosen for the passivation step, as the process was conducted on already contacted nanowire devices with chemically sensitive contact structures on top. There are many possibilities to optimise the passivation results by the chemical parameter selection; for an overview see [BMH⁺11].

In Figure 3.3, comparative EBIC linescans along a pn-GaAs nanowire before and after the passivation process are displayed. The green lines indicate the fits applied for extracting the diffusion lengths. It is obvious that the signal gradient is slightly increased 10 hours after the passivation procedure. Four days after the treatment, the diffusion lengths have reached the initial values again. The IV-characteristic of the device remains virtually unchanged during the whole passivation process (inset of Figure 3.3).

The experiment underlines the importance of an effective nanowire passivation. The values for L obtained on passivated nanowires in this work are still comparable to nanowires without passivation and way below the bulk values. However, the simple passivation process applied led to increased diffusion lengths. Moreover, ammonium sulphide passivation is known to be unstable in air, depending on the passivation parameters [OSW⁺93, HCL⁺96]. The EBIC measurements were conducted 10 hours after passivation. Measuring directly after the passivation process might reveal a much stronger effect. Furthermore, the effectiveness of the passivation process depends much on the choice of chemical reaction parameters, as described above. Further optimisation of these will also lead to a larger increase in diffusion lengths. Alternative approaches for long-term stable passivation treatments are shown in references [JPNT04] and [MWK⁺11].

3.4 Carrier diffusion lengths in ZnO nanowires

According to section 2.1.6, the slope of both the EBIC and CL signals towards a junction can be used to investigate the carrier dynamics in contacted semiconductor nanowires. However, for some materials either of the methods might be non-applicable owing to the physical properties of the material. The GaAs nanowire devices do not show any remarkable CL signal and cannot be investigated with this technique. On the other hand, ZnO nanowires exhibit a pronounced PPC effect. When exposed to electron irradiation, the conductivity of ZnO nanowire devices is significantly enhanced for a long time. This phenomenon, in combination with some unavoidable charging of the sample, leads to a complete overlay of the EBIC signal of the junction. Hence, the carrier dynamics in ZnO nanowire devices have been investigated via CL in this work instead of EBIC.

Despite the problems described before, minority carrier diffusion length measurements in ZnO nanowires via EBIC [LSF⁺11, SFC⁺11] and also SPCM [SDG10] have been reported in literature. The EBIC studies have been conducted on Sb doped p-type wires. The respective minority carrier diffusion length was found to be increased by applied heating as well as the duration of the e-beam irradiation, which was traced back to the activation of a dopant-related acceptor complex [LSF⁺11]. SPCM studies were conducted on n-type wires with diameters between 25 nm and 60 nm, revealing a dramatic decrease in diffusion length for smaller diameters that was traced back to a disproportional increase of mid-bandgap defect states for nanowire diameters smaller than 40 nm [SDG10]. A critical point in both studies is the open question of the nature of the observed carriers. As ZnO exhibits a relatively high exciton binding energy of 60 meV, it is likely that even at room temperature excited carriers will form excitons and the observation of free minority carriers is rather implausible [HDP⁺11].

At low temperatures the situation is more defined. Here, carrier dynamics are strongly dominated by excitons [RVK⁺08, RVW⁺08]. For the investigation of exciton dynamics, spatially resolved as well as time resolved measurements can be used. Time resolved emission characteristics allow for an indirect conclusion of the exciton dynamics. Willander et al. [WYW⁺08] extracted the influence of the surface on the lifetime of PL emission from ZnO nanowire ensembles in dependence of the nanowire diameter. The surface related decay lifetime is influenced by the surface recombination velocity combined with the carrier diffusion length. They found a decreasing exciton diffusion length for decreasing nanowire diameters. However, Oh et al. [OLP⁺07] found different optical properties for

3 Carrier diffusion lengths in semiconductor nanowires

ZnO nanowires from the same growth process via CL, showing that measurements on ensembles of nanowires could be misleading in view of possible inhomogeneities among the nanostructures. PL measurements on single CdS and ZnO nanowires revealed an increasing influence of the surface on the exciton recombination with decreasing nanowire diameter [THJ⁺06, WVBS06, VW08, RGW⁺10]. Higher spatial resolution can be obtained by time-resolved CL, as was applied for the characterisation of GaAs pyramidal nanostructures by Merano et al. [MSC⁺05].

The determination of diffusion lengths with the method described in chapter 2 has been shown by Ino et al. for excitons in GaN thin films [IY08]. Recently, the carrier depletion and exciton diffusion length in a 200 nm diameter ZnO single nanowire Schottky device have been investigated by Hwang et al. [HDP⁺11]. The authors varied the bias voltage applied to the device in order to change the extent of the depletion zone and enable the determination of the diffusion length along the nanowire axis. As excitons can be considered as neutral particles from the outside, applied bias voltage has no adulterant influence on the estimated exciton diffusion lengths. The diffusion length was found to be constantly around ≈ 200 nm along the nanowire axis.

3.5 CL investigations on ZnO nanowire Schottky junctions

ZnO nanowire Schottky devices have been produced following the scheme in Figure 2.2. ZnO nanowires with diameters from ≈ 100 nm to 300 nm have been used. Silicon with a 850 nm thick SiO₂-layer on top was used as substrate. Contact structures were formed by photolithography and the evaporation of 40 nm Ti and 90 nm Au. The CL measurements were performed with 10 keV electron energy at a temperature of 12 K. In order to avoid charging of the sample and to have the possibility of applying a bias voltage, the samples were contacted with conductive silver, whereby one contact was grounded and connected to the SEM holder while the other contact was connected to an external voltage source. Two samples with multiple nanowires have been investigated, hereafter referred to as samples #1 and #2.

The measurement of the exciton diffusion lengths is based on the assumption, that the CL signal vanishes towards the Schottky contact, as excitons created nearby diffuse into

3.5 CL investigations on ZnO nanowire Schottky junctions

the depletion layer of the contact. There, they are ionised and cannot contribute to the CL signal any more, but contribute to current. In this view, excitons created in the contact pad region are totally neglected. However, a closer look at the CL image in Figure 2.6 reveals a very weak but still visible luminescence from the contact-pad covered area of the investigated nanowire. In Figure 3.4, the CL spectrum of an uncovered nanowire is compared to the spectrum taken from an ensemble of 3 nanowires of comparable size covered by the Ti-Au contact pad. Both spectra show a near band-edge emission (NBE) peak at a photon energy close to the bandgap of ZnO. This peak is attributed to the direct recombination of excitons [RVK⁺08, RVW⁺08]. Additionally, a broad green defect-related deep level emission (DLE) with a central energy of 2.45 eV is visible on both positions, commonly attributed to defect centres near the crystal surface [RDM⁺09]. In comparison to the spectrum of the uncovered wire, the intensity of the covered wires is lowered by orders of magnitude. In addition, a change in the ratio between DLE and NBE is visible: the DLE appears less pronounced for the covered nanowires. This behaviour is in accordance to findings from literature, where coverage of ZnO nanowires with noble metals was found to influence the DLE/NBE ratio [RDM⁺09] and especially Ti coverage enhanced the NBE efficiency [FSW⁺11, DG11].

Covering with polymers was also found to suppress the DLE [RVW⁺08]. During the photolithography step, the nanowires are covered with photoresist, which should yield a similar effect. However, the resist is washed away with acetone subsequently to the contact evaporation. ZnO nanowires have been shown to be very sensitive to acetone exposure, as the acetone is able to reduce oxygen species that have been chemisorbed at the nanowire surface [CHC⁺08]. On the other hand, the acetone exposure does not lead to a long-term effect, as the initial wire properties are retained within seconds. Thus, it is very unlikely that the emission characteristics of the uncovered nanowires are influenced by any residues of the photolithography process.

A third feature that is visible in the spectra is the appearance of an additional weak defect related red emission band at ≈ 1.9 eV only for the uncovered nanowire. The low overall intensity of the covered wires can be explained by absorption in the contact pads as well as ionisation of the excitons and separation of the electron-hole pairs at the nanowire-contact pad interface. Since the luminescence of the covered parts of the wires is by orders of magnitude weaker, the extraction of the diffusion length from the CL image can be conducted following the method displayed in Figure 2.6 with the use of equation 2.11.

3 Carrier diffusion lengths in semiconductor nanowires

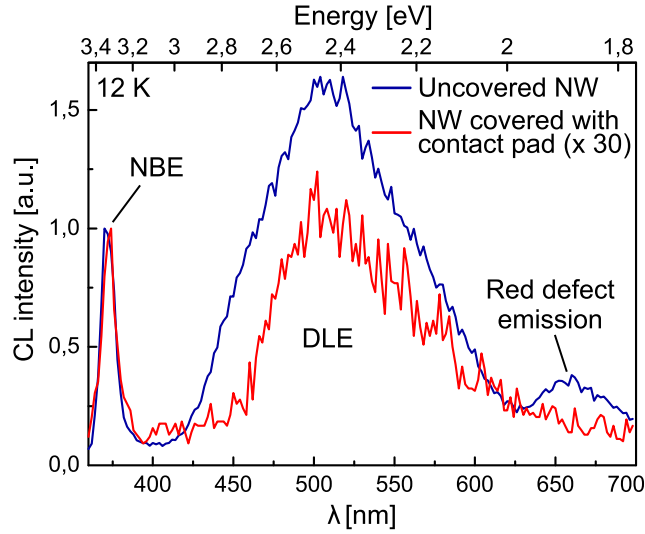


Figure 3.4: CL spectra of a single uncovered nanowire and an ensemble of 3 nanowires covered by a contact pad. Both spectra were recorded with the same integration time. The uncovered wire shows orders of magnitude higher overall intensity. Compared to the NBE, the intensity of the DLE is significantly reduced for the covered nanowires.

The CL setup can be used either in monochromatic or in panchromatic mode. With the monochromatic setup, it is possible to selectively detect only the direct recombination of excitons by monitoring the NBE. Previous studies on the luminescence properties of ZnO have shown that also the major part of the defect related emission cannot be observed under sub-bandgap excitation [Lau73, HTS⁺06]. From this one can conclude that the defect related emission is mainly caused by energy transfer from excitons that are trapped on the defect states while diffusing through the nanowire. Thus, it should make no significant difference for the estimation of the diffusion length, if the panchromatic or the monochromatic CL mode is applied in order to measure the diffusion length of the excitons in the wire, as always an emission primordially caused by an exciton is observed. Taking this consideration into account, the panchromatic mode was chosen for the diffusion length determination, as it offered a better signal-to-noise ratio. Exemplary monochromatic and a panchromatic image of an ensemble of nanowires of sample #2 are displayed in Figure 3.5. Due to the geometry of the CL setup, the contacted samples with wiring on top could not be adjusted in the focal point of the parabolic mirror to optimise the light detecting efficiency, explaining the poor contrast in the monochromatic images. With the panchromatic mode, it was possible to detect a sufficient amount of light within a reasonable time

3.5 CL investigations on ZnO nanowire Schottky junctions

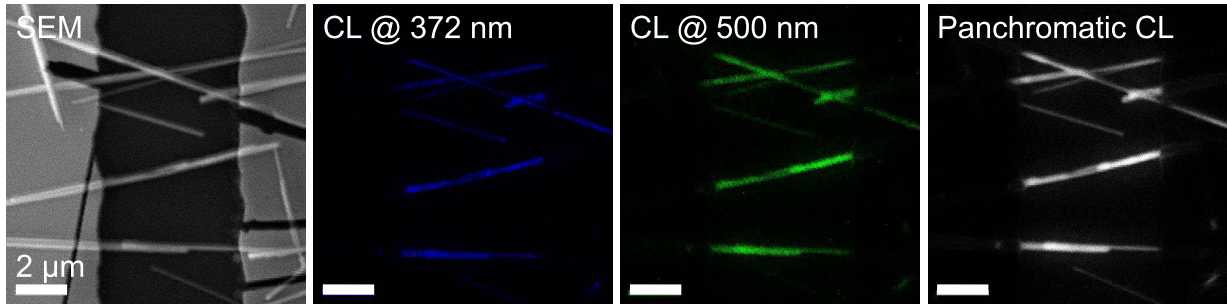


Figure 3.5: Monochromatic and panchromatic CL images of an ensemble of nanowires on sample #2 taken with identical exposure parameters. Even if the shape of all nanowires is clearly recognisable in the monochromatic images recorded at the spectral position of the NBE (372 nm) and DLE (500 nm), the poor contrast of the images is not sufficient for a successful extraction of the exciton diffusion lengths. In the panchromatic mode, significantly more light could be detected, giving enhanced contrast.

(≈ 2 min per image) anyway. Longer exposure times could not be used, as thermal drift inside the SEM would lead to a significant distortion of the CL images.

Following the method displayed in Figure 2.6, CL images of 27 nanowire contact areas were investigated in order to determine the exciton diffusion length. During the experiment, the Schottky diodes were always reverse biased with 15 V by an external voltage source. The extracted diffusion lengths are displayed in Figure 3.6. On the first view the data does not look very promising. The exciton diffusion lengths of nanowires with diameters of 150 nm and more librate around a value of 200 nm. This value, at least, is equal to the diffusion length that Hwang et al. determined for a 200 nm diameter ZnO wire [HDP⁺11], and is therefore in accordance to literature.

For smaller diameters the values obtained for the diffusion length are widely spread, including higher values. An increasing diffusion length with decreasing nanowire diameter seems unlikely, as one would expect a higher probability for the exciton to diffuse towards the surface and recombine on a surface defect for a smaller diameter. This would effectively reduce the diffusion length like observed on the GaAs nanowires. There must be another reason for the wide spreading of the estimated diffusion length values for the nanowires between 100 and 150 nm diameter.

From the error bars in Figure 3.6 it is obvious, that even in panchromatic mode the method for the diffusion length measurement provides a relatively high uncertainty, owing to the relatively poor resolution of the Jeol SEM and the even in panchromatic mode poor

3 Carrier diffusion lengths in semiconductor nanowires

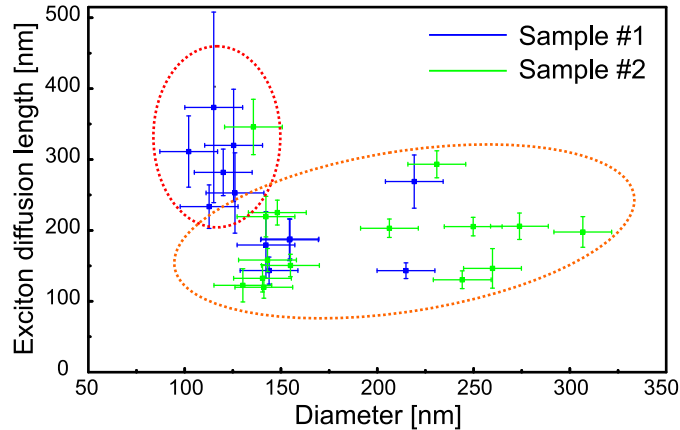


Figure 3.6: Diameter dependency of the exciton diffusion length of ZnO nanowires. The values are widely spread and do not follow a clear trend. The nanowires can be roughly classified in two groups: Nanowires with diffusion lengths librating around 200 nm, marked with the orange dotted ellipsoid, and nanowires with diffusion lengths spread to higher values, marked with the red ellipsoid.

light detection efficiency due to the non-optimum position of the wired sample. By surveying the data sample by sample, it stands out that all but one of the widely-spread values have been obtained by nanowires from sample #1. Nanowires from the same growth substrate have been used for both samples investigated in the study. However, the nanowires used for sample #1 were taken from a different position of this substrate than the wires on sample #2, which might lead to different properties of the nanowires. The emission characteristics of ZnO nanowires are strongly related to the local growth conditions [LLA⁺09]. The difference in the diameter distribution of the two samples is also an indication for differing nanowire properties. In the study of Oh et al. [OLP⁺07], different optical properties of nanowires from the same growth process have been found. The differences in emission characteristics were found to also be correlated to changed transport properties of the wires. In order to find or exclude a similar phenomenon in our experiment, the contact wirings from both samples were removed and the samples investigated in the CL again in order to get a more detailed view on the optical properties of the individual nanowires.

Room temperature CL revealed a strongly differing ratio of the NBE and DLE intensities I_{NBE} and I_{DLE} for the investigated nanowires with values ranging between 0.1 and 1.2, irrespective of the nanowire diameter, as reported by other groups [STN04]. As the I_{NBE}/I_{DLE} ratio of the identically prepared nanowires can differ so extremely, an investi-

3.5 CL investigations on ZnO nanowire Schottky junctions

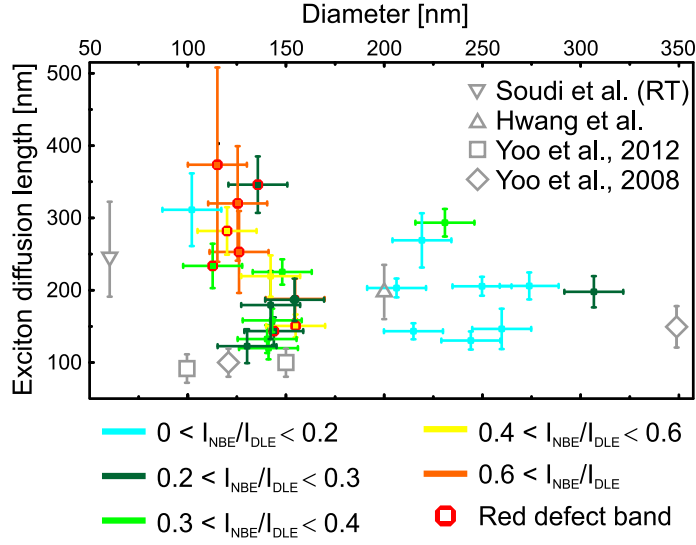


Figure 3.7: Diameter dependency of the exciton diffusion length of ZnO nanowires, colour-coded with respect to the intensity ratio I_{NBE}/I_{DLE} of the single nanowires. Nanowires with a pronounced red emission band are marked with a red octagon. While there is only little dependency of the measured diffusion length on the I_{NBE}/I_{DLE} ratio, most of the spread values accumulating for lower diameters are obtained from nanowires with a pronounced red emission band. For comparison, values obtained from other groups for ZnO [SDG10, HDP⁺11] and $Mg_{0.2}Zn_{0.8}O$ [YYD08, YLC⁺12] nanorods are included in the diagram.

gation of the metal layer influence on single nanowires can only be conducted on the same nanowire, priorly and subsequently to the metal evaporation. In addition, this finding puts the interpretation of the decreased DLE intensity for the covered nanowires in Figure 3.4 in another context.

A clear relationship between the I_{NBE}/I_{DLE} ratio and the exciton diffusion length could not be found, as can be seen in the colour-coded diagram displayed in Figure 3.7. However, the diagram reveals a dependence of the measured exciton diffusion length on the occurrence of the above mentioned red defect luminescence.

The red luminescence band at ≈ 1.9 eV has been prevalently observed in ZnO nanostructures [FCL⁺04, CSS05, TCL⁺06, PMM⁺08, RBBW09]. The emission is often attributed to oxygen interstitials [MLC⁺08]. An additional point defect seems not to be a possible explanation of the increased exciton diffusion length measured for some of the samples featuring the red emission band. Therefore, it is more likely that the measured deviations

3 Carrier diffusion lengths in semiconductor nanowires

are originating from somewhere else. The different emission characteristics of the single nanowires are pointing to a different defect configuration. Measuring in the panchromatic CL mode has been legitimated by the assumption that a direct excitation of the defect luminescence is not favoured and all observed luminescence is originally initialised by an excited electron-hole pair. However, it might be possible that some of the nanowires exhibit defect states that are sensitive to sub-bandgap excitation. In this case, the direct excitation of defects would generate a CL signal, which is added to the exciton related signal and might lead to misinterpretation in the panchromatic mode. Little is known about the ability of sub-bandgap excitation of the ZnO defect states. Thus, to exclude this possible error, monochromatic diffusion length measurements should be conducted. The suggested mechanism is not necessarily solely responsible for the large deviation of some of the measured diffusion length values, but the obviously wider spread values estimated for the nanowires with a pronounced red emission point to a systematic error that is related to the emission characteristics of the individual nanowires.

In addition to the results on the exciton diffusion length obtained in this work, some values from literature are displayed in Figure 3.7 in order to allow a comparison. As already mentioned, our values are in good accordance to the values obtained by Hwang et al. for a 200 nm diameter ZnO wire [HDP⁺11]. Values obtained by CL on Mg_{0.2}Zn_{0.8}O nanorods by Yoo et al. [YYD08, YLC⁺12] are a bit lower than the values obtained for pure ZnO nanowires in this work, caused by the different material compositions. Souidi et al. measured a value of 240 nm "minority carrier" diffusion length, which is a bit above the average value estimated in our study for the wires not affected by the red emission band [SDG10]. In addition, this value has been obtained by SPCM at room temperature. Yoo found a decreasing exciton diffusion length in the MgZnO nanorods with increasing temperature in the range between 5 and 80 K. Thus, the value obtained by Souidi seems a bit too high compared to those estimated within this thesis.

In consideration of the fact that the diffusion lengths of the nanowires are strongly related to the surface conditions of the single nanowires and even nanowires prepared on the same sample under identical conditions show different diffusion lengths, it is reasonable to classify the values obtained in this work as realistic and in accordance with literature. On the contrary, values of a few μm obtained via EBIC by Lin and Schwarz [LSF⁺11, SFC⁺11] seem to be rather unrealistic and might be based on misinterpreted side-effects during the EBIC measurement that could also be observed on our nanowire devices.

3.6 Conclusions

Within this chapter, the diffusion lengths of the respective minority carriers have been estimated for both the p-type and n-type part of an axial GaAs nanowire pn-junction. The minority carrier diffusion length of a material is a key parameter for the use especially in photovoltaic devices and significantly decreased in nanowires compared to bulk material due to enhanced surface recombination. Using EBIC, it was possible to measure the diffusion length directly at the pn-junction, which will be the most important element of a future nanowire solar cell.

From the diameter dependency of the diffusion lengths it is possible to determine the surface recombination velocity. On the n-type side of the junction, this parameter was found to be lower than expected for the dopant concentration adjusted during synthesis. This fits to the actual picture of VLS growth dynamics, where it takes some time until the growth catalyst is supersaturated with the dopant material after turning on the dopant source and a constant doping level is reached. Surface passivation gives a possibility to increase the minority carrier diffusion lengths again if needed for application. It was shown in this chapter, that with a simple passivation process using aqueous ammonium sulphide the carrier diffusion lengths can be significantly increased. The characterisation of charge carrier dynamics with EBIC is well-suited for the application in nanowire based (photovoltaic) devices, as it is possible to excite and analyse charge carriers with a very high spatial resolution inside the SEM. The results obtained in this chapter will guide the further improvement of GaAs in particular and semiconductor nanowire solar cells.

In the second part of this chapter, the exciton diffusion lengths of ZnO nanowire Schottky devices have been estimated by spatially resolved CL measurements. It was found that the emission properties of identically prepared VLS grown nanowires from the same growth process can differ extremely, independent of the nanowire diameter. The diffusion length measurement in panchromatic mode becomes unreliable for nanowires with an enhanced red defect emission, pointing to the occurrence of emission caused by sub-bandgap excitation. Thus, the monochromatic CL mode should be used if possible in order to get more reliable results.

The results of the diffusion length measurements on ZnO wires further point out the necessity of well-defined growth conditions in order to produce nanowires with reliable electro-optical properties. While the estimated diffusion lengths are more or less in accor-

3 Carrier diffusion lengths in semiconductor nanowires

dance with literature, an evaluation of the applicability of the nanowires in devices is hampered by the differences in diffusion and emission characteristic between single nanowires, even from the same growth run.

4 Ion implantation in ZnO nanowires

This chapter reports on ion implantation in ZnO nanowires. The experiments regarding hydrogen implantation in ZnO nanowires have been conducted in collaboration with Apurba Dev and Tobias Voss from the University of Bremen. Nanowire growth, implantation and electrical characterisation have been done in Jena, while the optical characterisation was conducted in Bremen. Some electrical measurements were done in close collaboration with Henry Holland-Moritz within the scope of his examination thesis [Hol11]. Parts of the results have been published in [DNR⁺10] and [RBG⁺10]. The results regarding persistent ion beam induced conduction in section 4.3 have been obtained in collaboration with Andreas Johannes within the scope of his diploma thesis [Joh11] and are partly published in [JNGR11].

4.1 Motivation

The electrical properties of a semiconductor are strongly influenced by the doping level (compare section 2.1). For the implementation of bottom-up grown semiconductor nanostructures into electrical devices it is necessary to have access to a doping mechanism that provides extremely exact and reproducible doping results. However, doping semiconductor nanowires during growth is rather challenging, especially in the case of compound semiconductors where the VLS growth model cannot be fully applied, as the more volatile component usually has almost no solubility within the applied catalyst [BNGR10]. An additional dopant atom species added during the growth process makes it even more complicated to predict the resulting nanowire stoichiometry and doping level.

The radial uniformity of the dopant distribution in VLS grown nanowires has been investigated by atom probe measurements [PHS⁺09] as well as stepwise surface etching combined with quantitative SPCM [APHL09] or Kelvin force microscopy [KBR10]. In all those studies an enhanced surface doping was detected, caused by enhanced dopant

4 Ion implantation in ZnO nanowires

aggregation at or diffusion towards the nanowire surface. The effect is even more pronounced for nanowires with a tapered structure caused by concurrent vapor-solid (VS) growth [BSM⁺06] at the nanowire sidewalls during the growth process [PHS⁺09, KRA⁺09]. All in all, the radial dopant profile of nanowires doped during growth is not smoother than profiles obtained by post-growth doping via diffusion as determined by capacitance-voltage measurements in [GTK⁺09].

In addition to radial dopant inhomogeneities, axial dopant concentration gradients often occur during VLS nanowire growth. The doping level depends on the concentration of dopant atoms inside the seed particle used for the growth. When the dopant supply is switched on, it usually takes a certain time to reach the desired dopant concentration inside the catalyst particle. Therefore, VLS-grown nanowires often show an axial inhomogeneous doping profile in the part of the nanowire grown directly after switching the dopant supply on or off [GRB⁺09]. For tapered nanowires with enhanced doping concentration in the conical shell, an axial doping gradient along the nanowire, caused by the ratio between a lower doped nanowire core and higher doped taper, is also visible [KRA⁺09]. Some possibilities exist to take advantage of nanowires with highly doped tapers [SPLF⁺09], but for many applications a homogeneous dopant profile along the nanowire is desirable. In a two-stage approach Koren et al. were able to reduce nonuniform doping in phosphorus-doped silicon nanowires by applying a high H₂ partial pressure during growth and annealing afterwards [KHG⁺11]. However, homogeneous doping profiles are hard to achieve in semiconductor nanowires during growth and reliable and controllable doping routines are of importance for future semiconductor nanowire device integration [PNR07].

A possible alternative to doping during growth is post-growth doping via ion implantation. This method provides a homogeneous dopant profile and the possibility to adjust the dopant concentration in an exact manner without being restrained by any solubility limits [RBGN10, BNGR10]. However, damage production inside the implanted crystal has to be taken into account and annealed subsequent to the implantation. Although post-growth annealing in order to achieve a homogeneous doping profile can act beneficially in some material systems [KHG⁺11], great care must be taken with regards to the out-diffusion of already implanted dopants [SWG⁺08] as well as catalyst diffusion into the nanowire [KHG⁺11].

So far, ion implantation in semiconductor nanowires has been introduced to different material systems in order to control the electrical, magnetic, and optical properties of the

nanostructures. An example of the successful doping of nanowires is the implantation of boron and phosphorus into silicon wires [CFR⁺08, HBR⁺09, KKND⁺09]. Here, not only uniform doping but even defined pn-junctions were realised via ion implantation. An example for tailoring the optical properties of semiconductor nanowires is the implantation of transition metal or rare earth elements into ZnO nanowires [GSM⁺08, MZLR09, RBG⁺10]. Following ion implantation and annealing, photoluminescence measurements revealed additional emission bands in the green spectral region. This could be attributed to intra-shell transitions of the implanted elements, and thus prove the successful incorporation of the dopants into the ZnO crystal. In the case of rare earth elements, ion implantation provides the only access to optically active dopants inside ZnO nanowires [GSM⁺08].

Although doping via ion implantation is a well known state-of-the-art technique in the semi-conductor industry, some new challenges arise for its application on nanostructures. For a spatially strongly confined structure, like a semiconductor nanowire of only a few nm in diameter, every single dopant atom might change the doping level significantly and thus cause a drastic change in the electrical properties. For example, a donor concentration of 10^{16} cm^{-3} equals the total amount of 2 dopant atoms in a nanowire with 25 nm diameter and 500 nm length. This precondition motivates the development of countable or even single ion implantation. Additionally, single dopant atoms and the controlled manipulation of their quantum states could give way to the development of fully new quantum bit devices [SdHK05]. In optoelectronic devices, single implanted optical emitters like rare earth elements in ZnO could work as single photon sources.

4.2 Hydrogen implantation in ZnO nanowires

Controllable p-type doping in ZnO is not easy to achieve and still subject to investigation. There are some studies about phosphorus-doped p-type ZnO [TOO⁺04, XWZ⁺07, CLB⁺08, LCZ⁺09]. However, in the case of nanowires, it is still not clear whether phosphorus doping really leads to stable p-type wires [DBL⁺11]. Other promising approaches are based on the use of nitrogen [YZJ⁺08a] or antimon [WCZ⁺11, LLC11] instead of phosphorus. While stable p-type doping remains an object of major interest for researchers, controlled n-type doping is also mandatory for device optimisation. It has been shown that the conductivity of ZnO can be enhanced by many orders of magnitude by introducing aluminium [ZLC⁺10], nickel [HLC⁺05], or gallium [YZJ⁺08b] as dopants. Within this chapter, hydrogen ion

4 Ion implantation in ZnO nanowires

implantation in ZnO nanowires is investigated. While the role of hydrogen in ZnO is still not fully understood, it is known that hydrogen can act as a shallow donor in ZnO [van00, CDC⁺01] and significantly enhance the bulk conductivity as well as the surface conductivity [ABC⁺10]. Compared to the heavier elements mentioned above, hydrogen ions cause only little and possibly even negligible damage inside the implanted material [DNR⁺10].

Hydrogen incorporation via plasma treatment, which primarily influences the properties of the near surface region in ZnO [IOH⁺03, PSG⁺03, PNI⁺05], has a tremendous impact of the electronic properties of ZnO nanostructures, where surface related effects govern a major fraction of the transport properties. While it is nearly impossible to derive the exact amount of hydrogen incorporated inside a nanowire during the exposure to hydrogen plasma, ion implantation allows for experiments at defined hydrogen concentrations. It is stated in the literature, that ZnO nanostructures can be used as hydrogen sensors, as the electric conductivity can be enhanced a few percent through simply exposing the structures to hydrogen gas [RKK⁺09]. However, the conductivity changes that occur after hydrogen plasma exposure or hydrogen implantation exceed this degree of change many times over.

4.2.1 Optical properties of hydrogen implanted nanowires

Hydrogen plasma treatment or annealing under hydrogen atmosphere has been demonstrated to enhance ZnO nanowire near bandgap emission (NBE) efficiency [HTN⁺04, LLZ⁺07]. An optimised emission efficiency constitutes a desirable case for any optical device. The effect even occurs in the case of a mild argon plasma containing only small amounts of hydrogen [DNR⁺10]. The emission spectra of pristine and plasma treated nanowires are compared in Figure 4.1. All measurements were conducted on nanowire ensembles left on the growth substrate. While the NBE is enhanced, deep level emission (DLE) from inner-bandgap defect states is significantly reduced. This DLE quenching is caused by passivation of the defect states [OIO⁺02] by the incorporated hydrogen atoms and remains stable over several weeks. Within the NBE region, displayed in detail in Figure 4.1 b, a new emission line at an energy of 3.363 eV appears. This line, commonly named I_4 , is attributed to the recombination of interstitial hydrogen bound excitons [BC08] and shows no long-term stability. Thus, the main contribution to the DLE quenching results from the deep level passivation, as the quenching is still visible after the volatile interstitial hydrogen donors are already diffused out of the crystal.

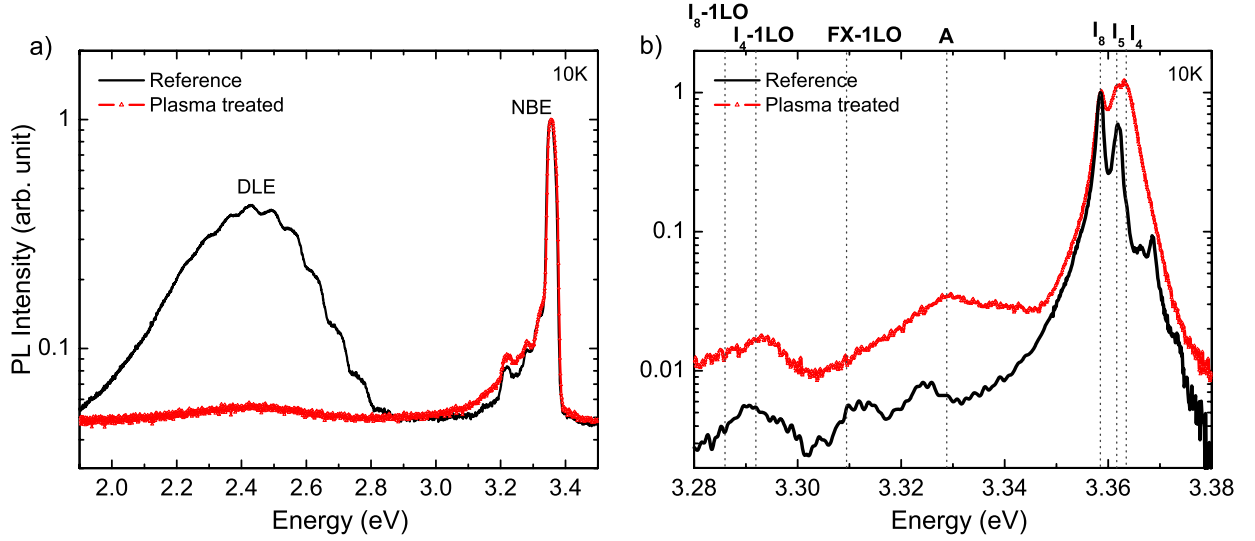


Figure 4.1: PL spectra of ZnO nanowires before and after mild argon plasma treatment. a) Survey spectrum. The quenching of the DLE after the plasma treatment is clearly visible. b) NBE spectrum. The I_4 emission line is attributed to excitons bound to interstitial hydrogen. This line is not stable in the long-term. Data taken from [DNR⁺10].

To investigate the effect of the incorporation of a discrete amount of hydrogen atoms, hydrogen-implanted nanowires were prepared by low energy ion implantation. H_2^+ implantation was carried out at room temperature with an ion energy of 600 eV. Calculations with the Monte Carlo package SRIM [ZBL85] estimate a projected range of the ions of about 7 nm. The damage caused by such an implantation is less than 0.02 defects/Å per ion. In ZnO most of the created point defects are annealed immediately at room temperature due to a high defect mobility [LAW⁺05], and one can thus assume that the nanowire remains practically undamaged during the implantation process. Two different fluences of $6.2 \cdot 10^{14}$ ions/cm² and $5 \cdot 10^{15}$ ions/cm² H_2^+ were used. The implanted H_2^+ -ion is believed to dissociate immediately when penetrating the ZnO nanowire and can be considered as two single 300 eV H^+ -ions. To prove this assumption, another sample was implanted with $1.1 \cdot 10^{15}$ ions/cm² 600 eV H^+ ions. However, due to the design of the accelerator, it was not possible to extract a reasonable amount of H_+ -ions at a lower ion energy within a reasonable timespan.

At low measuring temperatures, a strong quenching of the DLE is observed after the hydrogen implantation, in accordance with the plasma treated samples, as displayed in Figure 4.2 a). In comparison to the H^+ implanted sample, the H_2^+ implanted shows no

4 Ion implantation in ZnO nanowires

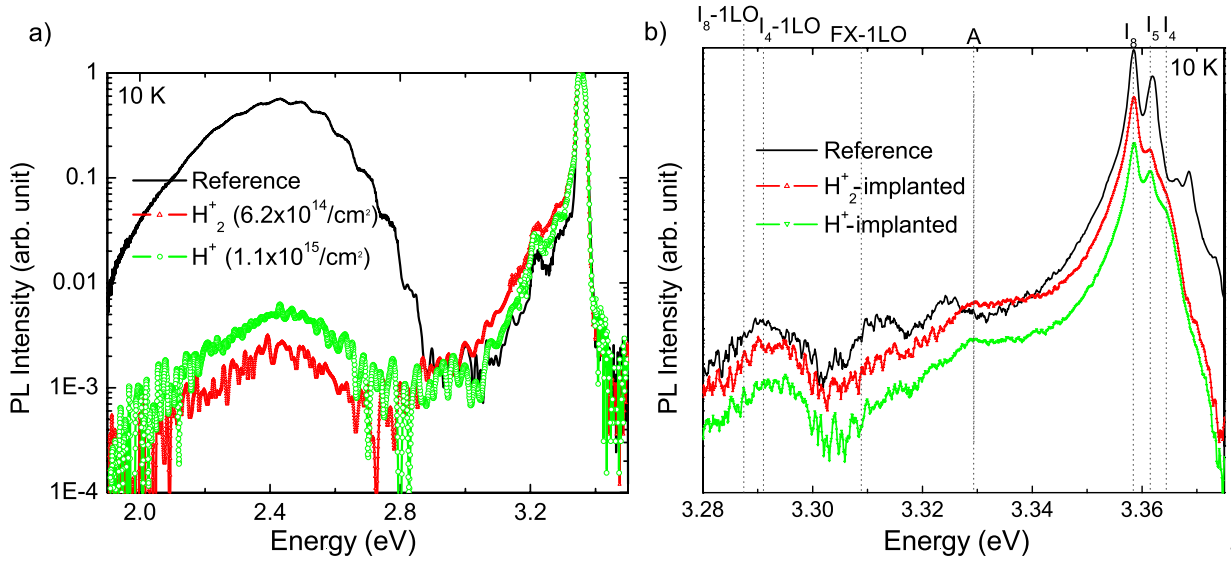


Figure 4.2: Comparison of PL spectra of plasma treated and hydrogen implanted ZnO nanowires. a) Survey spectrum. In both cases the quenching of the DLE is clearly visible. b) NBE spectrum. The I_4 emission line that is visible in the case of plasma treated nanowires does not show up in the spectrum of the implanted wires. Data taken from [DNR⁺10].

noteworthy difference. There is no sign of any implantation induced defect emission. The NBE region is shown in more detail in Figure 4.2 b). In contrast to the plasma treatment, the I_4 line attributed to the interstitial hydrogen does not appear for the implanted samples. For logistical reasons, the measurements could only be made three days after implantation. As such, it is possible that the majority of the interstitial hydrogen might have diffused out of the sample at room temperature.

In Figure 4.3 the PL spectra of samples implanted with different hydrogen fluences are compared. It is clearly visible that the quenching of the DLE becomes stronger with increasing H_2^+ fluence, indicating that hydrogen implantation is a powerful tool for targeted manipulation of the optical properties of ZnO nanostructures. Quantitative measurements with an integrated sphere [DNR⁺10] confirm the analogy between plasma treatment and ion implantation as well as the fluence dependency of the DLE quenching and the NBE enhancement.

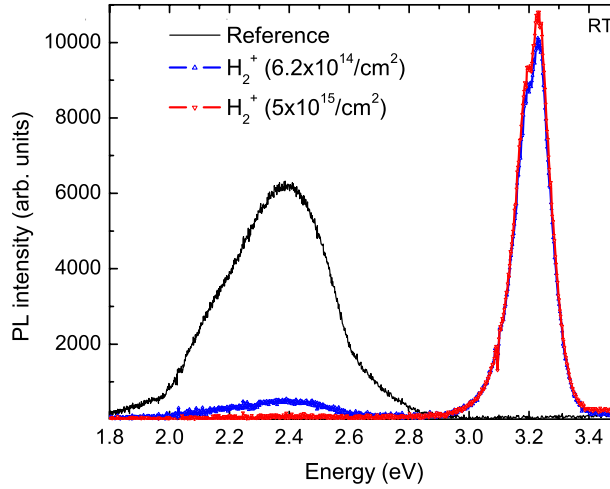


Figure 4.3: PL spectra of a pristine sample compared to nanowires implanted with two different fluences of H_2^+ . The DLE quenching gets more pronounced with increasing hydrogen fluence. Data taken from [DNR⁺10].

4.2.2 Electrical properties of hydrogen implanted nanowires

The impact of hydrogen implantation on the electrical properties of ZnO nanowires has been investigated on ZnO devices that were produced following the scheme in Figure 2.2. A thin gold layer or Ti/Au-bilayer was thermally evaporated as contact material. The devices usually consist of multiple nanowires bridging the two contact pads. As the number of wires per device differs from one to about 20 and the wires themselves are often asymmetrically contacted, the IV-characteristics of the devices can turn out quite differently. In Figure 4.4 two typical IV-characteristics are displayed. While the sample in 4.4 a) shows a rather linear characteristic, the sample in 4.4 b) turns out to be rectifying. However, both characteristics represent devices with multiple nanowires with Schottky barriers on each end, where the final IV-curve of the device is governed by the junctions with the lowest barriers in every direction. Besides the two types displayed in Figure 4.4, appearances of devices rectifying in the other direction as well as devices with a double-s-shaped characteristic are also common.

The contacted nanowires were measured inside the probe station prior to and after the implantation. Special attention had to be placed on the illumination constraints, as ZnO is known to be very sensitive to light exposure and exhibits persistent photoconductivity [LLZ⁺07,PHRJD⁺08,ZGH⁺09]. The samples used in this study also show a noteworthy

4 Ion implantation in ZnO nanowires

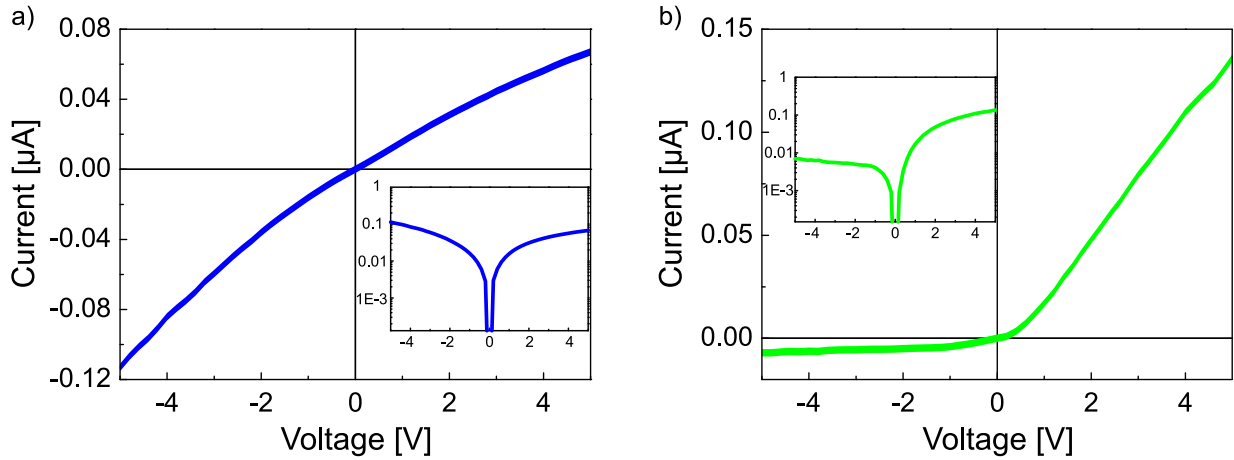


Figure 4.4: Typical characteristics of ZnO nanowire devices produced by photolithography. a) The device shows a rather linear characteristic. b) The device shows a more asymmetric, rectifying behaviour. Both devices consist of multiple nanowires bridging between the contacts. Insets show the same data on a logarithmic scale.

UV sensitivity, as visible in the comparison of IV-characteristics of the same sample under different illumination constraints, displayed in Figure 4.5. The measured current varies by two orders of magnitude depending on the illumination. Therefore, it is important to consistently measure with caution under the exact same conditions when comparing pre- and post-implantation IV-characteristics. Apparently, the shape of the characteristic does not change significantly. As with the issue of persistent photoconductivity, irradiation with energetic ions can induce a similar effect, namely, persistent ion beam induced conduction (PIC) [JNGR11]. As such, care with regards to this issue should also be taken when measuring implantation induced changes on the IV-characteristics. Under a vacuum atmosphere, PIC will last for several hours, whereas in ambient air, it will last for several minutes at most. A detailed view on the PIC effect in ZnO nanowires will be given in section 4.3.

Hydrogen implantation on contacted nanowires was carried out at different ion energies. Analogue to the optical measurements discussed above, implantation with 600 eV H_2^+ -ions and fluences of $1.5 \cdot 10^{14}$ ions/cm² and $1.15 \cdot 10^{15}$ ions/cm² were carried out. Those parameters are effectively tantamount to an implantation with 300 eV H_2^+ -ions at a doubled fluence. Furthermore, 10 keV H_2^+ -ions were used to increase the implantation depth. 10 keV H_2^+ instead of 5 keV H^+ -ions were chosen because of the higher yield of H_2^+ -ions at the accelerator system.

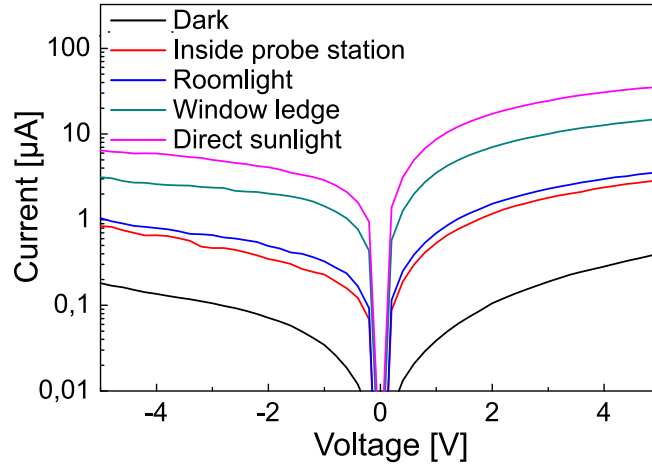


Figure 4.5: Comparison of the IV-characteristics of a ZnO nanowire device under different illumination constraints. The current is varied by two orders of magnitude due to light illumination at the measurement site.

The effect of the ion energy on the implantation depth is displayed in Figure 4.6. Iradina simulations (see chapter 2.2.2) show that, during the 5 keV hydrogen implantation, the nanowire is nearly completely riddled with hydrogen atoms (4.6 a)), whereas in the case of 300 eV, the ions are only implanted close to the surface (4.6 b)). Although the total amount of hydrogen incorporated is similar in both cases, the spatial distributions of the atoms differ greatly from one another. It is important to note that iradina Monte-Carlo simulations do not take into account any hydrogen diffusion ($T = 0$ K).

The IV-characteristics of the nanowire devices implanted with the low energetic ions are displayed in Figures 4.7 a) and b). The conductivity is enhanced by several orders of magnitude due to the irradiation. The enhancement factor seems to be fluence dependent in Figure 4.7 a); the implantation with the higher fluence reveals a further, moderate, increase in conductivity. However, the sample presented in Figure 4.7 b) shows different behaviour. In this case, the characteristic referring to the implantation with higher fluence was not recorded directly after implantation but the following day. Hence, parts of the hydrogen might have already diffused out of the sample when being incorporated on the volatile interstitial sites, similarly to the situation already observed during the optical measurements, presented above. This leads to the assumption that a part of the conductivity

4 Ion implantation in ZnO nanowires

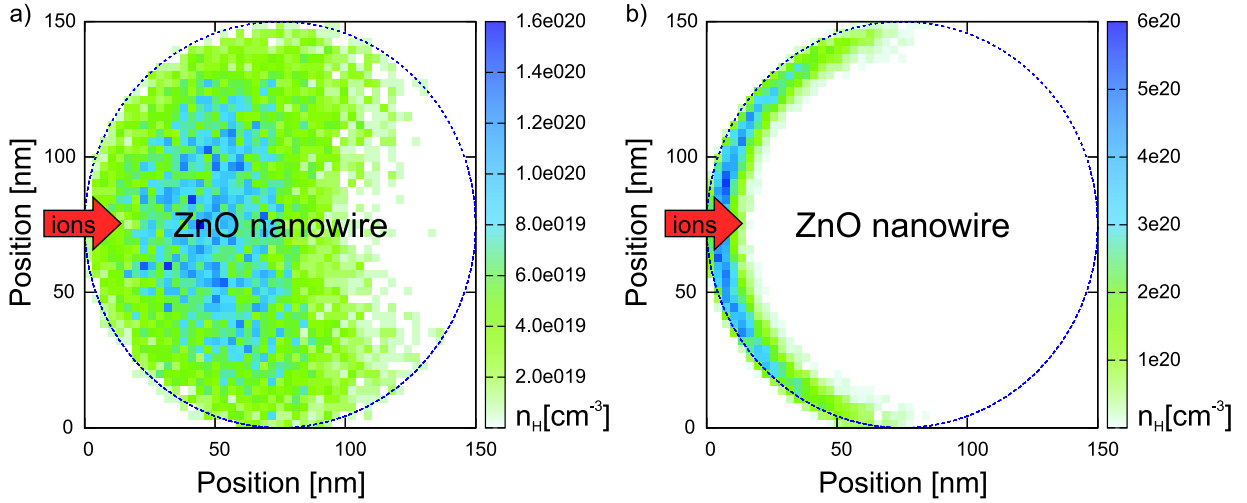


Figure 4.6: Comparison of implantation profiles of 5 keV H^+ -ions (a) and 300 eV H^+ -ions (b) in a ZnO nanowire with 150 nm diameter simulated with iradina [BR11]. The ions penetrate the nanowire from the left side, as indicated by the red arrow. The profiles are based on ions impinging evenly over the whole nanowire area. In both cases the simulated fluence was 10^{15} ions/cm².

increase is caused by implanted interstitial hydrogen donors. Additionally, a donor-related higher carrier concentration inside the wire leads to a thinner surface depletion layer as well as a positive effect on the Schottky type contact conductivity.

To investigate the long-term behaviour of the effect, both samples were measured three weeks after implantation took place. From Figure 4.7 a) and b) it is clear that the conductivity remains tremendously enhanced compared to the unimplanted state. Simultaneously, a noteworthy drop in conductivity in comparison to the state directly after the implantation is visible. This cutback in conductivity could be due to further outdiffusion of interstitial hydrogen and therefore less shallow donor states inside the nanowires. The permanently enhanced conductivity must therefore be related to the more stable substitutional hydrogen [BC08]. Hydrogen on an oxygen site can act as a shallow donor [JV06a] and therefore permanently increase the conductivity. Additionally, the positive influence of the substitutional hydrogen on the contact resistance can also lead to conductivity enhancement.

Generally, implantation induced changes of the properties of the Schottky contact to the nanowire have to be considered as a reason for the change in conductivity. On both devices a ≈ 100 nm thick gold layer was used to form the contact pads. The ZnO-Au Schottky diode is known to be very sensitive to the surroundings, as a major contribution to its electrical

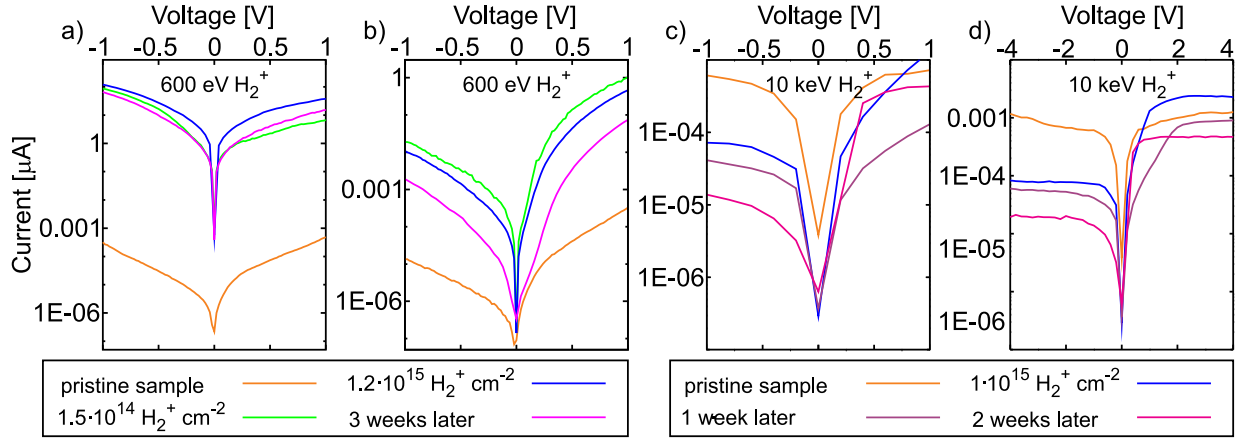


Figure 4.7: IV-characteristics of ZnO nanowire devices implanted with hydrogen. a) and b) show different samples implanted with low energy ions. The conductivity is massively increased after two subsequent implantations at the fluences mentioned in the legend. Three weeks after implantation the conductivity is significantly reduced but still orders of magnitude higher compared to the pristine sample. c) and d) present the IV-characteristic of a sample implanted with 10 keV H_2^+ ions. The previously symmetric characteristic becomes asymmetric after implantation. No significant conductivity increase is visible. From the plot over a wider voltage range in d) the shape of the characteristic appears altered following the implantation.

properties is governed by the behaviour of the near-surface states [MSW⁺05, LLZ⁺07]. Hydrogen induced passivation of near-surface defect states will reduce both the width of the surface depletion layer and the defect induced fermi level pinning at the surface [LLZ⁺07]. Both effects lead to a reduction of the Schottky barrier height and therefore to a higher conductivity of the contacted nanowire. In order to distinguish the influence of the contacts from the nanowire properties, four-point measurements would be needed. However, the penetration depth of the ions with 300 eV energy (7 nm in ZnO, compare Figure 2.2.2, in gold even less) is small compared to the contact pad thickness (100 nm) and it is very unlikely that any ion will permeate the contact pad and reach the nanowire-contact interface. Therefore, only ions that are impinging the nanowire near the contact junction will have an effect on the contact resistivity.

Implantation with 10 keV H_2^+ -ions was carried out on a nanowire device prepared with Ti-Au contacts. Besides this, the sample was prepared in the same way as the samples used for the lower ion energies. The IV-characteristics prior to and after the implantation are displayed in Figure 4.7 c) and over a wider voltage range in 4.7 d). It is obvious that

4 Ion implantation in ZnO nanowires

the desired effect, an enhancement of conductivity after hydrogen implantation, was not achieved with this sample. The same situation arose for several other samples prepared in the same way. For the exemplary sample presented here, the formerly nearly symmetric IV-characteristic had an altered, asymmetric shape after the implantation. Whereas the conduction was increased in one direction after the implantation, it was decreased in the other one. After one week, the conduction in both directions was worse than before the implantation. This further drop in conductivity can be explained by the outdiffusion of interstitial hydrogen. The initial drop must be due to implantation related defects. As irradiation and SRIM simulations do not predict notable amounts of defects due to the implanted hydrogen, impurities inside the accelerator might have caused some extra damage. Indeed, the accelerator LEILA was optimised for the implantation with ion energies below 1 keV. Thus, it is possible that the mass separation unit works less effectively for higher ion energies. Point defects in ZnO have often been assumed to be responsible for the intrinsic n-conductivity. Therefore, implantation induced defects should have a positive impact on the device conductivity. However, in [JV06b] Janotti and van de Walle conclude that point defects in ZnO cannot contribute to any conductivity, as most of the defects are not stable under ambient conditions, which also accounts for the Zinc interstitial shallow donor. Oxygen vacancies act as deep level donors that do not enhance the conductivity. As such, implantation defects induced by unwanted impurities in the ion beam are the most likely reason for the reduction in conductivity in the implanted devices. The change in symmetry of the IV-characteristic points to a more drastic degradation of the contacts, as an increase in nanowire resistivity would shift the IV-characteristic, but not alter the shape.

Within a totally different energy regime, tuning of the electrical characteristics of ZnO nanowire field effect transistors via high-energy proton irradiation has recently been presented by Hong et al. [HJS⁺10]. The authors showed that at low ion fluences of only $10^{10} - 10^{12}$ ions/cm² and a high proton energy of 10 MeV, a change in conductivity of irradiated ZnO nanowires can be obtained. However, they traced the conductivity change back to implantation induced charges in the substrate below the wires. The nanowires themselves remained unaffected by the protons, which is in accordance to measurements on bulk ZnO that show a remarkable resistance of the material to high energetic proton irradiation [AGH⁺01].

As described in section 2.1.2, the nanowire devices used in this section can also be driven as simple backgate FETs. In Figure 4.8 the transfer curve of the device from Figure

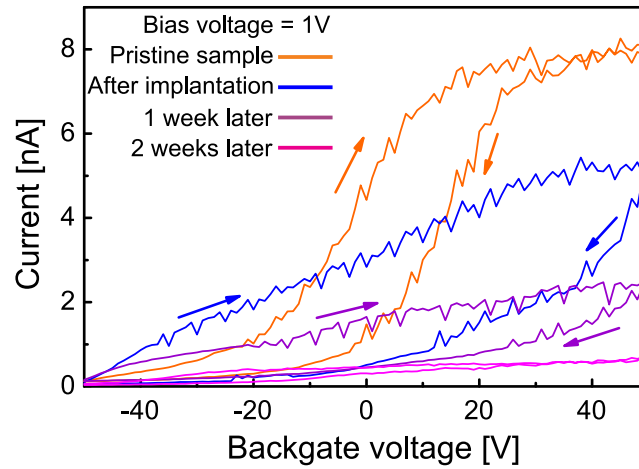


Figure 4.8: Transfer characteristics of a ZnO nanowire device implanted with $1 \cdot 10^{15}$ ions/cm² 10 keV hydrogen ions. After the implantation, the hysteresis of the transfer curve is significantly enhanced. The arrows indicate the direction of the measurement.

4.7 c) is shown. The device shows a typical n-type characteristic, which means that it is switched to the "on"-state (=conductive) with increasing gate voltage. It is visible that the unimplanted FET features a pronounced transfer hysteresis (orange line), which is further enhanced after the implantation process (blue line). Whereas the absolute current through the device decreases over a period of days after the implantation, the enhanced hysteresis stays visible.

Transfer hysteresis is a known effect for ZnO nanowire transistors and is attributed to the influence of adsorbed species on the nanowire surface [GSLY05, HJK⁺08, SHL⁺09]. Adsorbed species on the nanowire surface and the nanowire-gate interface are able to trap electrons when a positive gate voltage is applied. After switching off the gate voltage, the trapped carriers on the nanowire surface induce a depletion zone in the nanowire channel and therefore lower the conductivity. This phenomenon has recently gained major interest as it could be useful for the development of non-volatile memory [KKY⁺09, SCM⁺10]. The hysteresis behaviour is enhanced when the transistor is exposed to ambient air, and can be suppressed by layer coating passivation of the nanowire surface [HJK⁺08, SHL⁺09]. For the application in non-volatile storage devices a reliable hysteresis is desirable. Thus, several attempts have been made to control the hysteresis behaviour. Keem et al. used Al₂O₃ layers as gate dielectric to enhance the charge trapping ability of their devices, and therefore the hysteresis effect [KKY⁺09]. Sohn et al. functionalised the nanowire surface

4 Ion implantation in ZnO nanowires

with ferroelectric particles and realised a non-volatile multi-bit device [SCM⁺10]. Li et al. used redox-active molecules to functionalise and boost the charge-store capability of In₂O₃ nanowire transistors [LFS⁺04].

The transfer characteristics of the hydrogen implanted FET in Figure 4.8 show a significantly enhanced hysteresis subsequent to the hydrogen implantation. A comparable increase of the hysteresis loop was also observed for ZnO nanowire transistors annealed under a high-pressure hydrogen atmosphere [YHJ⁺11]. Yoon et al. attributed the appearance of the hysteresis to so-called mobile protons inside the substrate. Hydrogen atoms diffused into the gate oxide can accumulate either at the interface between oxide layer and nanowire or at the interface between oxide layer and gate electrode. By applying a gate voltage, the protons will move from one interface to the other with respect to the applied electric field. A positive gate voltage will drive the protons to the nanowire-oxide interface, where they can trap charge carriers and induce a depletion zone inside the nanowire, lowering the channel conductivity once the gate voltage is switched off. A negative gate voltage has the reverse effect. It is very likely that implantation with hydrogen ions leads to a similar effect. However, the hysteresis observed in Figure 4.8 must not necessarily result from mobile protons, as implantation induced defects can also induce a hysteresis in nanowire FETs, as observed for boron and phosphorus implanted silicon nanowires in [CFR⁺08]. Despite the uncertain origin of the hysteresis, the effect could be very interesting for the development of non-volatile memory devices, as ion implantation exhibits a simple access to modify the transfer hysteresis of ZnO nanowire transistors.

4.3 Persistent ion beam induced conductivity

As already mentioned in the previous section, the irradiation of ZnO nanowires with energetic ions can induce an additional increase in conductivity, similar to the already well-known PPC. This persistent ion beam induced conductivity (PIC) effect [JNGR11] is independent of the implanted ion species and will last for several minutes up to hours depending on the atmosphere applied to the sample. In this section the PIC effect will be further investigated and compared to the similar PPC effect.

The experiments have been conducted on nanowire devices assembled following the scheme in section 2.1.2. A 50 nm thick titanium layer as adhesive agent followed by a 50 nm thick gold layer were used to form the contacts. FIB preparation was used to cut all

4.3 Persistent ion beam induced conductivity

contact-connecting nanowires but one in order to receive single nanowire transistors. The devices typically exhibit a s-shaped IV-characteristic governed by the Schottky contacts formed by the ZnO nanowire and the Ti-Au contact pads. The samples were placed on a chip carrier, contacted via wedge bonding, and subsequently mounted on the high-vacuum flange equipped with electrical feed-throughs described in section 2.2.3 in order to allow electrical characterisation of the samples in-situ inside the implantation chamber. The implantations and the in-situ measurements were conducted using the implanter ROMEO in Jena.

In Figure 4.9 b), the current measured through a nanowire device at a constant bias of 1 V is displayed (the wiring scheme is displayed in Figure 4.9 a)). The sample was mounted inside the evacuated implantation chamber of the implanter at a pressure of 10^{-6} mbar. During the whole experiment the sample was kept in dark. While monitoring the current, two short 12s implantations each with $5 \cdot 10^{10}$ ions/cm² He⁺ were applied. Helium was chosen for two reasons. First, as a noble gas it will not be embedded in the ZnO crystal but diffuse out and not cause any doping. Additionally, the light helium ions cause only a small number of defects inside the crystal and therefore implantation related side effects on the conductivity are minimised. The current through the nanowire increased from $\approx 0.5 \mu\text{A}$ to $\approx 2.5 \mu\text{A}$ after the first implantation at 1000s. Directly after stopping the implantation, a steady but slowly decay of the current occurs, that does not reach the initial value of the relaxed device in accessible time. A second implantation step at 3000s leads to a comparable current increase from $\approx 2 \mu\text{A}$ to $\approx 4 \mu\text{A}$. Permanent ion irradiation of the device leads to a further increase of the current until reaching a saturation level, with the maximum current varying from device to device. The behaviour and also the dimension of the current increase are comparable to PPC effects reported in literature [BSS⁺11] as well as measured on our own devices (see Figure 4.10). The decay of the current is dramatically increased when the chamber is vented with ambient air, as happened at 6000s, demonstrating the influence of the chemical environment on the PIC effect.

Current decay curves of ion irradiated as well as comparable UV irradiated samples under constant bias and different atmospheres are displayed in Figure 4.10 in order to compare the chemical sensitivity of PIC and PPC decay times. It is obvious that in both cases the decay rate drastically increases when the device is exposed to ambient air and therefore to oxygen and water molecules. The analogue behaviour supposes that PIC and PPC rely on the same mechanisms. To exclude a pure dependence on the pressure, the experiment has also been conducted within a noble gas atmosphere for the UV irradiated sample,

4 Ion implantation in ZnO nanowires

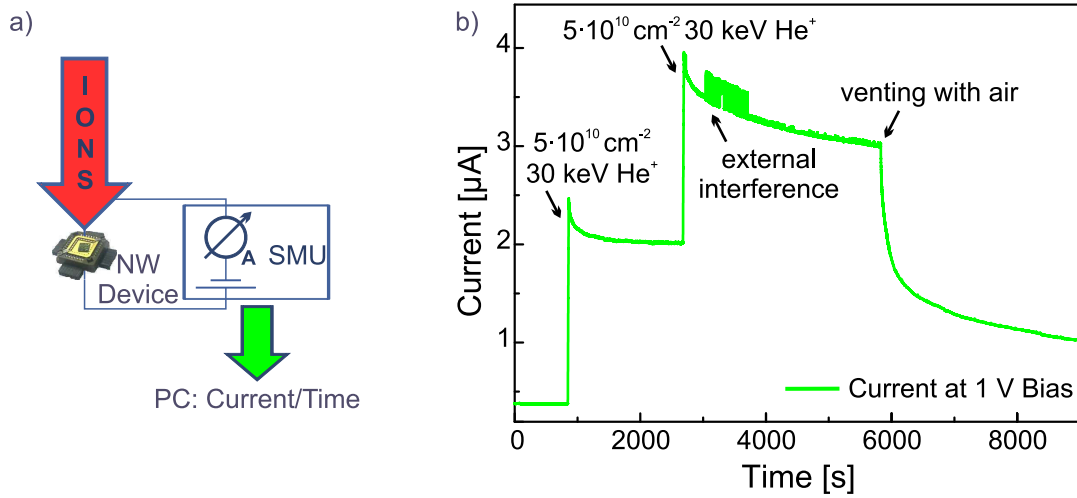


Figure 4.9: a) Wiring scheme for the in-situ current measurement. The current through the device is monitored during ion irradiation. Thus, ion induced changes in current transport can be detected. b) Current measured through a ZnO nanowire device during two short implantation steps with 30 keV He⁺-ions. A clearly visible current increase during each implantation step is followed by a steady but slow current decay. After venting with ambient air, the current decay rate is massively enhanced. Unintentional switching of the SMU measurement range resulted in a disturbance in the measured curve marked "external interference".

revealing that the current decay rate is pressure independent and indeed governed by the exposure to ambient air and therefore O₂ and H₂O molecules. This stands in accordance to literature regarding PPC [SHL⁺09], where the huge PPC effect in zinc oxide nanowires is commonly attributed to excited charge carriers that can populate quasi-stable, surface-oxygen bound states [PHRJD⁺08]. For the PIC effect, ions instead of photons are exciting electron-hole pairs inside the nanowire. Besides this, PPC and PIC seem to rely on the same mechanisms.

The nanowire surface exposed to the ion beam of a single nanowire transistor can be estimated to about 1 µm² for a nanowire channel of 200 nm width and 5 µm length. Therefore, the ion fluence of each implantation step applied to the device in Figure 4.9 equals about 500 ions per nanowire. As those 500 ions are causing a current increase of 2 µA, the average increase caused by a single ion should be detectable with the SMU that can measure down to pA resolution.

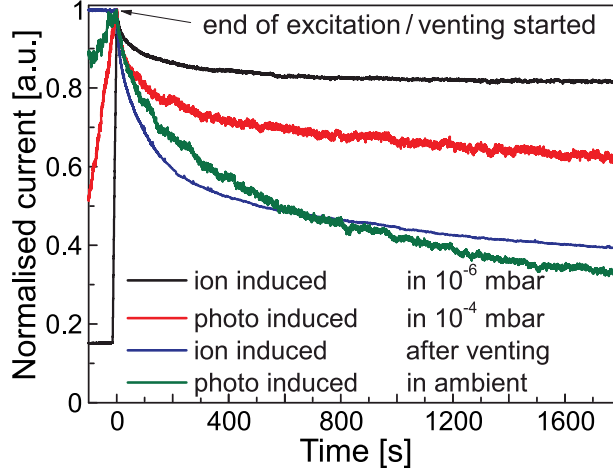


Figure 4.10: Comparison of the decay of PIC and PPC under different atmospheres. The maximum current of the devices before the decay sets in is normalised to one. It is obvious that the ion irradiated and the UV exposed samples show a similar behaviour. The slightly weaker decay of the ion induced conductivity in vacuum might be caused by the different vacuum pressure.

An upper limit of the total number of electron-hole pairs excited by the incoming ions can be estimated very roughly by dividing the ion energy through the bandgap of the irradiated material. In our experiment, this results in $30 \text{ keV} / 3.4 \text{ eV} \approx 9000$ electron-hole pairs or 18000 excited charge carriers per impinging ion. The true number of excited carriers will indeed be significantly smaller [Kle68]. Given an ion current of only 6 nA/cm^2 as in our experiment and a carrier lifetime of 100 ps [RGW⁺10], we obtain a maximum density of generated carriers of $\approx 3 \cdot 10^8 \text{ cm}^{-3}$. With 1 V bias applied to the $5 \mu\text{m}$ nanowire channel and a mobility of $20 \text{ cm}^2/\text{Vs}$ [BSS⁺11] the directly ion induced current should be less than 1 fA, more than six orders of magnitude below the observed average current change of 4 nA per impinging ion.

As mentioned above, the exaggerated current excitation efficiency of PIC in ZnO could in principle be sufficient to detect single ions impinging a ZnO nanowire. In Figure 4.11 the current through a ZnO single nanowire device during the implantation with 150 keV Tb^+ ions is displayed. The ion current was reduced to 5 pA/cm^2 , resulting in the theoretical value of one ion hitting the nanowire about every three seconds. The device was fully relaxed prior to implantation. During the 350 s of ion exposure, the current at 1 V bias rose from 0.5 nA to 6 nA. It is clearly visible, that the conductivity is increasing in distinct steps, most likely caused by the impact of single ions to the nanowires.

4 Ion implantation in ZnO nanowires

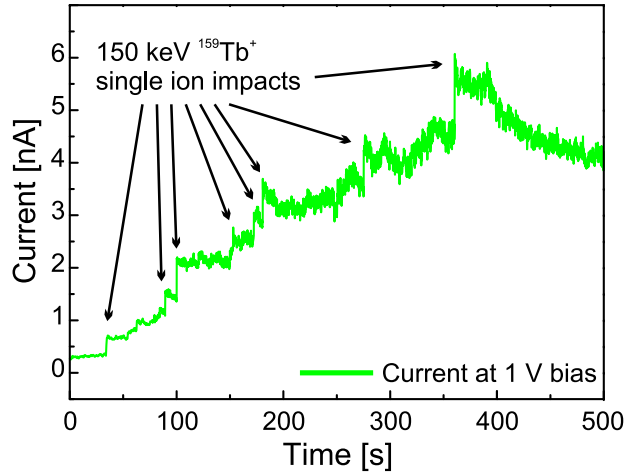


Figure 4.11: Current measured through a ZnO nanowire device during an implantation with 150 keV Tb^+ -ions at an ion current of $5 pA/cm^2$. A current increase in distinct steps, most likely related to single ion impacts can be observed.

However, the number of eight visible events during 350 s of implantation is much less than the expected ~ 100 impacts. Therefore, not every ion hitting the nanowire causes a significant increase in conductivity. Ions only glancing the nanowire might not deposit sufficient energy to induce a detectable current increase. Additionally, there could be differences in PIC excitation efficiency depending on the impact position. As the electrical characteristics of the nanowire devices are governed by the Schottky barriers between the nanowire and the Ti-Ai contact pads, an ion impinging on the region near the metal contact most likely induces a larger change in conductivity than an ion hitting the center of the nanowire channel, where it has nearly no effect on the contact properties. This behaviour is in accordance with the giant response of nanowires with ZnO-Pt Schottky contacts to UV light reported in literature [ZGH⁺09]. In that study, the PPC of ZnO nanowire devices with platinum contacts have been compared to devices with "ohmic" Ti-Au contacts. The platinum based contact structures, that feature a larger Schottky barrier, exhibit a much more pronounced PPC. The gigantic difference in photoresponse between the samples with different Schottky barrier heights confirm that at least a large fraction of the PPC is caused by excitation of the near-contact region of the devices. As so far most of the models for PPC in ZnO nanowire transistors do not take the changes to the contact behaviour in account [PHRJD⁺08], they might have to be expanded in this direction. This does not mean that those models are essentially wrong. Instead, one has to consider the impact of

the increased nanowire conductivity to the contact behaviour when investigating a device whose electrical characteristics are governed by the contact resistivity.

Finally, the strongly localised PIC response to an energetic ion beam within the Schottky contact area of a single nanowire transistor is also an interesting issue for the development of a spatially confined ion detector, which will be discussed in the following section.

4.4 Countable ion implantation in ZnO nanowires

The necessity of a precise doping method for the production of advanced semiconductor nanoscaled devices and the potential for the use of single dopant atoms in quantum computing and optoelectronics motivate the development of single ion implantation (SII) methods. Studies on nanoscaled FETs have shown a significant influence on the individual number of dopant atoms to the electrical properties of the devices [ONF⁺07,LRW⁺08,PWJ⁺09]. Generally, the selective implantation of a single atom into a nanosized target can only be achieved by either extremely confining the ion beam or the possibility of detecting single ions from a broader beam [Sch10a]. The former can be achieved by the use of an advanced focused ion beam system [SKH⁺02,SOKO05]. The number of implanted ions is counted by detection of ion impact induced secondary electrons. However, this approach is limited to the ion species that are available for focussed ion beam systems, which have to be driven with liquid metal sources. A wider variety of elements would be accessible due to the use of an ultra-cold laser trap ion source [SLF⁺09], which is, however, quite a complex unit.

The second approach, which is using a broader distributed ion beam for implantation and detecting and counting the implanted ions in a specified area, has the advantage of making less complex demands on the ion beam used for implantation. On the contrary, the detection of single ion impacts is still necessary in order to achieve assured single atom doping. To guarantee that only a specific area of a nanostructure is hit by the ion, implantation can be conducted through a nanosized mask, which is often stationary applied on the sample via lithographic processes [BWR⁺07,JYH⁺05,MJY⁺11]. A promising approach for the integration of a movable mask with accurate positioning on the sample area of interest is the implantation through a nanosized hole in a scanning probe cantilever [PPL⁺05,PLS⁺05,NKB⁺09]. Besides ion implantation methods, the integration of single dopants into semiconductor nanowires has also been demonstrated by using a scanning tunneling microscope (STM) as an atomically accurate fabrication tool [KF11].

4 Ion implantation in ZnO nanowires

However, that approach is not suitable for application in bottom-up grown semiconductor nanowires.

As conventional ion sources are not capable of emitting a predefined amount of ions at a distinct point in time, the detection of single ions is mandatory for any approach of SII. The monitoring of secondary electrons created by the impinging ion becomes less accurate for the detection of single charged ions in the range of only a few keV in nanostructures, owing to the dependency of the secondary electron yield on the surface morphology, on the ion energy, and on the charge state of the ion [Sch10a]. An alternative could be Geiger mode detectors, that have been shown to be capable of detecting single 125 keV helium ions within a distance of 75 μm on the same substrate [BSC10]. For the implantation in already contacted semiconductor nanowire devices, impinging ions can be detected also in-situ by either monitoring implantation induced current changes in transport channels [SKN⁺08, BWR⁺07, WSB⁺09, JTA⁺10] or by detecting the electron-hole pairs created by the ion impact [JYH⁺05, MJY⁺11].

The stepwise increasing current of the ZnO nanowire device in Figure 4.11, attributed to the impacts of single ions, is also an example for the detection of single ions via current changes. Contrary to the often investigated implantation induced current increase or decrease in silicon devices [SKN⁺08, BWR⁺07, WSB⁺09], where the current change is usually attributed to the creation of defects or the electrically active incorporated dopant atom, our experiment makes use of the PIC effect explained in the previous section. From this aspect, the spatial containment of the PIC effect to the depletion zone, that was suggested in the discussion of section 4.3, is quite interesting. A strongly localised sensitive area near the Schottky region allows a refined and accurate conclusion about the lateral position of the detected ion impact.

The device measured in Figure 4.11 was a single nanowire device, consisting of a ZnO nanowire contacted with Schottky-contacts on both sides. When a bias voltage is applied, one of the Schottky contacts is under forward bias, and the other is under reverse bias. The current will be governed by the contact under reverse bias condition, as the resistivity of a Schottky diode is higher in reverse direction. Ion beam induced conductivity changes on the contact biased in forward direction will therefore have only minor impact on the overall conductivity of the device. Thus, the device represents a detector for single ions that is spatially confined to the area near to the reverse-biased Schottky contact. An estimation of the extent of the sensitive region is not possible from our setup. However, one can

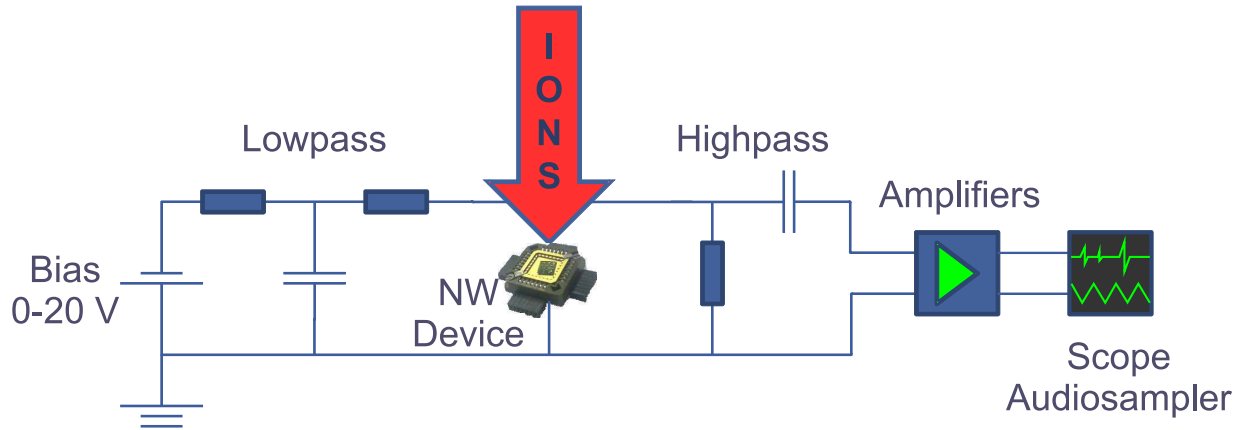


Figure 4.12: Wiring scheme for the in-situ detection of implanted ions. The device is biased by an external voltage source with a low-pass filter in between for levelling voltage source induced high-frequency noise. Through a high-pass filter the device is connected to an amplifier system. The amplified signal can be displayed with an oscilloscope or recorded by a multi-channel analyser or a rededicated audio sampler.

evaluate that only carriers excited within a distance from the contact that is smaller than the carrier diffusion length are able to have an impact on the contact resistance. Therefore, the sensitive region should be restricted to the first few hundred nanometers of the nanowire with respect to the contact pad.

Alternative to the recording of implantation induced conductivity changes, the detection of carriers generated by the ion impact can be used as a measure for the detection of single ion impacts [MSL⁺02, JYH⁺05, MJY⁺11], adapting the working principle of a semiconductor detector. An advantage of this procedure is, that, if the number of charge carriers generated can be detected, one can distinguish between ions that are incorporated inside the nanowire and ions that are just strafing the nanowire and create only a smaller amount of free carriers. In Ref. [JYH⁺05] the implantation took place into a reverse biased semiconductor detector PIN-diode that was covered by a PMMA mask with an opening on the position where the implantation should take place. The opening was placed over the depleted channel of the diode. Charge carriers created inside the channel by an impinging ion were instantaneously extracted to the diode contacts and therefore a current pulse could be detected. This detection mechanism should theoretically also work with our ZnO nanowire Schottky devices as well as with the GaAs nanowire pn-devices from chapter 3.

4 Ion implantation in ZnO nanowires

In both cases, the depletion layer of the reverse-biased junction could act as the active detection region.

The measurement setup is displayed in Figure 4.12. A nanowire device is biased by an external voltage source, and a low pass filter avoids high frequency noise generated by the source. A high pass filter eliminates most lower frequency signals and conducts only ion induced signal peaks through to the amplifiers. The amplified signal can be viewed on an oscilloscope or sampled on a PC. A Canberra 2006E pre-amplifier and Canberra 2022 amplifier [can91] were used for the signal amplification. Signals were recorded with the audio sampler of a standard office PC at 88.2kHz sampling rate. Apart from the nanowire device on the high-vacuum flange, all parts of the setup were placed outside the implantation chamber.

A ZnO nanowire device was mounted to the setup and irradiated with 30 keV He⁺ ions and an ion current of 30 pA/cm⁻². This corresponds to approximately two ions impinging on the nanowire per second. The stored scope signal is displayed in Figure 4.13 a), an extract from the signal recorded in parallel at the audio sampler is shown in Figure 4.13 b). On the upper channel of the scope display the signal from the amplifier was stored. A certain noise level with emerging distinct peaks is visible. The signal of the beam sweep unit, which scans the ion beam over the sample in order to get a homogeneously irradiated area, is applied to the second channel of the scope. It clearly shows that the signal peaks from the amplifier are related to the beam sweep signal, positioned roughly at the middle of the beam sweep range, which proves that the peaks only appear when the ion beam is scanned over the ZnO nanowire sample placed in the middle of the irradiated area. The data from the audio sampler proves that the peaks are randomly dispersed and not every scan over the sample results in a signal peak, excluding ion beam induced charging of the sample holder as an origin of the signal.

To confirm the successful detection of single ions and exclude further ion irradiation related side effects, the experiment was also conducted on samples without nanowires between the contact pads and on samples with short circuited contact pads. In both cases, no signal was detected. This excludes implantation induced changes in the contact pads or the gate oxide as well as secondary electrons from being responsible for the detected signal. If the ion beam was blanked off the sample, no signal peaks were recorded likewise.

For a fluence of $1 \cdot 10^{11}$ ions/cm², about 1000 ions are expected to impinge on the nanowire. However, comparable to the ion impacts monitored by current changes in section 4.3, only

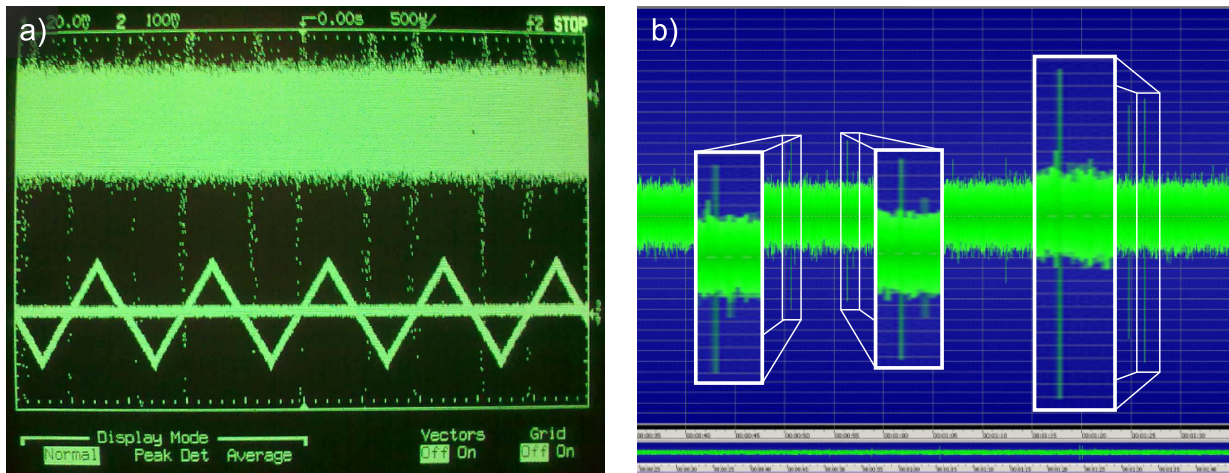


Figure 4.13: Images showing the detector signal in a) recorded with an oscilloscope and in b) with a PC audio sampler. On the scope the detector signal was applied to the upper channel, while the beam sweep signal was displayed on the lower channel, both channels recorded in storage mode. A clear correlation between the beam sweep and the detector events is visible, indicating that events are only recorded when the beam sweeps across the sample position. Peaks do not occur every time the beam sweeps across the sample, as it can be seen in the audio sampler measurement. Countable peaks that are easy to distinguish from noise level are recorded at random intervals during implantation. The insets show enlarged views of the peaks inside the thin white boxes.

47 signal peaks and therefore much less than expected could be detected. Again, this points to the fact that not the whole nanowire but only the region near the Schottky junction acts as an active area. The amount of excited carriers for an ion impact in the middle of the nanowire channel and an impact in the active area are equal; however, only in the latter case carriers will be injected into the depletion zone and a current signal pulse, that is intensified by the attached amplifier, will be detected. Interestingly, a comparable signal to that displayed in Figure 4.13 could also be detected when no bias voltage was applied. In this case, electron-hole pairs excited inside the space charge region of the Schottky contact are separated by the internal electrical field and detected as a current pulse.

The SII experiments have also been conducted with 200-300 nm diameter GaAs nanowire devices with axial pn-junctions. However, it was not possible to obtain any useful results with these devices. Most likely, this miss is caused by insufficient sensitivity of our home-built setup. Although the low and high pass filter significantly reduce the noise level, the

4 Ion implantation in ZnO nanowires

setup is still far from ideal conditions. At higher amplifier gain factors, switching the room light or even just think shutting the door of the accelerator hall generates signal peaks.

The required sensitivity of the setup is defined by the amount of electron-hole pairs that are expected during a single ion impact. In order to estimate this number, one has to account for the so called "nuclear defect" or pulse-height defect (PHD) [LSS63, HW66]. From studies on semiconductor detectors it is known, that for energetic ions with energies below 1 MeV energy losses due to nuclear collision in the target (compare section 2.2) become significant [Hsi76]. According to SRIM simulations only 84% of the energy of a 30 keV He⁺ ion are lost by electronic stopping in GaAs, whereas 15% are transferred to phonons and about 1% is used for the creation of defects in the target. The distribution is in accordance to experimentally obtained results for the energy loss in silicon [Hsi76]. Thus, about 25 keV of energy can contribute to the generation of electron-hole pairs in the case of a 30 keV He⁺ ion. The ionisation energy that is needed to generate an electron-hole pair is roughly about three times the bandgap energy [Kle68], which results in the amount of approximately 6000 electron-hole pairs per ion inside the irradiated GaAs nanowire device.

It should be noted that not every ion will create the same amount of charge carriers, as due to the nanowire geometry the ions are able to leave the nanowire before being stopped. However, as 30 keV He⁺ ions have an average longitudinal range of 175 nm in GaAs, a significant fraction of the implanted ions is believed to be incorporated within the implanted nanowire and therefore fulfilling the estimation of the amount of generated electron-hole pairs.

In the article on SII with a PIN-diode by Jamieson et al. [JYH⁺05], the successful detection of ≈ 1000 created electron-hole pairs per ion impact is reported. Even though this result could only be achieved with a great effort in noise reduction, it indicates that the amount of carriers generated inside our nanowire device should be sufficient for the detection of single ions. For the implantation of heavier ions, one additionally has to take a larger PHD in account. In the case of ⁶⁴Zn⁺ ions, which can be used for p-type doping of GaAs nanowires [SWG⁺08], according to SRIM only 23% of the ion energy are lost to electronic stopping for 30 keV ions. However, the increased PHD effect is partially compensated, as for heavier ions usually higher energies are necessary for implantation in order to reach an appropriate implantation depth. Thus, the detection of single ions with the GaAs nanowire devices should be possible with a better shielded, low-noise measurement setup.

Finally, the detection of single ions in the space charge region of a nanowire Schottky junction has been shown and proposed to work also on a pn-junction. However, this is not a limiting fact. Equivalent to the analogue response of different types of particle detectors and Schottky or pn-diodes to single ion impacts [YJH⁺02], any intrinsic semiconducting nanowire should be able to work as a nanosized particle detector if a large external field is applied to separate the ion induced charge carriers.

4.5 Conclusion

Ion implantation is a very useful tool in order to tailor the properties of semiconductor nanowires. Within this chapter, the modification of the electrical and optical properties of ZnO nanowires by hydrogen implantation was shown. After the implantation, the nanowires exhibit an increased near bandgap emission while the deep level emission was successfully suppressed. This effect on the optical properties of the nanowires turned out to be stable over weeks. Low energy implantation carried out on already contacted devices revealed a significantly enhanced conductivity. After some time, the conductivity drastically drops but still remains improved compared to the pristine sample. This behaviour can be traced back to the implanted hydrogen, that was incorporated either interstitial or substitutional. As the former is responsible for a short-lived conductivity enhancement and diffuses out of the nanowire within days, the latter is more stable and responsible for the remaining increased conductivity. Implantation with higher ion energies did decrease the long-term conductivity of the implanted wires, which can most likely be traced back to unintended implantation induced defects. The nanowires exhibited a hysteresis in the transfer characteristics, that could be useful for non-volatile memory applications. The hysteresis could be widened by hydrogen implantation. This effect is caused either by incorporated hydrogen in the substrate or implantation induced defects.

In ZnO nanowires, ion irradiation can induce PIC, an increase of conductivity persistent over a time-scale of hours. The effect was found to be similar to the well known PPC effect, caused by excited charge carriers that can populate quasi-stable, surface-oxygen bound states. The current increase of a few nA per incoming ion in an irradiated, biased nanowire allows for the in-situ detection of single ion impacts. Finally, single ion detection by measuring the carriers generated by an impinging ion in a biased nanowire device

4 Ion implantation in ZnO nanowires

was shown, using the nanowire like a semiconductor detector. The usage of nanowires as detectors gives rise to the detection of single ion impacts on a spatially confined area.

5 Biofunctionalisation of ZnO nanowires

In this chapter the biofunctionalisation of ZnO nanowires for the attachment of DNA target molecules is described. The functionalisation experiments have been conducted in collaboration with Bettina Rudolph, Barbara Seise, and Wolfgang Fritzsche from the Institute of Photonic Technologies (IPHT) in Jena. XPS measurements have been carried out in collaboration with Marc Brötzmann from the University of Göttingen. The fluorescence microscopy studies have been obtained in close collaboration with Ulrich Christian Schröder within the scope of his diploma thesis [Sch10b]. Irma Slowik and Jana Sommerfeld also assisted with the experiments. Parts of the results have been published in [NSS⁺11].

5.1 Nanowire biosensors

Semiconductor nanowires are well suited for application in electrical sensing devices, owing to their superb surface-to-volume ratio and the quasi one-dimensional current transport. As the sensing mechanism is based on the interaction of the nanowire surface with the environment, specific functionalisation of the surface with biological capture molecules will make the nanowire surface and therefore the sensing device sensible to the specific respective biological target molecule. In this way, a label-free biosensor based on semiconductor nanowires can be build, where the nanowire has the character of an active channel in a field effect transistor whose conductivity is governed by the field effect induced by the assembly of charged target molecules on the semiconductor surface. Examples for such biosensors, which are usually based on Si nanowires, can be found in references [CWPL01,PTZL07,CSPD⁺08]. As a further advantage, the reported high sensitivity, coming close to single molecule detection, can be combined with the possibility of arranging the nanowires in a very dense assembly owing to their nanosized dimension.

Up to know, biosensors based on other semiconducting materials than Si have played a minor role in science. Si-based nanowire biosensors are CMOS compatible and therefore

5 Biofunctionalisation of ZnO nanowires

quite easy to integrate into existing semiconductor device fabrication lines. Furthermore, Si is biocompatible and techniques for the functionalisation of Si are well understood. Although ZnO nanowires are not innately CMOS compatible, there are some arguments that motivate the use of ZnO nanowires for biosensing devices. First, ZnO is very stable under ambient conditions and especially its surface is stable under oxygen-rich conditions, which is an advantage over Si. The stability under physiological conditions, which is important for biosensing applications, depends strongly on the crystal quality of the nanostructures. However, it can be assumed as sufficient for structures grown by thermal evaporation methods [ZXW06, CXL⁺08, ISN⁺11] which usually offer an advanced crystal quality compared to wet chemical grown ZnO nanowires. Second, ZnO is non-toxic and biocompatible [Wan09]. Third, ZnO nanostructures can be produced fast, cheap, and in a wide manner of different shapes and forms [HWF⁺01, Wan09]. The DNA capture molecule immobilisation with organosilanes as linker molecules has been successfully shown by Corso and co-workers on planar ZnO surfaces [CDH08], where the biomolecule layer was used to act as an acoustic wave sensor. With the use of ZnO nanowires instead of planar films, the metal oxide itself can be used to build an electrically working biosensor. Biosensors based on ZnO nanostructures have been reported in a few studies, using both electrostatic adsorption [FAA⁺10, AAI⁺10, LCY⁺11] as well as organosilane modification with subsequent covalent bonding for immobilisation [CKJL10]. In the latter case, the biofunctionalisation of ZnO nanowires with biotin for streptavidin detection has been shown using organosilanes with aldehyde-functionality that bind the amino-group of biotin. The nanowire based protein sensors could detect streptavidin bonding down to the very low concentration of 2.5 nmol, underlining the capability of ZnO nanowires for the electrical detection of biomolecules.

In reference [CKJL10], the attachment of the positively charged streptavidin molecules led to an increased probe current through the nanowire. For the attachment of negatively charged DNA target molecules on the nanowire surface, a contrary effect is expected: the current through the intrinsically n-type ZnO nanowire should decrease as the charged target molecules induce a carrier depletion zone inside the nanowire. In another approach ZnO nanostructures have been functionalised with target molecules to use the fluorescence-enhancement capability of the ZnO for fluorescence detection of biomolecules [KDH06, DKH06]. In this type of application, nanowires also showed enhanced sensing abilities compared to conventional structures. However, the authors did not pursue the way to electrical label-free biosensing any further and limited themselves to fluorescence detection.

Within this study, the biofunctionalisation of ZnO nanowires with DNA capture molecules was investigated in order to achieve a label-free working ZnO nanowire biosensor. However, to ensure the successful functionalisation, molecules labelled with fluorescence have been used to control the attachment of DNA to the nanowires in the first place. A sensor consisting of electrically contacted, functionalised nanowires will not require the usage of labelled DNA anymore.

5.2 Nanowire preparation and functionalisation

Prior to biofunctionalisation, an oxygen plasma was applied to the as-grown nanowires for 30 min at 5 Pa oxygen pressure with a plasma energy of 50 W. This step is necessary to remove adsorbed molecules from the nanowire surface to maintain it clean and reactive. The samples were stored in a cabinet dryer afterwards at 100 °C for at least 5 min to remove water residues from the surface, as this treatment is known to enhance the dissociative adsorption of water on the ZnO surface [RKK⁺09]. Subsequent to the cleaning process silanisation took place in 10 mM GOPS (produced by Sigma-Aldrich) in a water-free toluene solution. The silanisation mechanism is displayed in Figure 5.1. The samples were incubated while stirring constantly for at least 6 h at 70 °C. The samples were rinsed 3 times subsequently with pure toluene for 5 min in each case and then dried with compressed air.

The 5'-amino-modified oligonucleotides (synthesised by Eurofins MWG Opera) were dissolved in 5x PBS buffer (pH 7.4) with a concentration of 10 µmol for the biofunctionalisation. The single stranded DNA sequence of the applied oligonucleotides consists of 27 bases and is shown in Table 5.1. The fluorescence markers, which are linked to the 3'-end and enable the detection of the molecules with fluorescence microscopy, are also listed in Table 5.1. The DNA solution was pipetted onto the nanowire samples and incubated over night under wet conditions to immobilise the nucleotides on the GOPS surface via the 5'-amino linker (see Figure 5.1 b). Afterwards the samples were rinsed for 10 minutes in 15 mmol tris-HCl-buffer (pH 8) in order to get rid of unbound DNA and then dried with compressed air.

Control samples were prepared both leaving out the GOPS silanisation step and with DNA that does not have an amino linker attached to investigate if the DNA binding follows the scheme with the covalent binding step in Figure 5.1. For further characterisation the

5 Biofunctionalisation of ZnO nanowires

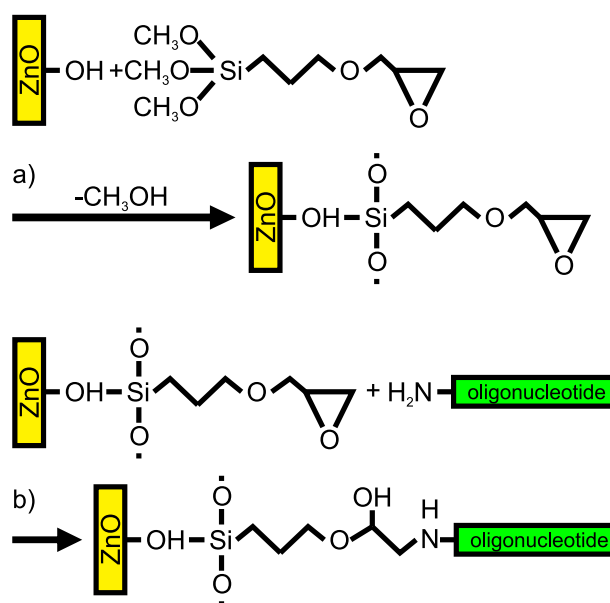


Figure 5.1: In a toluene environment (a) the bifunctional GOPS molecule is attached to the ZnO nanowire surface. In a second step (b), the oligonucleotide is linked to the epoxy group of the GOPS. [CDH08]

Table 5.1: DNA sequence and fluorescence markers of the oligonucleotides used for the ZnO nanowire biofunctionalisation

5'-modification	sequence from 5'-3'	3'-modification
C6-aminolink	TCT TAG TTC CTC GTG TAC GAC TTT TTT	FITC
C6-aminolink	TCT TAG TTC CTC GTG TAC GAC TTT TTT	Cy3

biofunctionalised nanowires were mechanically transferred to silicon or glass substrates by a gentle pressure imprint of the treated growth substrate.

5.3 Characterisation of functionalised nanowires

Fluorescence microscopy was used to check the immobilisation of DNA capture molecules on the ZnO surface. Samples with two different types of fluorescence markers were prepared for characterisation (compare Table 5.1). Specimens marked with Cy3 turned out to be

5.3 Characterisation of functionalised nanowires

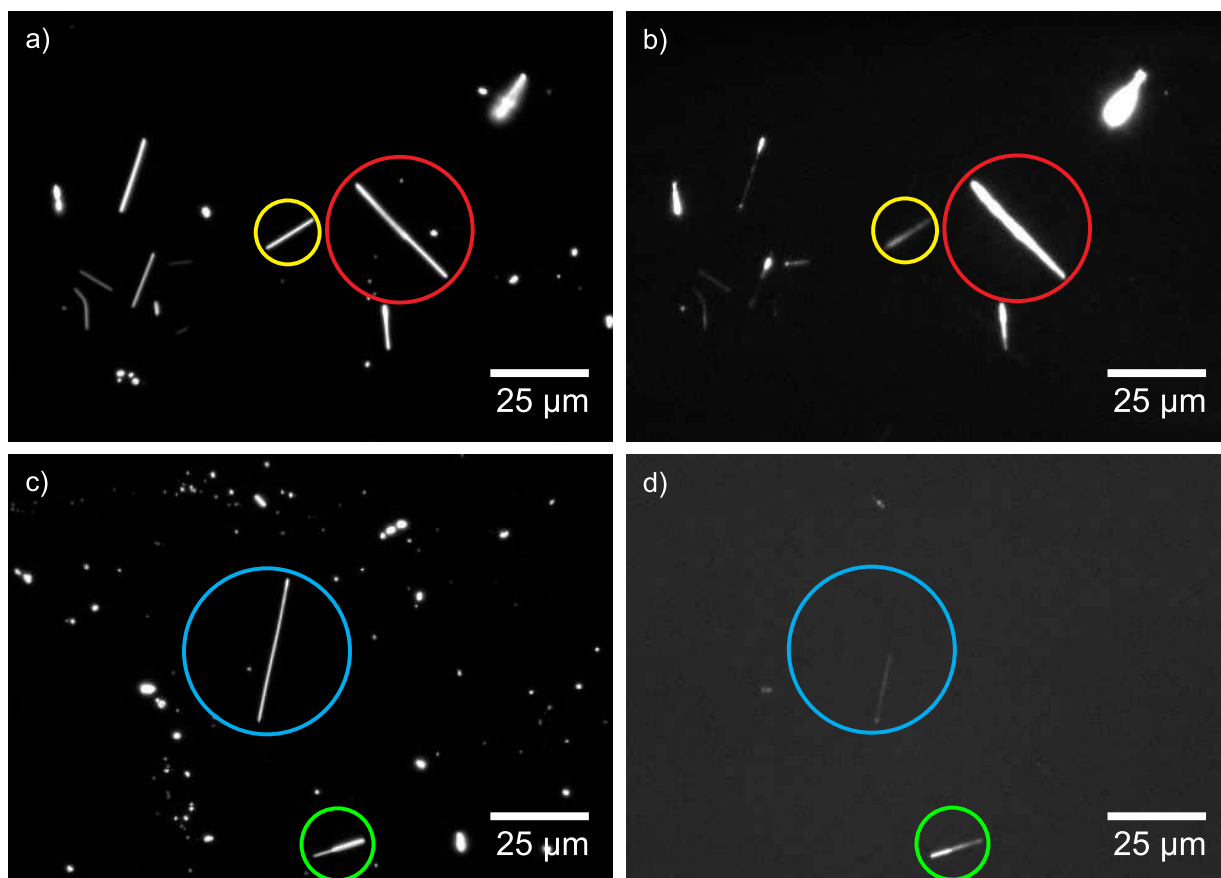


Figure 5.2: Dark field (left side) and fluorescence (right side) images of biofunctionalised ZnO nanowires. Nanowires in the upper row have been modified with Cy3 marked DNA, nanowires in bottom row with FITC marked DNA. Note that the nanowires marked with the red and yellow circles in (b) show different fluorescence intensities along the nanowire axis. The nanowire marked blue in (d) only shows fluorescence at one side, the nanowire marked green shows higher fluorescence intensity at the side that is appearing darker in the respective dark field image.

much more photo stable than samples marked with FITC. Thus, mainly Cy3 marked samples have been investigated here.

Dark field and fluorescence images of DNA biofunctionalised ZnO nanowires are shown in Figure 5.2 (a-d). Every nanowire that can be identified in the dark field image is also showing a fluorescence signal, proving the presence of biomolecules on the nanowire surface. However, intensities differ extremely; this might be explained by different nanowire diameters. Additionally, the intensity of the emitted light often appears non-uniformly

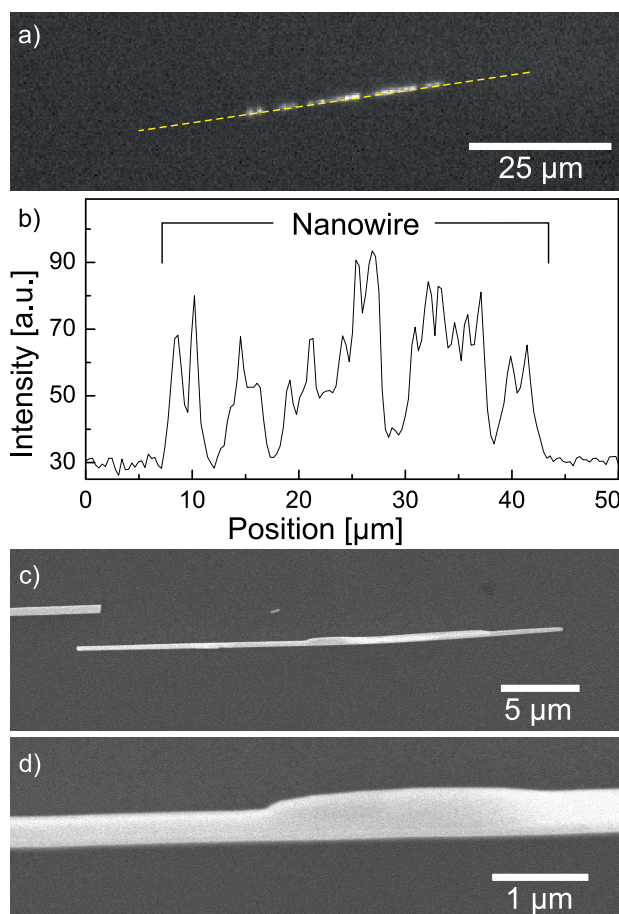


Figure 5.3: In (a) a fluorescence image of a biofunctionalised nanowire with intensity fluctuations along the nanowire axis is shown. In (b) the intensity plot along the dotted yellow line is plotted. The intensity value fluctuates by more than one order of magnitude and even disappears at two points. Images (c) and (d) show SEM images of a typical nanowire used in this study with alternating thickness along the wire axis. At larger magnification in (d) the thickness variation is clearly visible.

along the nanowire axis, as for the nanowires marked with the green and blue circles in Figure 5.2 (d). Such intensity gradients might be caused by only fragmentary DNA coverage of the nanowire surface or by variations of the nanowire thickness.

In Figure 5.3 (a) the fluorescence image of a biofunctionalised nanowire with strong intensity fluctuations is shown. The intensity profile was extracted along the dotted yellow line following the wire axis and plotted in Figure 5.3 (b). The intensity is not only fluctuating, but even going down to background noise level in some regions of the wire, leading to the assumption, that on these sites the functionalised nanowire might not be covered with

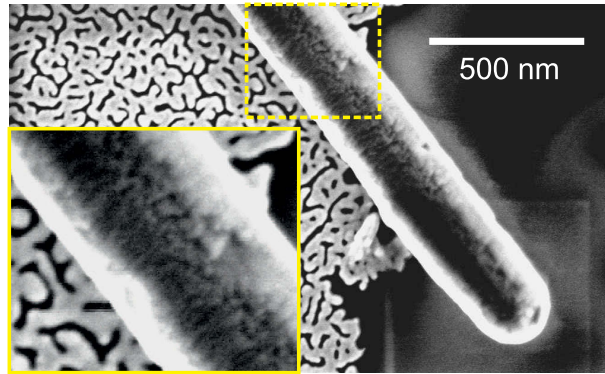


Figure 5.4: FE-SEM study of a biofunctionalised ZnO nanowire. The inset shows an enlarged view of the yellow dotted rectangle in the top middle of the picture. To avoid charging interferences, the nanowire was imprinted to a substrate covered with a thin gold layer. The picture shows a rough but homogeneous coverage of the nanowire surface. Single biomolecules cannot be resolved within the FE-SEM.

DNA at all. Besides patchy coverage with DNA, thickness variations along the wire axis will also lead to variations in fluorescence intensity. The SEM images of a typical nanowire used for the bifunctionalisation in Figure 5.3 (c) and (d) reveal a nanowire diameter that is varying by a factor of two along the wire axis. In Figure 5.4 a high resolution FE-SEM picture of a functionalised nanowire is displayed. The detailed surface morphology of the functionalised wire is not clearly resolvable even at the highest magnification. The larger scaled inset of the picture presents a uniform-looking coverage of the nanowire; however, the uniformity of the DNA coverage might vary from nanowire to nanowire.

In order to confirm that the functionalisation mechanism is really working on ZnO surfaces, a single crystalline ZnO bulk sample was also functionalised only on one half and the DNA surface coverage investigated on both halves subsequently. A comparison of the bright field and the fluorescence images (Figure 5.5) of this sample reveals a homogeneous fluorescence signal and therefore DNA surface coverage only on the biofunctionalised side of the sample.

Although these results show that a uniform DNA coverage is achievable on ZnO surfaces with the utilised process, the DNA immobilisation might be hampered on parts of the nanowire due to a locally craggy nanowire surface caused by thickness variations like displayed in Figure 5.3 (d). Furthermore, nanowires sticking together during the silanisation process could also lead to a non-uniform DNA coverage, as well as damages of the

5 Biofunctionalisation of ZnO nanowires

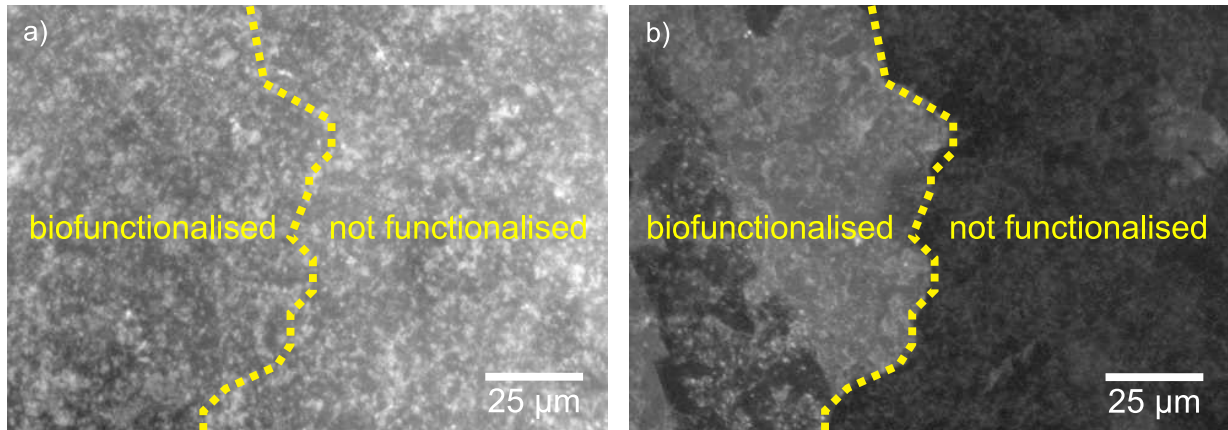


Figure 5.5: Bright field (a) and fluorescence (b) image of a partially biofunctionalised ZnO bulk crystal surface. The sample is showing a homogeneous fluorescence of the biofunctionalised area, underlining that the GOPS treatment is applicable for the successful accumulation of DNA monolayer to ZnO surfaces.

DNA layer during the imprint process. All those issues could be overcome with a more advanced nanowire growth setup [FWZ06]. The observed thickness variations might result from furnace-related instabilities of the growth conditions. Nanowires sticking together during the silanisation process could be avoided by using directional nanowire growth from a seed array [FWZ06]. Damages of the DNA layer during the imprint could also be circumvented by using ordered nanowire arrays, maybe combined with a more advanced imprint method [FHJ⁺08].

To exclude autofluorescence or luminescence of the nanowires as an origin of the detected fluorescence signal, untreated as well as silanised but not functionalised nanowires were also investigated with the fluorescence microscope. As can be seen from Figure 5.6, no interfering autofluorescence or luminescence signals appear. ZnO nanostructures are known to show a green defect luminescence that can be dramatically enhanced when the nanowires are coated [RDM⁺09]. In order to avoid defect luminescence being misinterpreted as fluorescence, the samples were investigated not only with the bandpass filter fitting to the dye used for functionalisation, but also with filters passing other wavelength ranges in the green part of the light spectrum. Without any exception, the samples only showed fluorescence at wavelengths referable to the specific dye attached to the immobilised DNA, indicating that a possible misinterpretable defect luminescence signal can be neglected.

5.3 Characterisation of functionalised nanowires

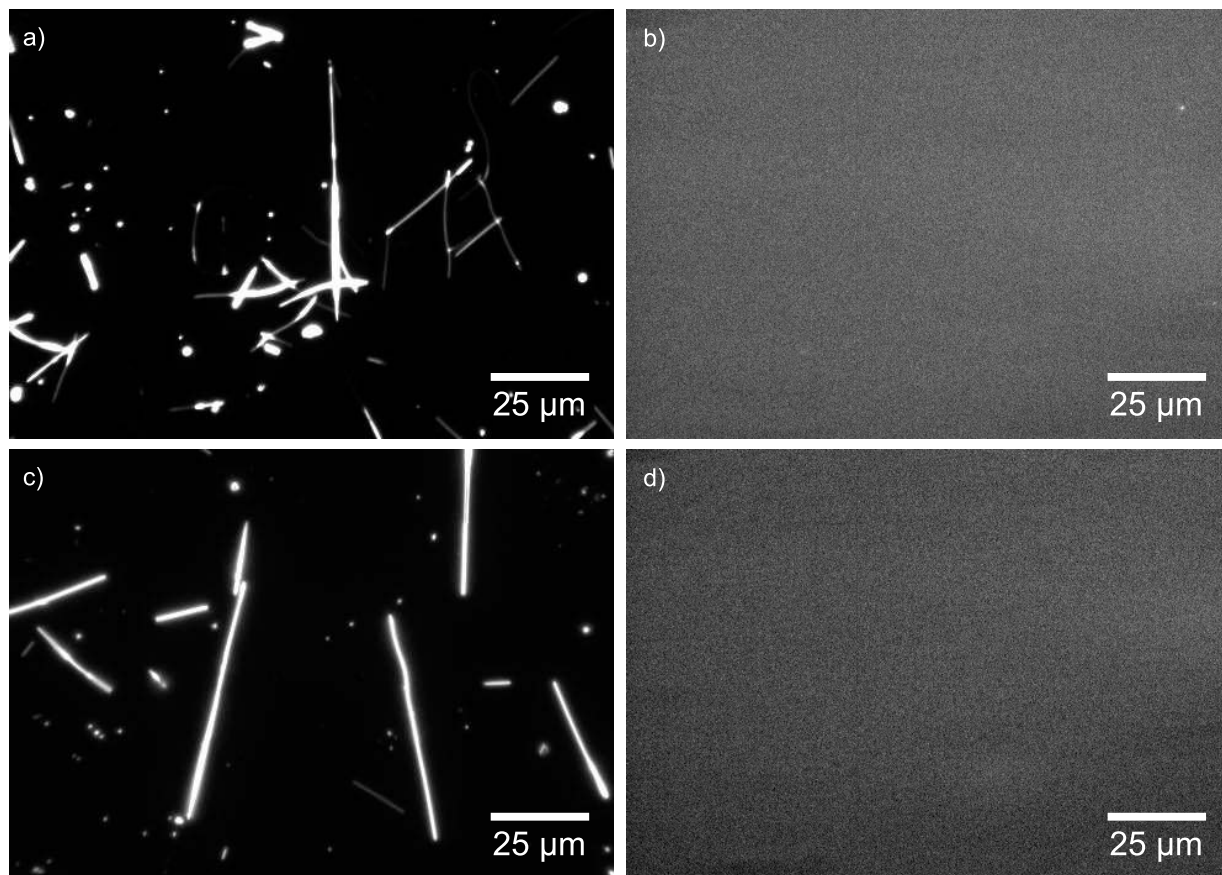


Figure 5.6: Reference experiments with untreated nanowires. In (a) and (b), the dark field and fluorescence images of an unmodified nanowire sample are shown. In (c) and (d), the dark field and fluorescence image of a silanised but not biofunctionalised nanowire sample are shown. In both cases, the fluorescence measurement does not show any sign of unexpected distracting signal.

Thus, it is clear that the above observed fluorescence is caused by the fluorescence marked DNA attached to the nanowires.

It is also known that ZnO nanostructures act fluorescence-enhancing themselves by affecting the self-quenching properties of fluorophores [HLZ⁺10]. This could seemingly lead in theory to fluorescing wires on top of a dye-covered substrate. As mentioned above, the wires investigated here were first functionalised and then subsequently transferred to a clean and dye-free substrate. Thus, fluorescence enhancement of substrate-bonded fluorescence markers can also be excluded as the origin of the observed fluorescence.

5 Biofunctionalisation of ZnO nanowires

Having demonstrated the successful attachment of DNA to the nanowires, some questions regarding character and stability of the bonding between DNA molecules and nanowire surface still need to be clarified. A critical point is whether the attachment of the DNA to the ZnO nanowire is really due to chemisorption, as suggested in the reaction scheme in Figure 5.1, or just by unspecific physisorption to the surface. While it is well known that the amino-modified DNA can covalently bond to the functional group of the GOPS molecule, the bonding type between GOPS and ZnO nanowire has not been investigated before. A method that can be used to investigate the binding character between a monolayer and a substrate is X-ray photoelectron spectroscopy (XPS). In this method, the kinetic energy of photoelectrons which escape from a substrate under X-ray radiation at a particular wavelength is analyzed. The kinetic energy directly depends on the binding energy of the electron inside the sample and is therefore characteristic for the atom and even the atomic orbital the electron comes from. XPS is very surface sensitive and therefore an adequate method for the investigation of monolayers [WWW03]. To show with XPS whether a layer is bound covalently or not to a substrate can be challenging, as the photoelectron yield from a monolayer is quite low. Franquet et al. [FBT⁺06] investigated the interfacial bonding between silane films and aluminum surfaces and could distinguish a signal peak in the Al XPS spectra that was originating from Al atoms within a covalent Al-O-Si bonding. The energy of the respective photoelectrons was shifted by 1.3 eV compared to hydrogenated Al surface atoms. There are no XPS studies on silanised ZnO surfaces so far. However, the interface between ZnO nanoparticles and mesoporous silica was investigated by Yao et al. [YSBZ00]. In the case of covalent cross-linking bonds of Zn-O-Si between the nanoparticles and the SiO₂ material a peak shift of the Zn 2p_{3/2} signal of 0.6 eV was observed.

With the intent to confirm the covalent attachment of GOPS to the ZnO surface, XPS measurements have been performed on both silanised and untreated nanowires. A shift in the Zn 2p_{3/2} signal as reported in [YSBZ00] could prove the covalent character of the silanisation process. Unexpectedly, there was no significant difference in the XPS signal of the treated and the untreated nanowires, as visible in Figure 5.7 (a). Following the argumentation before, this would hint to an unspecific, non-covalent bonding of the GOPS to the nanowire surface. However, in the XPS survey image that was also recorded during the measurement the Si atom related emission peaks are missing. A detailed scan in the spectral area around the Si 2s peak at 151 eV (Figure 5.7 (b)) shows the absence of any Si related signal. This hints at too weak a signal from the nanowire surface layer to detect

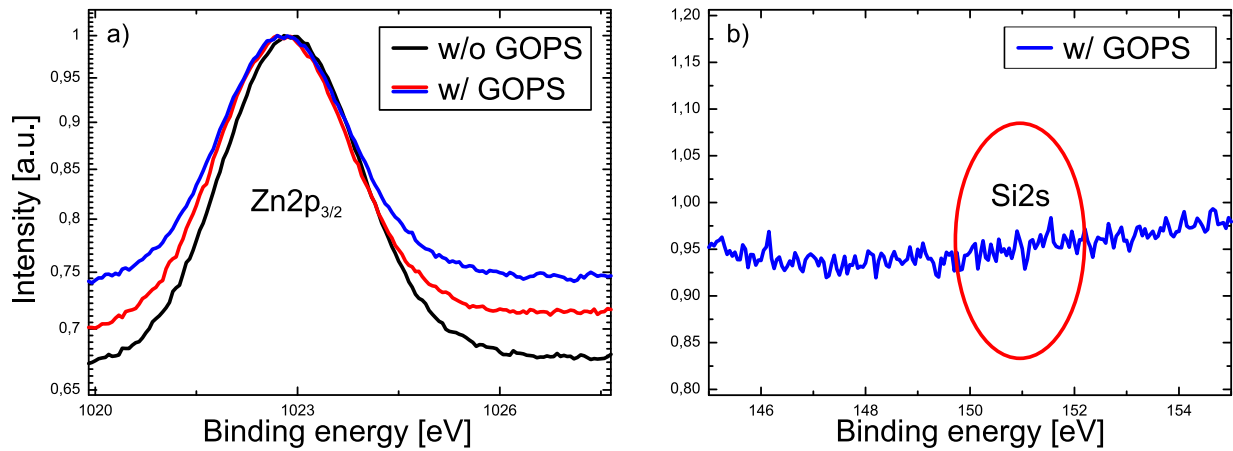


Figure 5.7: In (a): XPS spectra of the Zn $2p_{3/2}$ peak for untreated and GOPS silanised nanowire. There is no significant effect due to the silanisation visible. In (b): Detailed scan in the spectral area of the Si $2s$ peak. There is no Si related signal detectable at all.

anything, including a significant shift of the Zn $2p_{3/2}$ peak. The XPS measurements have been carried out on disorderly grown, pristine nanowire samples, which is most likely the cause for the absence of surface-related signals. Following the nanowire surface, more photoelectrons are directed sideways than in the case of thin film measurements. Due to the spaghetti-like sample geometry, a major fraction of the excited photoelectrons might be recaptured by other nanowires crossing the flight path before reaching the detector array. The channeltron detectors of the used setup were quite old, resulting in a relatively low photoelectron yield. However, this circumstance cannot explain the missing surface related signals, as the measurement time was extended to compensate the poor detector efficiency.

As the XPS measurements could not be used to clarify the character of the bonding of the GOPS to the ZnO surface, several control samples were prepared, leaving out specific steps in the functionalisation process. In Figure 5.8 (a) a fluorescence image of a silanised and biofunctionalised nanowire is shown. Both images were recorded using the same microscope settings and exposure times. Compared to the image in Figure 5.8 (b), a much more pronounced fluorescence is noticeable. The nanowire in Figure 5.8 (b) was not silanised and covered with DNA without the 5'-amino linker, which makes unspecific physisorption the only possible binding mechanism between nanowire and DNA molecules. This leads to the conclusion, that during the functionalisation process sketched in Figure 5.1 a more stable bonding is achieved.

5 Biofunctionalisation of ZnO nanowires

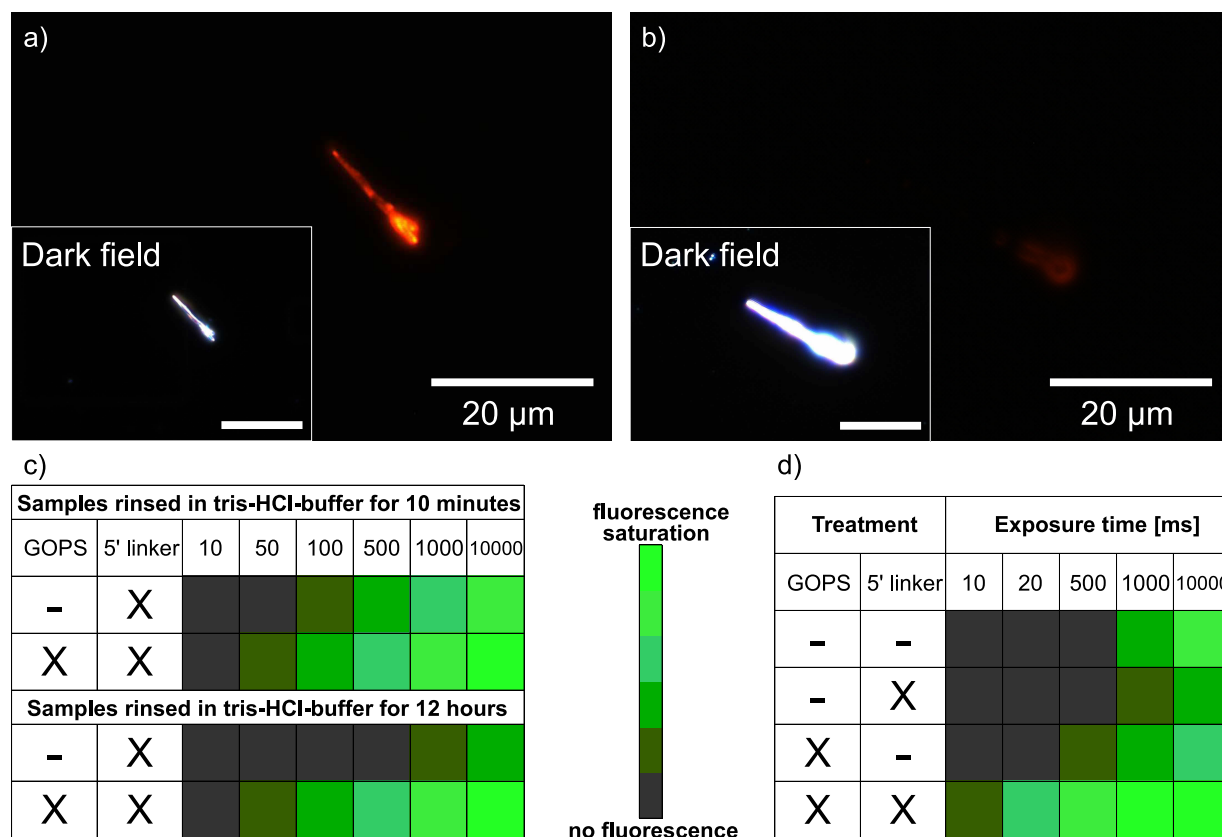


Figure 5.8: In (a) a typical fluorescence image of a silanised and biofunctionalised nanowire is shown. In (b) an image of a nanowire is shown that was treated the same way, but leaving out the silanisation step and using DNA without a 5'-amino linker. In (c) a comparison of a sample with GOPS and a sample without GOPS rinsed in tris-HCl-buffer solution for different periods of time is presented. In order to quantify the fluorescence intensities, the apparent magnitudes resulting from different exposure times have been classified into six levels of intensity between no fluorescence at all and fluorescence saturation. In (d) the fluorescence intensities of various control samples are compared in the same way.

The amino linker attached to the DNA molecule is in principle able to bond directly to the ZnO surface itself, without the GOPS silanisation step. In Figure 5.8 (c), a comparison of the fluorescence intensity between a sample silanised with GOPS prior to DNA attachment and a sample where the silanisation step was left out is presented. Both samples were biofunctionalised with DNA with amino linker. The samples have been rinsed in tris-HCl-buffer solution for 10 minutes and then measured. To quantify the intensities of different fluorescent samples, all signals were integrated for different lengths of time and the resulting apparent magnitudes were classified into six levels of fluorescence intensity between no

fluorescence at all and fluorescence saturation. As expected, the silanised sample is showing the strongest fluorescence. However, after rinsing both samples for another 12 hours, the fluorescence of the sample silanised with GOPS and then functionalised has not dropped, whereas the fluorescence of the control sample is less present than before. This indicates that in the presence of GOPS the bonding achieved between DNA and ZnO surface is much more durable and stable.

In Figure 5.1 (d) the fluorescence intensities of various control samples varying the presence of GOPS and the DNA attached amino linker are compared. It is reconfirmed that the fluorescence is most pronounced in the case of both GOPS treatment and DNA with amino linker. All the other control samples show significant less fluorescence, indicating that a strong, presumably covalent bonding between the DNA and the nanowire is only achieved with both coupling groups present (epoxy group at GOPS and amino group at DNA) in order to form a covalent bond, as drafted in the reaction scheme in Figure 5.1.

5.4 Conclusions

Biofunctionalisation of ZnO nanowires with DNA capture molecules gives way to label-free nanowire biosensors featuring high selectivity and sensitivity. In this chapter the successful functionalisation could be verified with fluorescence microscopy. The bifunctional linker GOPS was used to immobilise the DNA capture molecules on the nanowire surface. Variations of the nanowire thickness and shadowing effects result in fluorescence variations along the nanowire axes. The presumably covalent character of the bonding between DNA layer and ZnO nanowire surface was shown indirectly by comparing several samples prepared in different ways. The next step on the road to nanowire biosensing will be contacting of the functionalised wires in order to receive an electrically working sensing device.

5 Biofunctionalisation of ZnO nanowires

6 Summary and outlook

Among the large variety of bottom-up grown semiconductor nanostructures, semiconductor nanowires are of outstanding interest, since they are promising candidates for integration into future electronic and photonic devices. For the use in devices like transistors, sensors, LEDs, and solar cells, it is essential to know and understand the nature of the nanowires. Furthermore, the selective control of the nanowire properties, by modifying either the wire composition or the surface conditions, allows the development of novel, functional elements for next generation semiconductor devices.

This thesis reports on both, the characterisation and the selective modification of semiconductor nanowires. Scanning electron microscopy based methods are shown for the determination of the carrier diffusion lengths in ZnO and GaAs nanowires. The change of the electrical properties of ZnO nanowires during ion beam implantation is investigated as an example for the targeted modification of the nanowire properties. Here, the ion-nanowire interaction enables the detection of single ion impacts. Biofunctionalisation of ZnO nanowires is also shown, demonstrating the suitability of surface-modified nanowires for the use in biosensing devices. The thesis is divided into three parts, addressing the diffusion length measurements, the ion implantation experiments, and the surface biofunctionalisation.

The diffusion lengths of the respective minority carriers for both the p-type and n-type parts of axial GaAs nanowire pn-junctions have been estimated via EBIC. The measurements were conducted directly at the junction, giving access to the properties of the most important part of the devices. The surface recombination velocity was derived from the diameter dependency of the diffusion lengths. The velocity determined on the n-type side of the nanowires is lower than expected for the dopant concentration adjusted during synthesis. This effect could be attributed to the VLS growth dynamics, where the correct adjustment of the desired doping concentration is delayed by the growth catalyst. Thus, the doping concentration is lower than expected directly at the junction. A simple passi-

6 Summary and outlook

vation process based on aqueous ammonium sulphide was applied to the nanowire devices. After this surface passivation, the carrier diffusion lengths were significantly increased.

The exciton diffusion lengths at ZnO nanowire Schottky devices were investigated by spatial resolved CL measurements. Identically prepared nanowires from the same growth process exhibited extremely different emission properties, independent on the nanowire diameter. The diffusion length measurements were carried out in panchromatic mode in order to receive a good signal-to-noise ratio. The parameter could be determined successfully for most of the investigated nanowires. The method yielded unreliable results for nanowires with an enhanced red defect emission, pointing to the occurrence of sub-bandgap excitation caused emission. Monochromatic measurements could lead to more reliable results in this case.

The influence of hydrogen implantation on the optical and electrical properties of ZnO nanowires was investigated. Hydrogen implantation was found to increase the near bandgap emission while the deep level emission was suppressed. This change of the optical properties is stable over several weeks. Low energy hydrogen implantation on ZnO nanowire devices lead to an enhanced nanowire conductivity. After some time, the conductivity dropped again but eventually remained improved when compared to the pristine sample. This behaviour is attributed to the nature of the implanted hydrogen atoms. Interstitial incorporated hydrogen is responsible for an unstable increase in conductivity, an effect that vanishes after some days. Substitutional incorporated hydrogen leads to a stable and durably increase.

Implantation with higher ion energy led to a decrease in the long-term conductivity. This could be attributed to the unintended creation of implantation induced defects. Hydrogen was initially chosen for implantation because of the low number of defects generated during the implantation. The experiment showed, that still enough defects are created to antagonise the positive effects of the implantation. The implanted nanowires exhibited a transfer curve hysteresis, which could be widened by hydrogen implantation. The effect is related either to incorporated hydrogen in the substrate or implantation induced defects and could be useful for non-volatile memory applications.

The ion implantation of any ion species in ZnO nanowires can also induce a persistently increased conductivity over a time scale of hours. This effect, labelled PIC, was found to be very similar to the well known illumination induced PPC effect, which is related to the existence of quasi-stable, surface oxygen bound states. Due to PIC, the current through a

biased nanowire was increased by a few nA with every implanted ion. This behaviour can be monitored and used for the detection of single implanted ions. Furthermore, nanowire transistors have been used to detect the impact of single ions by separating the charge carriers generated inside the nanowire, following the principle of a classical semiconductor detector.

The biofunctionalisation of ZnO nanowires with DNA was conducted in order to develop a label-free DNA sensor on a nanowire basis. The bifunctional linker molecule GOPS was applied to the nanowires to immobilise the DNA capture molecules via covalent bonding on the surface. The successful immobilisation of the DNA was verified by fluorescence microscopy. Measurements on the long-term stability of the DNA attachment confirmed the presumably covalent character of the bonding between ZnO nanowires and DNA molecules. Variations of the nanowire thickness and shadowing effects resulted in variations of the DNA coverage along the nanowire axes.

In summary, the results obtained in this thesis give new insights on some aspects of the work with semiconductor nanowires. The measurement of the carrier diffusion length inside a SEM allows the validation of the functionality of surface passivation methods. Furthermore, such measurements can be applied to nanowires modified by any other technique to investigate the impact of the applied modification methods on the carrier transport. Both EBIC and CL can be applied for the diffusion length estimation. Thus, it is possible to choose the best-suited method for the material of interest. Especially investigations on nanostructures benefit from the SEM based methods due to the good spatial resolution.

Ion beam implantation has been shown as an effective method for the modification of semiconductor nanowire properties. The availability of any type of ion species without the restriction to any solubility limits makes ion implantation a preferred technique for doping of semiconductor nanowires. Implantation-related side effects like defect production have to be taken care of, even for the implantation of hydrogen ions. EBIC and CL characterisation of implanted nanostructures might help to verify the impact of ion beam doping on the suitability of the implanted nanostructures in photovoltaic and other optoelectronic devices in the future.

The detection of single ions hitting a nanowire by the detection of the interaction between impinging ion and the nanowire itself is aimed at two different directions. First, the countable implantation into semiconductor nanowires is very interesting for the development of devices that need a single dopant atom. An example for such a device is a

6 Summary and outlook

single photon source. A single atom optical emitter, namely the activated dopant that was implanted in the nanowire, is only able to emit one photon at a time. Furthermore, single dopants are of great interest for the development of quantum electronic devices. Second, a nanosized ion detector is realised by the spatially confined detection of the impinging ions with a nanowire device. Such a detector would also recognise ions that are piercing through the nanowire. Thus, the nanowire device might be attractive for the use on top of an implantation target as a movable detector, which is able to detect the impact of single ions with a high spatial resolution.

The results on the biofunctionalisation of the nanowires revealed the applicability of these structures in DNA sensing devices. A detailed characterisation of the electrical properties of the nanowires is of course mandatory for a further device integration. The next step on the the road to a label-free DNA sensor will be the electrical contacting of the functionalised wires, e.g. by dielectrophoretic methods. Then, electrical measurements will follow and reveal whether the wires can be used as biosensors or must be additionally modified. In addition, optical measurements by CL will be conducted. Spatially resolved CL might reveal information on bilayer-caused changes in the extend of the depletion zone in functionalised devices.

The results and findings obtained during the work on this thesis will help to continue the research on semiconductor nanowires towards application. Examples of the characterisation and the selective modification of semiconductor nanowires were presented. Further research based on the requirements established in this work will open the door to new findings on and new applications for semiconductor nanowires in the near future.

Bibliography

- [AAI⁺10] ALI, S. M. U., N. H. ALVI, Z. IBUPOTO, O. NUR, M. WILLANDER and B. DANIELSSON: *Selective potentiometric determination of uric acid with uricase immobilized on ZnO nanowires*. Sensors and Actuators B: Chemical, 2010.
- [ABC⁺10] ANWAND, W., G. BRAUER, T. E. COWAN, V. HEERA, H. SCHMIDT, W. SKORUPA, H. VON WENCKSTERN, M. BRANDT, G. BENNDORF and M. GRUNDMANN: *Structural characterization of H plasma-doped ZnO single crystals by Hall measurements and photoluminescence studies*. physica status solidi (a), 207(11):2426–2431, 2010.
- [ACC⁺06] ANGELUCCI, R., F. CORTICELLI, M. CUFFIANI, G. M. DALLAVALLE, L. MALFERRARI, A. MONTANARI, F. ODORICI, R. RIZZOLI and G. P. VERONESE: *A novel position detector based on nanotechnologies: the NanoChanT project*. Nuclear Physics B-Proceedings Supplements, 150:140–143, 2006.
- [ACD⁺06] ANGELUCCI, R., M. CUFFIANI, G. M. DALLAVALLE, S. GUATELLI, A. JAGMINAS, L. MALFERRARI, A. MONTANARI, F. ODORICI, M. G. PIA, R. RIZZOLI et al.: *Simulation with GEANT4 of a Novel Position Detector Based on Nanotechnologies*. In *Nuclear Science Symposium Conference Record, 2006*. IEEE, volume 3, pages 1480–1484. IEEE, 2006.
- [AGH⁺01] AURET, F. D., S. A. GOODMAN, M. HAYES, M. J. LEGODI, H. A. VAN LAARHOVEN and D. C. LOOK: *Electrical characterization of 1.8 MeV proton-bombarded ZnO*. Applied Physics Letters, 79(19):3074, 2001.
- [AHP⁺08] ALLEN, J. E., E. R. HEMESATH, D. E. PEREA, J. L. LENSCH-FALK, Z. Y. LI, F. YIN, M. H. GASS, P. WANG, A. L. BLELOCH, R. E. PALMER et al.: *High-resolution detection of Au catalyst atoms in Si nanowires*. Nature nanotechnology, 3(3):168–173, 2008.
- [APHL09] ALLEN, J. E., D. E. PEREA, E. R. HEMESATH and L. J. LAUHON: *Nonuniform nanowire doping profiles revealed by quantitative scanning photocurrent microscopy*. Advanced Materials, 21(30):3067–3072, 2009.
- [App02] APPELL, D.: *Nanotechnology: Wired for success*. Nature, 419(6907):553–555, 2002.

Bibliography

- [ASC⁺09] ANNUNZIATA, A. J., D. F. SANTAVICCA, J. D. CHUDOW, L. FRUNZIO, M. J. ROOKS, A. FRYDMAN and D. E. PROBER: *Niobium superconducting nanowire single-photon detectors*. Applied Superconductivity, IEEE Transactions on, 19(3):327–331, 2009.
- [BA05] BAXTER, J. B. and E. S. AYDIL: *Nanowire-based dye-sensitized solar cells*. Applied Physics Letters, 86(5):053114–053114, 2005.
- [BAL⁺09] BAIRD, L., G. H. ANG, C. H. LOW, N. M. HAEGEL, A. A. TALIN, Q. LI and G. T. WANG: *Imaging minority carrier diffusion in GaN nanowires using near field optical microscopy*. Physica B: Condensed Matter, 404(23-24):4933–4936, 2009.
- [BC08] BANG, J. and K. J. CHANG: *Diffusion and thermal stability of hydrogen in ZnO*. Applied Physics Letters, 92:132109, 2008.
- [BDC02] BANERJEE, S., A. DAN and D. CHAKRAVORTY: *Review synthesis of conducting nanowires*. Journal of materials science, 37(20):4261–4271, 2002.
- [BHB⁺09] BRISENO, A. L., T. W. HOLCOMBE, A. I. BOUKAI, E. C. GARNETT, S. W. SHELTON, J. J. M. FRÉCHET and P. YANG: *Oligo-and polythiophene/ZnO hybrid nanowire solar cells*. Nano letters, 10(1):334–340, 2009.
- [BHS⁺09] BYUN, K. E., K. HEO, S. SHIM, H. J. CHOI and S. HONG: *Functionalization of Silicon Nanowires with Actomyosin Motor Protein for Bioinspired Nanomechanical Applications*. Small, 5(23):2659–2664, 2009.
- [BMB⁺11] BORSCHEL, C., M. E. MESSING, M. T. BORGSTROM, W. PASCHOAL, J. WALLENTIN, S. KUMAR, K. MERGENTHALER, K. DEPERT, C. M. CANALI, H. PETTERSSON et al.: *A new route towards semiconductor nanospintronics: highly Mn-doped GaAs nanowires realized by ion-implantation under dynamic annealing conditions*. Nano letters, 2011.
- [BMH⁺11] BRENNAN, B., M. MILOJEVIC, C. L. HINKLE, F. S. AGUIRRE-TOSTADO, G. HUGHES and R. M. WALLACE: *Optimisation of the ammonium sulphide (NH₄)₂S passivation process on In_{0.53}Ga_{0.47}As*. Applied Surface Science, 257(9):4082–4090, 2011.
- [BMS⁺06] BORCHERS, C., S. MÜLLER, D. STICHTENOTH, D. SCHWEN and C. RONNING: *Catalyst- Nanostructure Interaction in the Growth of 1-D ZnO Nanostructures*. J. Phys. Chem. B, 110(4):1656–1660, 2006.
- [BMSG10] BOLINSSON, J., K. MERGENTHALER, L. SAMUELSON and A. GUSTAFSSON: *Diffusion length measurements in axial and radial heterostructured nanowires using cathodoluminescence*. Journal of Crystal Growth, 2010.

- [BNGR10] BORSCHHEL, C., R. NIEPELT, S. GEBURT and C. RONNING: *Ion beam doping of semiconductor nanowires*. In *Nanoelectronics Conference (INEC), 2010 3rd International*, pages 40–41. IEEE, 2010.
- [BOC⁺11] BAIRD, L., C. P. ONG, R. A. COLE, N. M. HAEGEL, A. A. TALIN, Q. LI and G. T. WANG: *Transport imaging for contact-free measurements of minority carrier diffusion in GaN, GaN/AlGaN, and GaN/InGaN core-shell nanowires*. *Applied Physics Letters*, 98(13):132104–132104, 2011.
- [BP07] BOSI, M. and C. PELOSI: *The potential of III-V semiconductors as terrestrial photovoltaic devices*. *Progress in photovoltaics: Research and applications*, 15(1):51–68, 2007.
- [BR83] BINNIG, G. and H. ROHRER: *Scanning tunneling microscopy*. *Surface Science*, 126(1):236–244, 1983.
- [BR11] BORSCHHEL, C. and C. RONNING: *Ion beam irradiation of nanostructures-A 3D Monte Carlo simulation code*. *Nuclear Instruments and Methods in Physics Research Section B: Beam Interactions with Materials and Atoms*, 2011.
- [BSC10] BIELEJEC, E., J. A. SEAMONS and M. S. CARROLL: *Single ion implantation for single donor devices using Geiger mode detectors*. *Nanotechnology*, 21:085201, 2010.
- [BSM⁺06] BORCHERS, C., D. STICHTENOTH, S. MÜLLER, D. SCHWEN and C. RONNING: *Catalyst-nanostructure interaction and growth of ZnS nanobelts*. *Nanotechnology*, 17:1067, 2006.
- [BSS⁺11] BAO, J., I. SHALISH, Z. SU, R. GURWITZ, F. CAPASSO, X. WANG and Z. REN: *Photoinduced oxygen release and persistent photoconductivity in ZnO nanowires*. *Nanoscale Research Letters*, 6(1):404, 2011.
- [Bul09] BULGARINI, G.: *Luminescence of single ZnS nanowires implanted with Mn and rare earths*. Master’s thesis, Politecnico di Milano / Friedrich-Schiller-Universität Jena, 2009.
- [BWR⁺07] BATRA, A., C. D. WEIS, J. REIJONEN, A. PERSAUD, T. SCHENKEL, S. CABRINI, C. C. LO and J. BOKOR: *Detection of low energy single ion impacts in micron scale transistors at room temperature*. *Applied Physics Letters*, 91(19):193502–193502, 2007.
- [CAM⁺11] CORFDIR, P., M. ABID, A. MOUTI, P. A. STADELMANN, E. PAPA, J. P. ANSERMET, J. D. GANIÈRE and B. DEVEAUD-PLÉDRAN: *Biexciton emission and crystalline quality of ZnO nano-objects*. *Nanotechnology*, 22:285710, 2011.
- [can91] *Spectroscopy Amplifier Model 2022*. Canberra Industries, www.canberra.com/products/1102.asp, 1991.

Bibliography

- [CC94] CAVALCOLI, D. and A. CAVALLINI: *Evaluation of diffusion length at different excess carrier concentrations*. Materials Science and Engineering B, 24(1-3):98–100, 1994.
- [CDC⁺01] COX, S. F. J., E. A. DAVIS, S. P. COTTRELL, P. J. C. KING, J. S. LORD, J. M. GIL, H. V. ALBERTO, R. C. VILAO, J. P. DUARTE, N. A. DE CAMPOS, A. WEIDINGER, R. L. LICHTI and S. J. C. IRVINE: *Experimental confirmation of the predicted shallow donor hydrogen state in zinc oxide*. Physical Review Letters, 86(12):2601, 2001.
- [CDH08] CORSO, C. D., A. DICKHERBER and W. D. HUNT: *An investigation of antibody immobilization methods employing organosilanes on planar ZnO surfaces for biosensor applications*. Biosensors and Bioelectronics, 24(4):805–811, 2008.
- [CFC⁺06] CHANG, P. C., Z. FAN, C. J. CHIEN, D. STICHTENOTH, C. RONNING and J. G. LU: *High-performance ZnO nanowire field effect transistors*. Applied physics letters, 89:133113, 2006.
- [CFR⁺08] COLLI, A., A. FASOLI, C. RONNING, S. PISANA, S. PISCANEC and A. C. FERRARI: *Ion beam doping of silicon nanowires*. Nano letters, 8(8):2188–2193, 2008.
- [CFS74] CUNNINGHAM, J., E. FINN and N. SAMMAN: *Photo-assisted surface reactions studied by dynamic mass spectrometry*. Faraday Discuss. Chem. Soc., 58:160–174, 1974.
- [CHC⁺08] CHANG, S. J., T. J. HSUEH, I. C. CHEN, S. F. HSIEH, S. P. CHANG, C. L. HSU, Y. R. LIN and B. R. HUANG: *Highly sensitive ZnO nanowire acetone vapor sensor with Au adsorption*. Nanotechnology, IEEE Transactions on, 7(6):754–759, 2008.
- [CKJL10] CHOI, A., K. KIM, H. I. JUNG and S. Y. LEE: *ZnO nanowire biosensors for detection of biomolecular interactions in enhancement mode*. Sensors and Actuators B: Chemical, 148(2):577–582, 2010.
- [CL08] CHANG, P. C. and J. G. LU: *ZnO nanowire field-effect transistors*. Electron Devices, IEEE Transactions on, 55(11):2977–2987, 2008.
- [CLB⁺08] CAO, B. Q., M. LORENZ, M. BRANDT, H. VON WENCKSTERN, J. LENZNER, G. BIEHNE and M. GRUNDMANN: *p-type conducting ZnO: P microwires prepared by direct carbothermal growth*. physica status solidi (RRL)-Rapid Research Letters, 2(1):37–39, 2008.
- [CMP73] CASEY, H. C., B. I. MILLER and E. PINKAS: *Variation of minority-carrier diffusion length with carrier concentration in GaAs liquid-phase epitaxial layers*. Journal of Applied Physics, 44(3):1281–1287, 1973.

- [col12] *Ion gun model G-1.* Colutron Research Corporation, www.colutron.com/products/gun/gun.html, 2012.
- [CSC⁺10] CHUANG, L. C., F. G. SEDGWICK, R. CHEN, W. S. KO, M. MOEWE, K. W. NG, T. T. D. TRAN and C. CHANG-HASNAIN: *GaAs-Based Nanoneedle Light Emitting Diode and Avalanche Photodiode Monolithically Integrated on a Silicon Substrate.* Nano letters, 2010.
- [CSPD⁺08] CATTANI-SCHOLZ, A., D. PEDONE, M. DUBEY, S. NEPPL, B. NICKEL, P. FEULNER, J. SCHWARTZ, G. ABSTREITER and M. TORNOW: *Organophosphonate-based PNA-functionalization of silicon nanowires for label-free DNA detection.* ACS nano, 2(8):1653–1660, 2008.
- [CSS05] CROSS, R. B. M., M. M. D. SOUZA and E. M. SANKARA NARAYANAN: *A low temperature combination method for the production of ZnO nanowires.* Nanotechnology, 16:2188, 2005.
- [CW30] COCKCROFT, J. D. and E. T. S. WALTON: *Experiments with high velocity positive ions.* Proceedings of the Royal Society of London. Series A, 129(811):477–489, 1930.
- [CWPL01] CUI, Y., Q. WEI, H. PARK and C. M. LIEBER: *Nanowire nanosensors for highly sensitive and selective detection of biological and chemical species.* Science, 293(5533):1289, 2001.
- [CXL⁺08] CHENG, C., R. XIN, Y. LENG, D. YU and N. WANG: *Chemical stability of ZnO nanostructures in simulated physiological environments and its application in determining polar directions.* Inorganic chemistry, 47(17):7868–7873, 2008.
- [CZW⁺03] CUI, Y., Z. ZHONG, D. WANG, W. U. WANG and C. M. LIEBER: *High performance silicon nanowire field effect transistors.* Nano Letters, 3(2):149–152, 2003.
- [DBL⁺11] DIETRICH, C. P., M. BRANDT, M. LANGE, J. KUPPER, T. BÖNTGEN, H. VON WENCKSTERN and M. GRUNDMANN: *Defect properties of ZnO and ZnO: P microwires.* Journal of Applied Physics, 109:013712, 2011.
- [DDW⁺03] DHARA, S., A. DATTA, C. T. WU, Z. H. LAN, K. H. CHEN, Y. L. WANG, L. C. CHEN, C. W. HSU, H. M. LIN and C. C. CHEN: *Enhanced dynamic annealing in Ga⁺ ion-implanted GaN nanowires.* Applied Physics Letters, 82(3):451, 2003.
- [DG11] DHARA, S. and P. K. GIRI: *On the origin of enhanced photoconduction and photoluminescence from Au and Ti nanoparticles decorated aligned ZnO nanowire heterostructures.* Journal of Applied Physics, 110(12):124317–124317, 2011.

Bibliography

- [DKH06] DORFMAN, A., N. KUMAR and J. HAHM: *Nanoscale ZnO-Enhanced Fluorescence Detection of Protein Interactions*. *Advanced Materials*, 18(20):2685–2690, 2006.
- [DNR⁺10] DEV, A., R. NIEPELT, J. P. RICHTERS, C. RONNING and T. VOSS: *Stable enhancement of near-band-edge emission of ZnO nanowires by hydrogen incorporation*. *Nanotechnology*, 21:065709, 2010.
- [DPDC⁺11] DEMERS, H., N. POIRIER-DEMERS, A. R. COUTURE, D. JOLY, M. GUILMAIN, N. DE JONGE and D. DROUIN: *Three-dimensional electron microscopy simulation with the CASINO Monte Carlo software*. *Scanning*, 33(3):135–146, 2011.
- [DST⁺11] DAN, Y., K. SEO, K. TAKEI, J. H. MEZA, A. JAVEY and K. B. CROZIER: *Dramatic Reduction of Surface Recombination by in Situ Surface Passivation of Silicon Nanowires*. *Nano Letters*, 2011.
- [FAA⁺10] FULATI, A., S. M. U. ALI, M. ASIF, N. H. ALVI, M. WILLANDER, C. BRÄNNMARK, P. STRÅLFORS, S. I. BÖRJESSON, F. ELINDER and B. DANIELSSON: *An intracellular glucose biosensor based on nanoflake ZnO*. *Sensors and Actuators B: Chemical*, 2010.
- [FBT⁺06] FRANQUET, A., M. BIESEMANS, H. TERRYN, R. WILLEM and J. VEREECKEN: *Study of the interaction of hydrolysed silane solutions with pre-treated aluminium substrates*. *Surface and interface analysis*, 38(4):172–175, 2006.
- [FCL⁺04] FAN, Z., P. CHANG, J. G. LU, E. C. WALTER, R. M. PENNER, C. LIN and H. P. LEE: *Photoluminescence and polarized photodetection of single ZnO nanowires*. *Applied physics letters*, 85:6128, 2004.
- [Fey60] FEYNMAN, R. P.: *There's plenty of room at the bottom*. *Engineering and Science*, 23(5):22–36, 1960.
- [FHJ⁺08] FAN, Z., J. C. HO, Z. A. JACOBSON, R. YERUSHALMI, R. L. ALLEY, H. RAZAVI and A. JAVEY: *Wafer-scale assembly of highly ordered semiconductor nanowire arrays by contact printing*. *Nano letters*, 8(1):20–25, 2008.
- [FSW⁺11] FANG, Y. J., J. SHA, Z. L. WANG, Y. T. WAN, W. W. XIA and Y. W. WANG: *Behind the change of the photoluminescence property of metal-coated ZnO nanowire arrays*. *Applied Physics Letters*, 98:033103, 2011.
- [FWZ06] FAN, H. J., P. WERNER and M. ZACHARIAS: *Semiconductor Nanowires: From Self-Organization to Patterned Growth*. *Small*, 2(6):700–717, 2006.
- [GBCM11] GARNETT, E. C., M. L. BRONGERSMA, Y. CUI and M. D. MCGEHEE: *Nanowire Solar Cells*. *Annual Review of Materials Research*, 41:269–295, 2011.

- [GBS07] GUSTAFSSON, A., M. T. BJÖRK and L. SAMUELSON: *Locating nanowire heterostructures by electron beam induced current*. Nanotechnology, 18:205306, 2007.
- [GBSS10] GUSTAFSSON, A., J. BOLINSSON, N. SKOLD and L. SAMUELSON: *Determination of diffusion lengths in nanowires using cathodoluminescence*. Applied Physics Letters, 97(7):072114–072114, 2010.
- [GLR⁺10] GUTSCHE, C., A. LYSOV, I. REGOLIN, K. BLEKKER, W. PROST and F.-J. TEGUDE: *n-Type Doping of Vapor-Liquid-Solid Grown GaAs Nanowires*. Nanoscale Research Letters, pages 1–6, 2010.
- [GLR⁺11] GUTSCHE, C., A. LYSOV, I. REGOLIN, A. BRODT, L. LIBORIUS, J. FROHLEIKS, W. PROST and F.-J. TEGUDE: *Ohmic contacts to n-GaAs nanowires*. Journal of Applied Physics, 110:014305, 2011.
- [GMOY11] GRAHAM, R., C. MILLER, E. OH and D. YU: *Electric Field Dependent Photocurrent Decay Length in Single Lead Sulfide Nanowire Field Effect Transistors*. Nano letters, 2011.
- [GNG⁺12] GUTSCHE, C., R. NIEPELT, M. GNAUCK, A. LYSOV, W. PROST, C. RONNING and F.-J. TEGUDE: *Determination of minority carrier diffusion lengths directly from axial GaAs nanowire pn-junctions*. submitted to Nano Letters, 2012.
- [GPLN11] GU, Z., P. PRETE, N. LOVERGINE and B. NABET: *On optical properties of GaAs and GaAs/AlGaAs core-shell periodic nanowire arrays*. Journal of Applied Physics, 109:064314, 2011.
- [GRB⁺09] GUTSCHE, C., I. REGOLIN, K. BLEKKER, A. LYSOV, W. PROST and F.-J. TEGUDE: *Controllable p-type doping of GaAs nanowires during vapor-liquid-solid growth*. Journal of Applied Physics, 105(2):024305–024305, 2009.
- [GRD⁺06] GU, Y., J. P. ROMANKIEWICZ, J. K. DAVID, J. L. LENSCH, L. J. LAUHON, E. S. KWAK and T. W. ODOM: *Local photocurrent mapping as a probe of contact effects and charge carrier transport in semiconductor nanowire devices*. Journal of Vacuum Science & Technology B: Microelectronics and Nanometer Structures, 24:2172, 2006.
- [GSLY05] GOLDBERGER, J., D. J. SIRBULY, M. LAW and P. YANG: *ZnO nanowire transistors*. The Journal of Physical Chemistry B, 109(1):9–14, 2005.
- [GSM⁺08] GEBURT, S., D. STICHTENOTH, S. MULLER, W. DEWALD, C. RONNING, J. WANG, Y. JIAO, Y. Y. RAO, S. K. HARK and Q. LI: *Rare earth doped zinc oxide nanowires*. Journal of Nanoscience and Nanotechnology, 8(1):244–251, 2008.

Bibliography

- [GTK⁺09] GARNETT, E. C., Y. C. TSENG, D. R. KHANAL, J. WU, J. BOKOR and P. YANG: *Dopant profiling and surface analysis of silicon nanowires using capacitance–voltage measurements*. Nature Nanotechnology, 4(5):311–314, 2009.
- [Ham10] HAMAGUCHI, C.: *Basic semiconductor physics*. Springer Verlag, 2010.
- [HBR⁺09] HOFFMANN, S., J. BAUER, C. RONNING, T. STELZNER, J. MICHLER, C. BALLIF, V. SIVAKOV and S. H. CHRISTIANSEN: *Axial pn junctions realized in silicon nanowires by ion implantation*. Nano letters, 9(4):1341–1344, 2009.
- [HCL⁺96] HOU, X., X. CHEN, Z. LI, X. DING and X. WANG: *Passivation of GaAs surface by sulfur glow discharge*. Applied physics letters, 69:1429, 1996.
- [HDP⁺11] HWANG, J. S., F. DONATINI, J. PERNOT, R. THIERRY, P. FERRET and L. S. DANG: *Carrier depletion and exciton diffusion in a single ZnO nanowire*. Nanotechnology, 22:475704, 2011.
- [HJK⁺08] HONG, W. K., G. JO, S. S. KWON, S. SONG and T. LEE: *Electrical properties of surface-tailored ZnO nanowire field-effect transistors*. Electron Devices, IEEE Transactions on, 55(11):3020–3029, 2008.
- [HJS⁺10] HONG, W., G. JO, J. I. SOHN, W. PARK, M. CHOE, G. WANG, Y. H. KAHNG, M. E. WELLAND and T. LEE: *Tuning of the electronic characteristics of ZnO nanowire field effect transistors by proton irradiation*. ACS Nano, 4(2):818, 2010.
- [HLC⁺05] HE, J. H., C. S. LAO, L. J. CHEN, D. DAVIDOVIC and Z. L. WANG: *Large-scale Ni-doped ZnO nanowire arrays and electrical and optical properties*. Journal of the American Chemical Society, 127(47):16376–16377, 2005.
- [HLZ⁺10] HU, W., Y. LIU, Z. ZHU, H. YANG and C. M. LI: *Randomly Oriented ZnO Nanorods As Advanced Substrate for High-Performance Protein Microarrays*. ACS Applied Materials & Interfaces, 2(6):1569–1572, 2010.
- [Hol74] HOLT, D. B.: *Quantitative conductive mode scanning electron microscopy*. Quantitative Scanning Electron Microscopy, DB Holt, MD Muir, PR Grant, IM Boswarva, eds. (Academic Press, NY), pages 213–286, 1974.
- [Hol89] HOLT, D. B.: *SEM microcharacterization of semiconductors*, volume 12. Academic press, 1989.
- [Hol11] HOLLAND-MORITZ, H.: *Untersuchung der elektrischen Eigenschaften von Halbleiternanodrähten*. Master’s thesis, Friedrich-Schiller-Universität Jena, September 2011.

- [Hsi76] HSIEH, K. C.: *Observations on pulse-height defect for helium ions of energies ≤ 30 keV in silicon.* Nuclear Instruments and Methods, 138(4):677–679, 1976.
- [HT65] HIGUCHI, H. and H. TAMURA: *Measurement of the Lifetime of Minority Carriers in Semiconductors with a Scanning Electron Microscope.* Japanese journal of applied physics, 4(4):316–317, 1965.
- [HTN⁺04] HEO, Y. W., L. C. TIEN, D. P. NORTON, B. S. KANG, F. REN, B. P. GILA and S. J. PEARTON: *Electrical transport properties of single ZnO nanorods.* Applied Physics Letters, 85(11):2002, 2004.
- [HTS⁺06] HSU, J. W. P., D. R. TALLANT, R. L. SIMPSON, N. A. MISSERT and R. G. COPELAND: *Luminescent properties of solution-grown ZnO nanorods.* Applied physics letters, 88:252103, 2006.
- [hve12] *High Voltage ion accelerator.* High Voltage Engineering Europa B.V., www.highvolteng.com, 2012.
- [HW66] HAINES, E. L. and A. B. WHITEHEAD: *Pulse height defect and energy dispersion in semiconductor detectors.* Review of Scientific Instruments, 37(2):190–194, 1966.
- [Hwa69] HWANG, C. J.: *Optical Properties of n-Type GaAs. I. Determination of Hole Diffusion Length from Optical Absorption and Photoluminescence Measurements.* Journal of Applied Physics, 40(9):3731–3739, 1969.
- [HWF⁺01] HUANG, M. H., Y. WU, H. FEICK, N. TRAN, E. WEBER and P. YANG: *Catalytic growth of zinc oxide nanowires by vapor transport.* Advanced Materials, 13(2):113–116, 2001.
- [HZAL07] HAYDEN, O., G. ZHENG, P. AGARWAL and C.M. LIEBER: *Visualization of Carrier Depletion in Semiconducting Nanowires.* small, 3(12):2048–2052, 2007.
- [I⁺91] IJIMA, S. et al.: *Helical microtubules of graphitic carbon.* nature, 354(6348):56–58, 1991.
- [II94] ITO, H. and T. ISHIBASHI: *Surface recombination velocity in p-type GaAs.* Japanese journal of applied physics, 33(1A):88–89, 1994.
- [Inf04] INFINEON TECHNOLOGIES AG (MÜNCHEN): *Halbleiter: Technische Erläuterungen, Technologien und Kenndaten.* Publicis Corp. Publ., 2004.
- [IOH⁺03] IP, K., M. E. OVERBERG, Y. W. HEO, D. P. NORTON, S. J. PEARTON, C. E. STUTZ, S. O. KUCHEYEV, C. JAGADISCH, J. S. WILLIAMS, B. LUO, F. REN, D. C. LOOK and J. M. ZAVADA: *Hydrogen incorporation, diffusivity and evolution in bulk ZnO.* Solid State Electronics, 47:2255, 2003.
- [isi12] *ISI Web of Knowledge.* Thomson Reuters, www.isiknowledge.com, 2012.

Bibliography

- [ISN⁺11] ISRAR, M. Q., J. R. SADAF, O. NUR, M. WILLANDER, S. SALMAN and B. DANIELSSON: *Chemically fashioned ZnO nanowalls and their potential application for potentiometric cholesterol biosensor*. Applied Physics Letters, 98(25):253705–253705, 2011.
- [ITR11] *International technology roadmap for semiconductors - 2011 edition - Executive summary*. ITRS, 2011.
- [ITY⁺06] IP, K., G. T. THALER, H. YANG, S. YOUN HAN, Y. LI, D. P. NORTON, S. J. PEARTON, S. JANG and F. REN: *Contacts to ZnO*. Journal of crystal growth, 287(1):149–156, 2006.
- [IY08] INO, N. and N. YAMAMOTO: *Low temperature diffusion length of excitons in gallium nitride measured by cathodoluminescence technique*. Applied Physics Letters, 93:232103, 2008.
- [JG89] JOSHI, R. and R. O. GRONDIN: *Monte Carlo analysis of high-field hole diffusion coefficients in nondegenerate GaAs*. Applied Physics Letters, 54(24):2438–2439, 1989.
- [JLG75] JASTRZEBSKI, L., J. LAGOWSKI and H. C. GATOS: *Application of scanning electron microscopy to determination of surface recombination velocity: GaAs*. Applied Physics Letters, 27(10):537–539, 1975.
- [JNGR11] JOHANNES, A., R. NIEPELT, M. GNAUCK and C. RONNING: *Persistent ion beam induced conductivity in zinc oxide nanowires*. Applied Physics Letters, 99(25):252105, 2011.
- [Joh11] JOHANNES, A.: *In-situ characterisation of ion-doped zinc oxide nanowires*. Master's thesis, Friedrich-Schiller-Universität Jena, May 2011.
- [JPNT04] JIN, Z., W. PROST, S. NEUMANN and F.-J. TEGUDE: *Sulfur and low-temperature SiN passivation of self-aligned graded-base InGaAs/InP heterostructure bipolar transistors*. Journal of Vacuum Science & Technology B: Microelectronics and Nanometer Structures, 22:1060, 2004.
- [JTA⁺10] JOHNSON, B. C., G. C. TETTAMANZI, A. D. C. ALVES, S. THOMPSON, C. YANG, J. VERDUJN, J. A. MOL, R. WACQUEZ, M. VINET, M. SANQUER et al.: *Drain current modulation in a nanoscale field-effect-transistor channel by single dopant implantation*. Applied Physics Letters, 96:264102, 2010.
- [JV06a] JANOTTI, A. and C. G. VAN DE WALLE: *Hydrogen multicentre bonds*. Nature materials, 6(1):44–47, 2006.
- [JV06b] JANOTTI, A. and C. G. VAN DE WALLE: *New insights into the role of native point defects in ZnO*. Journal of Crystal Growth, 287:58, 2006.
- [JXW10] JING, E., B. XIONG and Y. WANG: *Low-temperature Au–Si wafer bonding*. Journal of Micromechanics and Microengineering, 20:095014, 2010.

- [JYH⁺05] JAMIESON, D. N., C. YANG, T. HOPF, S. M. HEARNE, C. I. PAKES, S. PRAWER, M. MITIC, E. GAUJA, S. E. ANDRESEN, F. E. HUDSON et al.: *Controlled shallow single-ion implantation in silicon using an active substrate for sub-20-keV ions*. Applied Physics Letters, 86:202101, 2005.
- [Kas02] KASEMO, B.: *Biological surface science*. Surface Science, 500(1-3):656–677, 2002.
- [KBR10] KOREN, E., N. BERKOVITCH and Y. ROSENWAKS: *Measurement of active dopant distribution and diffusion in individual silicon nanowires*. Nano letters, 10(4):1163–1167, 2010.
- [KDH06] KUMAR, N., A. DORFMAN and J. HAHM: *Ultrasensitive DNA sequence detection using nanoscale ZnO sensor arrays*. Nanotechnology, 17:2875, 2006.
- [kei12] *Keithley Instruments, Inc. www.keithley.com*, 2012.
- [KF11] KOENRAAD, P. M. and M. E. FLATTÉ: *Single dopants in semiconductors*. Nature materials, 10(2):91–100, 2011.
- [KHG⁺11] KOREN, E., J. K. HYUN, U. GIVAN, E. R. HEMESATH, L. J. LAUHON and Y. ROSENWAKS: *Obtaining uniform dopant distributions in VLS-grown Si nanowires*. Nano letters, 2011.
- [KHO⁺85] KROTO, H. W., J. R. HEATH, S. C. O'BRIEN, R. F. CURL and R. E. SMALLEY: *C 60: buckminsterfullerene*. Nature, 318(6042):162–163, 1985.
- [KKND⁺09] KANUNGO, P. D., R. KÖGLER, K. NGUYEN-DUC, N. ZAKHAROV, P. WERNER and U. GÖSELE: *Ex situ n and p doping of vertical epitaxial short silicon nanowires by ion implantation*. Nanotechnology, 20:165706, 2009.
- [KKY⁺09] KEEM, K., J. KANG, C. YOON, D. YEOM, D. Y. JEONG, B. PARK, J. PARK and S. KIM: *ZnO Nanowire-Based Nonvolatile Memory Devices with Al₂O₃ Layers as Storage Nodes*. Journal of Nanoscience and Nanotechnology, 9(7):4240–4243, 2009.
- [Kle68] KLEIN, C. A.: *Bandgap dependence and related features of radiation ionization energies in semiconductors*. Journal of Applied Physics, 39(4):2029–2038, 1968.
- [KRA⁺09] KOREN, E., Y. ROSENWAKS, J. E. ALLEN, E. R. HEMESATH and L. J. LAUHON: *Nonuniform doping distribution along silicon nanowires measured by Kelvin probe force microscopy and scanning photocurrent microscopy*. Applied Physics Letters, 95:092105, 2009.
- [KTEK⁺08] KELZENBERG, M. D., D. B. TURNER-EVANS, B. M. KAYES, A. MICHAEL, M. C. PUTNAM, N. S. LEWIS and H. A. ATWATER: *Photovoltaic measurements in single-nanowire silicon solar cells*. Nano letters, 8(2):710–714, 2008.

Bibliography

- [Lau73] LAUER, R. B.: *The IR photoluminescence emission band in ZnO*. Journal of Physics and Chemistry of Solids, 34(2):249–253, 1973.
- [LAW⁺05] LORENZ, K., E. ALVES, E. WENDLER, O. BILANI, W. WESCH and M. HAYES: *Damage formation and annealing at low temperatures in ion implanted ZnO*. Applied Physics Letters, 87:191904, 2005.
- [LCY⁺11] LIN, S. S., I. C. CHEN, J. YANG, T. J. HSUEH, C. L. HSU, H.E. LEE and T.Y. SHIEH: *A Study on One-Step Immobilization of Horse Immunoglobulin with Vertically Grown ZnO Nanorods Substrates*. Journal of The Electrochemical Society, 158:K107, 2011.
- [LCZ⁺09] LORENZ, M., B. CAO, G. ZIMMERMANN, G. BIEHNE, C. CZEKALLA, H. FRENZEL, M. BRANDT, H. VON WENCKSTERN and M. GRUNDMANN: *Stable p-type ZnO: P nanowire/n-type ZnO: Ga film junctions, reproducibly grown by two-step pulsed laser deposition*. Journal of Vacuum Science & Technology B: Microelectronics and Nanometer Structures, 27(3):1693–1697, 2009.
- [Lea82] LEAMY, H. J.: *Charge collection scanning electron microscopy*. Journal of Applied Physics, 53(6):R51–R80, 1982.
- [LFS⁺04] LI, C., W. FAN, D. A. STRAUS, B. LEI, S. ASANO, D. ZHANG, J. HAN, M. MEYYAPPAN and C. ZHOU: *Charge storage behavior of nanowire transistors functionalized with bis (terpyridine)-Fe (II) molecules: Dependence on molecular structure*. Journal of the American Chemical Society, 126(25):7750–7751, 2004.
- [LGY04] LAW, M., J. GOLDBERGER and P. YANG: *Semiconductor nanowires and nanotubes*. Annu. Rev. Mater. Res., 34:83–122, 2004.
- [LL06] LU, W. and C. M. LIEBER: *Semiconductor nanowires*. Journal of Physics D: Applied Physics, 39:R387, 2006.
- [LL07] LU, W. and C. M. LIEBER: *Nanoelectronics from the bottom up*. Nature Materials, 6(11):841–850, 2007.
- [LLA⁺09] LIU, J., S. LEE, Y. H. AHN, J. Y. PARK and K. H. KOH: *Tailoring the visible photoluminescence of mass-produced ZnO nanowires*. Journal of Physics D: Applied Physics, 42:095401, 2009.
- [LLC11] LU, M. P., M. Y. LU and L. J. CHEN: *p-Type ZnO nanowires: From synthesis to nano energy*. Nano Energy, Just accepted manuscript, 2011.
- [LLZ⁺07] LIAO, Z. M., K. J. LIU, J. M. ZHANG, J. XU and D. P. YU: *Effect of surface states on electron transport in individual ZnO nanowires*. Physics Letters A, 367(3):207, 2007.

- [LOG⁺11] LYSOV, A., M. OFFER, C. GUTSCHE, I. REGOLIN, S. TOPALOGLU, M. GELLER, W. PROST and F.-J. TEGUDE: *Optical properties of heavily doped GaAs nanowires and electroluminescent nanowire structures*. Nanotechnology, 22:085702, 2011.
- [LRW⁺08] LANSBERGEN, G. P., R. RAHMAN, C. J. WELLARD, I. WOO, J. CARO, N. COLLAERT, S. BIESEMANS, G. KLIMECK, L. C. L. HOLLENBERG and S. ROGGE: *Gate-induced quantum-confinement transition of a single dopant atom in a silicon FinFET*. Nature Physics, 4(8):656–661, 2008.
- [LSF⁺11] LIN, Y., M. SHATKHIN, E. FLITSIYAN, L. CHERNYAK, Z. DASHEVSKY, S. CHU and J. L. LIU: *Minority carrier transport in p-ZnO nanowires*. Journal of Applied Physics, 109:016107, 2011.
- [LSS63] LINDHARD, J., M. SCHARFF and H. E. SCHIOETT: *Range concepts and heavy ion ranges (Notes on atomic collisions, III)*. Kgl. Danske Videnskab., Selskab. Mat. Fys. Medd., 33(14), 1963.
- [LVO⁺11] LYSOV, A., S. VINAJI, M. OFFER, C. GUTSCHE, I. REGOLIN, W. MERTIN, M. GELLER, W. PROST, G. BACHER and F.-J. TEGUDE: *Spatially resolved photoelectric performance of axial GaAs nanowire pn-diodes*. Nano Research, 4(10):1–9, 2011.
- [MB10] MAJIDI, H. and J. B. BAXTER: *Electrodeposition of CdSe coatings on ZnO nanowire arrays for extremely thin absorber solar cells*. Electrochimica Acta, 2010.
- [MDS⁺09] MARKSTEINER, M., A. DIVOCHIY, M. SCLAFANI, P. HASLINGER, H. ULBRICHT, A. KORNEEV, A. SEMENOV, G. GOL'TSMAN and M. ARNDT: *A superconducting NbN detector for neutral nanoparticles*. Nanotechnology, 20:455501, 2009.
- [MG74] MUIR, M. D. and P. R. GRANT: *Cathodoluminescence*. Quantitative Scanning Electron Microscopy, DB Holt, MD Muir, PR Grant, IM Boswarva, eds. (Academic Press, NY), pages 287–334, 1974.
- [mic12] *Fotolithografie*. MicroChemicals GmbH, Ulm, www.microchemicals.eu, 2012.
- [Mil10] MILZ, S.: *Konzepte zur Realisierung von einfachen Nanodrahtbauelementen für die Energiegewinnung*. Master's thesis, Friedrich-Schiller-Universität Jena, June 2010.
- [MJY⁺11] MCCALLUM, J. C., D. N. JAMIESON, C. YANG, A. D. ALVES, B. C. JOHNSON, T. HOPF, S. C. THOMPSON and J. A. VAN DONKELAAR: *Single-Ion Implantation for the Development of Si-Based MOSFET Devices with Quantum Functionalities*. Advances in Materials Science and Engineering, 2012, 2011.

Bibliography

- [MLC⁺08] MÜLLER, S., M. LORENZ, C. CZEKALLA, G. BENNDORF, H. HOCHMUTH, M. GRUNDMANN, H. SCHMIDT and C. RONNING: *Intense white photoluminescence emission of V-implanted zinc oxide thin films*. Journal of Applied Physics, 104(12):123504–123504, 2008.
- [Moh08] MOHAMMAD, S. N.: *Analysis of the vapor–liquid–solid mechanism for nanowire growth and a model for this mechanism*. Nano letters, 8(5):1532–1538, 2008.
- [MSC⁺05] MERANO, M., S. SONDEREGGER, A. CROTTINI, S. COLLIN, P. RENUCCI, E. PELUCCHI, A. MALKO, M. H. BAIER, E. KAPON, B. DEVEAUD et al.: *Probing carrier dynamics in nanostructures by picosecond cathodoluminescence*. Nature, 438(7067):479–482, 2005.
- [MSL⁺02] MCKINNON, R. P., F. E. STANLEY, N. E. LUMPKIN, E. GAUJA, L. D. MACKS, M. MITIC, V. CHAN, K. PECEROS, T. M. BUEHLER, A. S. DZURAK et al.: *Nanofabrication processes for single-ion implantation of silicon quantum computer devices*. Smart materials and structures, 11:735, 2002.
- [MSW⁺05] MOSBACKER, H. L., Y. M. STRZHEMECHNY, B. D. WHITE, P. E. SMITH, D. C. LOOK, C. W. LITTON, D. C. REYNOLDS and L. J. BRILLSON: *Role of near-surface states in ohmic-Schottky conversion of Au contacts to ZnO*. Applied Physics Letters, 87(1):12102, 2005.
- [MWK⁺11] MARIANI, G., P. S. WONG, A. M. KATZENMEYER, F. LÉONARD, J. SHAPIRO and D. L. HUFFAKER: *Patterned Radial GaAs Nanopillar Solar Cells*. Nano Letters, 11(6):2490–2494, 2011.
- [MZLR09] MÜLLER, S., M. ZHOU, Q. LI and C. RONNING: *Intra-shell luminescence of transition-metal-implanted zinc oxide nanowires*. Nanotechnology, 20:135704, 2009.
- [NKB⁺09] NAYDENOV, B., R. KOLESOV, A. BATALOV, J. MEIJER, S. PEZZAGNA, D. ROGALLA, F. JELEZKO and J. WRACHTRUP: *Engineering single photon emitters by ion implantation in diamond*. Applied physics letters, 95(18):181109–181109, 2009.
- [NKR⁺04] NOBIS, T., E. M. KAIASHEV, A. RAHM, M. LORENZ, J. LENZNER and M. GRUNDMANN: *Spatially inhomogeneous impurity distribution in ZnO micropillars*. Nano Letters, 4(5):797–800, 2004.
- [NSS⁺11] NIEPELT, R., U. C. SCHRÖDER, J. SOMMERFELD, I. SLOWIK, B. RUDOLPH, R. MÖLLER, B. SEISE, A. CSAKI, W. FRITZSCHE and C. RONNING: *Biofunctionalization of zinc oxide nanowires for DNA sensory applications*. Nanoscale Research Letters, 6(1):511, 2011.
- [OG91] O'REGAN, B. and M. GRATZEL: *A low-cost, high-efficiency solar cell based on dye-sensitized colloidal TiO₂ films*. Nature, 353(6346):737–740, 1991.

- [ÖHM10] ÖZGÜR, U., D. HOFSTETTER and H. MORKOÇ: *ZnO devices and applications: a review of current status and future prospects*. Proceedings of the IEEE, 98(7):1255–1268, 2010.
- [OIO⁺02] OHASHI, N., T. ISHIGAKI, N. OKADA, T. SEKIGUCHI, I. SAKAGUCHI and H. HANEDA: *Effect of hydrogen doping on ultraviolet emission spectra of various types of ZnO*. Applied physics letters, 80:2869, 2002.
- [OLP⁺07] OH, Y. M., K. M. LEE, K. H. PARK, Y. KIM, Y. H. AHN, J. Y. PARK and S. LEE: *Correlating luminescence from individual ZnO nanostructures with electronic transport characteristics*. Nano letters, 7(12):3681–3685, 2007.
- [ONF⁺07] ONO, Y., K. NISHIGUCHI, A. FUJIWARA, H. YAMAGUCHI, H. INOKAWA and Y. TAKAHASHI: *Conductance modulation by individual acceptors in Si nanoscale field-effect transistors*. Applied Physics Letters, 90:102106, 2007.
- [OSW⁺93] OSHIMA, M., T. SCIMECA, Y. WATANABE, H. OIGAWA and Y. NANNICHI: *Oxidation of sulfur-treated GaAs surfaces studied by photoluminescence and photoelectron spectroscopy*. Japanese journal of applied physics, 32(1B):518–522, 1993.
- [PBPR07] PARISH, C., D. BATCHELOR, C. PROGL and P. RUSSELL: *Tutorial: Electron Beam-Induced Current in the Scanning Electron Microscope*. Microscopy and Analysis, 121:11, 2007.
- [PHRJD⁺08] PRADES, J. D., F. HERNÁNDEZ-RAMÍREZ, R. JIMENEZ-DIAZ, M. MANZANARES, T. ANDREU, A. CIRERA, A. ROMANO-RODRIGUEZ and J. R. MORANTE: *The effects of electron–hole separation on the photoconductivity of individual metal oxide nanowires*. Nanotechnology, 19:465501, 2008.
- [PHS⁺09] PEREA, D. E., E. R. HEMESATH, E. J. SCHWALBACH, J. L. LENSCH-FALK, P. W. VOORHEES and L. J. LAUHON: *Direct measurement of dopant distribution in an individual vapour–liquid–solid nanowire*. Nature nanotechnology, 4(5):315–319, 2009.
- [PJG⁺09] PARKINSON, P., H. J. JOYCE, Q. GAO, H. H. TAN, X. ZHANG, J. ZOU, C. JAGADISH, L. M. HERZ and M. B. JOHNSTON: *Carrier Lifetime and Mobility Enhancement in Nearly Defect-Free Core-Shell Nanowires Measured Using Time-Resolved Terahertz Spectroscopy*. Nano letters, 9(9):3349–3353, 2009.
- [PLS⁺05] PERSAUD, A., J. A. LIDDLE, T. SCHENKEL, J. BOKOR, T. IVANOV and I. W. RANGELOW: *Ion implantation with scanning probe alignment*. Journal of Vacuum Science & Technology B: Microelectronics and Nanometer Structures, 23:2798, 2005.

Bibliography

- [PMM+08] PATRA, M. K., K. MANZOOR, M. MANOTH, S. R. VADERA and N. KUMAR: *Studies of luminescence properties of ZnO and ZnO: Zn nanorods prepared by solution growth technique*. Journal of Luminescence, 128(2):267–272, 2008.
- [PNI+05] PEARTON, S. J., D. P. NORTON, K. IP, Y. W. HEO and T. STEINER: *Recent progress in processing and properties of ZnO*. Progress in Materials Science, 50:293, 2005.
- [PNR07] PEARTON, S. J., D. P. NORTON and F. REN: *The Promise and Perils of Wide-Bandgap Semiconductor Nanowires for Sensing, Electronic, and Photonic Applications*. Small, 3(7):1144–1150, 2007.
- [PPAD06] PAUC, N., M. R. PHILLIPS, V. AIMEZ and D. DROUIN: *Carrier recombination near threading dislocations in GaN epilayers by low voltage cathodoluminescence*. Applied physics letters, 89:161905, 2006.
- [PPL+05] PERSAUD, A., S. J. PARK, J. A. LIDDLE, T. SCHENKEL, J. BOKOR and I. W. RANGELOW: *Integration of scanning probes and ion beams*. Nano letters, 5(6):1087–1091, 2005.
- [PR07] PARISH, C. M. and P. E. RUSSELL: *Scanning Cathodoluminescence Microscopy*. Advances in Imaging and Electron Physics, 147:1–135, 2007.
- [PSG+03] POLYAKOV, A. Y., N. B. SMIRNOV, A. V. GOVORKOV, K. IP, M. E. OVERBERG, Y. W. HEO, D. P. NORTON, S. J. PEARTON, B. LUO, F. REN and J. M. ZAVADA: *Hydrogen plasma treatment effects on electrical and optical properties of n-ZnO*. Journal of Applied Physics, 94(1):400, 2003.
- [PTZL07] PATOLSKY, F., B. P. TIMKO, G. ZHENG and C. M. LIEBER: *Nanowire-based nanoelectronic devices in the life sciences*. MRS bulletin, 32(02):142–149, 2007.
- [PWJ+09] PIERRE, M., R. WACQUEZ, X. JEHL, M. SANQUER, M. VINET and O. CUETO: *Single-donor ionization energies in a nanoscale CMOS channel*. Nature nanotechnology, 5(2):133–137, 2009.
- [PYE+07] PIECHAL, B., J. YOO, A. ELSHAER, A. C. MOFOR, G. C. YI, A. BAKIN, A. WAAG, F. DONATINI and L. S. DANG: *Cathodoluminescence of single ZnO nanorod heterostructures*. physica status solidi (b), 244(5):1458–1461, 2007.
- [RBBW09] RESHCHIKOV, M. A., A. BEHRENDTS, A. BAKIN and A. WAAG: *Photoluminescence from ZnO nanowires*. Journal of Vacuum Science & Technology B: Microelectronics and Nanometer Structures, 27:1688, 2009.

- [RBG⁺10] RONNING, C., C. BORSCHHEL, S. GEBURT, R. NIEPELT, S. MÜLLER, D. STICHTENOTH, J. P. RICHTERS, A. DEV, T. VOSS, L. CHEN et al.: *Tailoring the properties of semiconductor nanowires using ion beams*. *physica status solidi (b)*, 247(10):2329–2337, 2010.
- [RBGN10] RONNING, C., C. BORSCHHEL, S. GEBURT and R. NIEPELT: *Ion beam doping of semiconductor nanowires*. *Materials Science and Engineering: R: Reports*, 70(3-6):30–43, 2010.
- [RDM⁺09] RICHTERS, J. P., A. DEV, S. MÜLLER, R. NIEPELT, C. BORSCHHEL, C. RONNING and T. VOSS: *Influence of metallic coatings on the photoluminescence properties of ZnO nanowires*. *physica status solidi (RRL)-Rapid Research Letters*, 3(5):166–168, 2009.
- [RGL⁺10] REGOLIN, I., C. GUTSCHE, A. LYSOV, K. BLEKKER, Z. A. LI, M. SPASOVA, W. PROST and F.-J. TEGUDE: *Axial pn-Junctions formed by MOVPE using DEZn and TESn in vapour-liquid-solid grown GaAs Nanowires*. *Journal of Crystal Growth*, 2010.
- [RGW⁺10] REPARAZ, J. S., F. GÜELL, M. R. WAGNER, A. HOFFMANN, A. CORNET and J. R. MORANTE: *Size-dependent recombination dynamics in ZnO nanowires*. *Applied Physics Letters*, 96:053105, 2010.
- [Ric10] RICHTERS, J. P.: *Optische Eigenschaften von ZnO-Nanodrähten: Einfluss von Oberflächenbehandlungen und hohen Anregungsdichten*. mbv, Mensch-und-Buch-Verl., 2010.
- [RKK⁺09] RA, H. W., R. KHAN, J. T. KIM, B. R. KANG, K. H. BAI and Y. H. IM: *Effects of surface modification of the individual ZnO nanowire with oxygen plasma treatment*. *Materials Letters*, 63(28):2516–2519, 2009.
- [RVK⁺08] RICHTERS, J. P., T. VOSS, D. S. KIM, R. SCHOLZ and M. ZACHARIAS: *Enhanced surface-excitonic emission in ZnO/Al₂O₃ core-shell nanowires*. *Nanotechnology*, 19:305202, 2008.
- [RVW⁺08] RICHTERS, J. P., T. VOSS, L. WISCHMEIER, I. RÜCKMANN and J. GUTOWSKI: *Influence of polymer coating on the low-temperature photoluminescence properties of ZnO nanowires*. *Applied Physics Letters*, 92:011103, 2008.
- [SBW⁺08] SCHLENKER, E., A. BAKIN, T. WEIMANN, P. HINZE, D. H. WEBER, A. GÖLZHÄUSER, H. H. WEHMANN and A. WAAG: *On the difficulties in characterizing ZnO nanowires*. *Nanotechnology*, 19:365707, 2008.
- [Sch00] SCHARF, R. (editor): *Physik - Themen, Bedeutung und Perspektiven physikalischer Forschung*. Deutsche Physikalische Gesellschaft e. V. (DPG), 1 edition, 2000.

Bibliography

- [Sch08] SCHIETTEKATTE, F.: *Fast Monte Carlo for ion beam analysis simulations*. Nuclear Instruments and Methods in Physics Research Section B: Beam Interactions with Materials and Atoms, 266(8):1880–1885, 2008.
- [Sch10a] SCHENKEL, T.: *Single Ion Implantation and Deterministic Doping*. Technical Report LBNL Paper LBNL-3622E, Lawrence Berkeley National Laboratory, 2010.
- [Sch10b] SCHRÖDER, U. C.: *Biofunktionalisierung von ZnO-Nanodrähten für die Nukleinsäuresensorik*. Master's thesis, Friedrich-Schiller-Universität Jena, November 2010.
- [SCM⁺10] SOHN, J. I., S. S. CHOI, S. M. MORRIS, J. S. BENDALL, H. J. COLES, W. K. HONG, G. JO, T. LEE and M. E. WELLAND: *Novel Nonvolatile Memory with Multibit Storage Based on a ZnO Nanowire Transistor*. Nano letters, 2010.
- [SDG10] SOUDI, A., P. DHAKAL and Y. GU: *Diameter dependence of the minority carrier diffusion length in individual ZnO nanowires*. Applied Physics Letters, 96:253115, 2010.
- [SdHK05] SARMA, S. D., ROGERIO DE SOUSA, XUEDONG HU and BELITA KOILLER: *Spin quantum computation in silicon nanostructures*. SOLID STATE COMMUNICATIONS, 133:737, 2005.
- [Ser01] SERVICE, R. F.: *Molecules Get Wired*. Science, 294(5551):2442–2443, 2001.
- [SFC⁺11] SCHWARZ, C., E. FLITSIYAN, L. CHERNYAK, V. CASIAN, R. SCHNECK, Z. DASHEVSKY, S. CHU and J. L. LIU: *Impact of forward bias injection on minority carrier transport in p-type ZnO nanowires*. Journal of Applied Physics, 110(5):056108–056108, 2011.
- [SHH⁺09] SEMENOV, A., P. HAAS, H. W. HÜBERS, K. ILIN, M. SIEGEL, A. KIRSTE, D. DRUNG, T. SCHURIG and A. ENGEL: *Intrinsic quantum efficiency and electro-thermal model of a superconducting nanowire single-photon detector*. Journal of Modern Optics, 56(2-3):345–351, 2009.
- [SHL⁺09] SOHN, J. I., W. K. HONG, M. J. LEE, T. LEE, H. SIRRINGHAUS, D. J. KANG and M. E. WELLAND: *The influence of surface chemical dynamics on electrical and optical properties of ZnO nanowire field effect transistors*. Nanotechnology, 20:505202, 2009.
- [SKH⁺02] SHINADA, T., H. KOYAMA, C. HINOSHITA, K. IMAMURA and I. OHDOMARI: *Improvement of focused ion-beam optics in single-ion implantation for higher aiming precision of one-by-one doping of impurity atoms into nano-scale semiconductor devices*. Japanese journal of applied physics, 41(3A):L287–L290, 2002.

- [SKN⁺08] SHINADA, T., T. KUROSAWA, H. NAKAYAMA, Y. ZHU, M. HORI and I. OHDOMARI: *A reliable method for the counting and control of single ions for single-dopant controlled devices*. Nanotechnology, 19:345202, 2008.
- [SLF⁺09] SCHNITZLER, W., N. M. LINKE, R. FICKLER, J. MEIJER, F. SCHMIDT-KALER and K. SINGER: *Deterministic ultracold ion source targeting the Heisenberg limit*. Physical review letters, 102(7):70501, 2009.
- [SN06] SZE, S. M. and KWOK K. NG: *Physics of Semiconductor Devices*. John Wiley & Sons, Inc., 2006.
- [SOKO05] SHINADA, T., S. OKAMOTO, T. KOBAYASHI and I. OHDOMARI: *Enhancing semiconductor device performance using ordered dopant arrays*. Nature, 437(7062):1128–1131, 2005.
- [Som96] SOMORJAI, G. A.: *Modern surface science and surface technologies: An introduction*. Chemical reviews, 96(4):1223–1236, 1996.
- [SPLF⁺09] SCHLITZ, R. A., D. E. PEREA, J. L. LENSCH-FALK, E. R. HEMESATH and L. J. LAUHON: *Correlating dopant distributions and electrical properties of boron-doped silicon nanowires*. Applied Physics Letters, 95:162101, 2009.
- [STN04] SHALISH, I., H. TEMKIN and V. NARAYANAMURTI: *Size-dependent surface luminescence in ZnO nanowires*. Physical Review B, 69(24):245401, 2004.
- [sus12] SÜSS MicroTec AG. www.suss.com, 2012.
- [SW09] SCHATZ, G. and A. WEIDINGER: *Nukleare Festkörperphysik: Kernphysikalische Messmethoden und ihre Anwendungen*. Vieweg+Teubner, 2009.
- [SWG⁺08] STICHTENOTH, D., K. WEGENER, C. GUTSCHE, I. REGOLIN, F.-J. TEGUDE, W. PROST, M. SEIBT and C. RONNING: *P-type doping of GaAs nanowires*. Applied Physics Letters, 92(16):163107–163107, 2008.
- [T⁺74] TANIGUCHI, N. et al.: *On the basic concept of nanotechnology*. In *Proc. Intl. Conf. Prod. Eng. Tokyo, Part II, Japan Society of Precision Engineering*, pages 18–23, 1974.
- [TCL⁺06] TAM, K. H., C. K. CHEUNG, Y. H. LEUNG, A. B. DJURIŠIĆ, C. C. LING, C. D. BELING, S. FUNG, W. M. KWOK, W. K. CHAN, D. L. PHILLIPS et al.: *Defects in ZnO nanorods prepared by a hydrothermal method*. The Journal of Physical Chemistry B, 110(42):20865–20871, 2006.
- [THJ⁺06] TITOVA, L. V., T. B. HOANG, H. E. JACKSON, L. M. SMITH, J. M. YARRISON-RICE, J. L. LENSCH and L. J. LAUHON: *Low-temperature photoluminescence imaging and time-resolved spectroscopy of single CdS nanowires*. Applied physics letters, 89:053119, 2006.

Bibliography

- [TOO⁺04] TSUKAZAKI, A., A. OHTOMO, T. ONUMA, M. OHTANI, T. MAKINO, M. SUMIYA, K. OHTANI, S. F. CHICHIBU, S. FUKU, Y. SEGAWA et al.: *Repeated temperature modulation epitaxy for p-type doping and light-emitting diode based on ZnO*. Nature Materials, 4(1):42–46, 2004.
- [Tou05] TOURNEY, C.: *Apostolic succession*. Engineering and Science, 68(1):16–23, 2005.
- [TPKL11] TAJIK, N., Z. PENG, P. KUYANOV and R. R. LAPIERRE: *Sulfur passivation and contact methods for GaAs nanowire solar cells*. Nanotechnology, 22:225402, 2011.
- [Uen92] UENO, H.: *Au wire bonding to Cu pad using Ti thin film*. Japanese journal of applied physics, 31:1547, 1992.
- [van00] VAN DE WALLE, C. G.: *Hydrogen as a cause of doping in zinc oxide*. Physical Review Letters, 85(5):1012, 2000.
- [VSM⁺07] VOSS, T., G. T. SVACHA, E. MAZUR, S. MÜLLER, C. RONNING, D. KONJHODZIC and F. MARLOW: *High-Order Waveguide Modes in ZnO Nanowires*. Nanoletters, 7:3675, 2007.
- [VW08] VOSS, T. and L. WISCHMEIER: *Recombination dynamics of surface-related excitonic states in single ZnO nanowires*. Journal of Nanoscience and Nanotechnology, 8(1):228–232, 2008.
- [Wan07] WANG, Z. L.: *Nanopiezotronics*. Advanced Materials, 19(6):889–892, 2007.
- [Wan09] WANG, Z. L.: *ZnO nanowire and nanobelt platform for nanotechnology*. Materials Science and Engineering: R: Reports, 64(3-4):33–71, 2009.
- [WB11] WALLENTIN, J. and M. T. BORGSTRÖM: *Doping of semiconductor nanowires*. Journal of Materials Research, 26(17):2142–2156, 2011.
- [WCLK11] WHITE, R., A. COLLI, H. LI and J. KIVIOJA: *Input/output pulse operation of ZnO nanowire threshold integrators*. Nanotechnology, 22:025207, 2011.
- [WCY⁺07] WU, J. J., G. R. CHEN, H. H. YANG, C. H. KU and J. Y. LAI: *Effects of dye adsorption on the electron transport properties in ZnO-nanowire dye-sensitized solar cells*. Applied physics letters, 90:213109, 2007.
- [WCZ⁺11] WANG, G., S. CHU, N. ZHAN, Y. LIN, L. CHERNYAK and J. LIU: *ZnO homojunction photodiodes based on Sb-doped p-type nanowire array and n-type film for ultraviolet detection*. Applied Physics Letters, 98:041107, 2011.
- [WDJ⁺09] WACASER, B. A., K. A. DICK, J. JOHANSSON, M. T. BORGSTRÖM, K. DEPERT and L. SAMUELSON: *Preferential interface nucleation: an expansion of the VLS growth mechanism for nanowires*. Advanced Materials, 21(2):153–165, 2009.

- [WE64] WAGNER, R. S. and W. C. ELLIS: *VAPOR-LIQUID-SOLID MECHANISM OF SINGLE CRYSTAL GROWTH*. Applied Physics Letters, 4:89, 1964.
- [WG09] WANG, M. C. P. and B. D. GATES: *Directed assembly of nanowires*. Mater Today, 12(5):34–43, 2009.
- [Wie02] WIEN, W.: *Untersuchungen über die elektrische Entladung in verdünnten Gasen*. Annalen der Physik, 313(6):244–266, 1902.
- [Wil98] WILLIAMS, J. S.: *Ion implantation of semiconductors*. Materials Science and Engineering, 253:8, 1998.
- [WK64] WITTRY, D. B. and D. F. KYSER: *Use of electron probes in the study of recombination radiation*. Journal of Applied Physics, 35(8):2439–2442, 1964.
- [WLS⁺11] WANG, Y., Z. LIAO, G. SHE, L. MU, D. CHEN and W. SHI: *Optical modulation of persistent photoconductivity in ZnO nanowires*. Applied Physics Letters, 98(20):203108, 2011.
- [WOPS81] WIGHT, D. R., P. E. OLIVER, T. PRENTICE and V. W. STEWARD: *Diffusion lengths in p-type MOCVD GaAs*. Journal of Crystal Growth, 55(1):183–191, 1981.
- [WSB⁺09] WEIS, C. D., A. SCHUH, A. BATRA, A. PERSAUD, I. W. RANGELOW, J. BOKOR, C. C. LO, S. CABRINI, D. OLYNICK, S. DUHEY et al.: *Mapping of ion beam induced current changes in FinFETs*. Nuclear Instruments and Methods in Physics Research Section B: Beam Interactions with Materials and Atoms, 267(8-9):1222–1225, 2009.
- [WVBS06] WISCHMEIER, L., T. VOSS, S. BÖRNER and W. SCHADE: *Comparison of the optical properties of as-grown ensembles and single ZnO nanowires*. Applied Physics A: Materials Science & Processing, 84(1):111–116, 2006.
- [WWW03] WATTS, J. F., J. WOLSTENHOLME and J. WILEY: *An introduction to surface analysis by XPS and AES*. Wiley Online Library, 2003.
- [WYW⁺08] WILLANDER, M., L. L. YANG, A. WADEASA, S. U. ALI, M. H. ASIF, Q. X. ZHAO and O. NUR: *Zinc oxide nanowires: controlled low temperature growth and some electrochemical and optical nano-devices*. J. Mater. Chem., 19(7):1006–1018, 2008.
- [XWZ⁺07] XIANG, B., P. WANG, X. ZHANG, S. A. DAYEH, D. P. R. APLIN, C. SOCI, D. YU and D. WANG: *Rational synthesis of p-type zinc oxide nanowire arrays using simple chemical vapor deposition*. Nano letters, 7(2):323–328, 2007.
- [YH86] YACOBI, B. G. and D. B. HOLT: *Cathodoluminescence scanning electron microscopy of semiconductors*. Journal of applied physics, 59(4):R1–R24, 1986.

Bibliography

- [YHJ⁺11] YOON, J., W.K. HONG, M. JO, G. JO, M. CHOE, W. PARK, J. I. SOHN, S. NEDIC, H. HWANG, M. E. WELLAND et al.: *Nonvolatile Memory Functionality of ZnO Nanowire Transistors Controlled by Mobile Protons*. ACS nano, 2011.
- [YJH⁺02] YANG, C., D. N. JAMIESON, S. M. HEARNE, C. I. PAKES, B. ROUT, E. GAUJA, A. J. DZURAK and R. G. CLARK: *Ion-beam-induced-charge characterisation of particle detectors*. Nuclear Instruments and Methods in Physics Research Section B: Beam Interactions with Materials and Atoms, 190(1):212–216, 2002.
- [YLC⁺12] YOO, J., D. LE SI, B. CHON, T. JOO and G. C. YI: *Exciton scattering mechanism in a single semiconducting MgZnO nanorod*. Nano Letters, 2012.
- [YNPR05] YANG, H. S., D. P. NORTON, S. J. PEARTON and F. REN: *Ti/ Au n-type Ohmic contacts to bulk ZnO substrates*. Applied Physics Letters, 87:212106, 2005.
- [YSBZ00] YAO, B., H. SHI, H. BI and L. ZHANG: *Optical properties of ZnO loaded in mesoporous silica*. Journal of Physics: Condensed Matter, 12:6265, 2000.
- [YY09] YUHAS, B. D. and P. YANG: *Nanowire-based all-oxide solar cells*. Journal of the American Chemical Society, 131(10):3756–3761, 2009.
- [YYD08] YOO, J., G.C. YI and L.S. DANG: *Probing Exciton Diffusion in Semiconductors Using Semiconductor-Nanorod Quantum Structures*. Small, 4(4):467–470, 2008.
- [YYF10] YANG, P., R. YAN and M. FARDY: *Semiconductor nanowire: What's next?* Nano letters, 10(5):1529–1536, 2010.
- [YZJ⁺08a] YUAN, G. D., W. J. ZHANG, J. S. JIE, X. FAN, J. A. ZAPIEN, Y. H. LEUNG, L. B. LUO, P. F. WANG, C. S. LEE and S. T. LEE: *p-type ZnO nanowire arrays*. Nano letters, 8(8):2591–2597, 2008.
- [YZJ⁺08b] YUAN, G. D., W.J. ZHANG, J. S. JIE, X. FAN, J. X. TANG, I. SHAFIQ, Z. Z. YE, C. S. LEE and S. T. LEE: *Tunable n-Type Conductivity and Transport Properties of Ga-doped ZnO Nanowire Arrays*. Advanced Materials, 20(1):168–173, 2008.
- [ZBL85] ZIEGLER, J. F., J.P. BIRSACK and U. LITTMARK: *The stopping and ranges of ions in solids*. Pergamon Press, New York, 1985.
- [ZGH⁺09] ZHOU, J., Y. GU, Y. HU, W. MAI, P. H. YEH, G. BAO, A. K. SOOD, D. L. POLLA and Z. L. WANG: *Gigantic enhancement in response and reset time of ZnO UV nanosensor by utilizing Schottky contact and surface functionalization*. Applied physics letters, 94:191103, 2009.
- [ZI80] ZIEGLER, J. F. and G. J. IAFRATE: *The stopping of energetic ions in solids*. Radiation Effects, 46(3-4):199–219, 1980.

- [ZLC⁺10] ZIMMERMANN, G., M. LANGE, B. CAO, M. LORENZ and M. GRUNDMANN: *Resistivity control of ZnO nanowires by Al doping*. physica status solidi (RRL)-Rapid Research Letters, 4(3-4):82–84, 2010.
- [ZSR⁺08] ZIMMLER, M. A., D. STICHTENOTH, C. RONNING, W. YI, V. NARAYANAMURTI, T. VOSS and F. CAPASSO: *Scalable Fabrication of Nanowire Photonic and Electronic Circuits Using Spin-on Glass*. Nanoletters, 8(6):1695, 2008.
- [ZXW06] ZHOU, J., N. S. XU and Z. L. WANG: *Dissolving behavior and stability of ZnO wires in biofluids: a study on biodegradability and biocompatibility of ZnO nanostructures*. Advanced Materials, 18(18):2432–2435, 2006.
- [ZZB10] ZIEGLER, J. F., M. D. ZIEGLER and J. P. BIRSACK: *SRIM—The stopping and range of ions in matter (2010)*. Nuclear Instruments and Methods in Physics Research Section B: Beam Interactions with Materials and Atoms, 268(11):1818–1823, 2010.

Bibliography

A List of publications

Publications directly related to this thesis

Determination of minority carrier diffusion lengths directly from axial GaAs nanowire pn-junctions

C. Gutsche, **R. Niepelt**, M. Gnauck, A. Lysov, W. Prost, C. Ronning, and F.-J. Tegude
submitted to NANO LETTERS (2012)

Stable enhancement of near-band-edge emission of ZnO nanowires by hydrogen incorporation

A. Dev, **R. Niepelt**, J.-P. Richters, C. Ronning, and T. Voss
NANOTECHNOLOGY 21, 065709 (2010)

Tailoring the properties of semiconductor nanowires using ion beams

C. Ronning, C. Borschel, S. Geburt, **R. Niepelt**, S. Müller, D. Stichtenoth, J. -P. Richters, A. Dev, T. Voss, L. Chen, W. Heimbrod, C. Gutsche, and W. Prost
PHYSICA STATUS SOLIDI (B) 247, 2329-2337 (2010)

Persistent ion beam induced conductivity in zinc oxide nanowires A. Johannes, **R. Niepelt**, M. Gnauck, and C. Ronning APPLIED PHYSICS LETTERS 99, 252105 (2011)

Biofunctionalization of zinc oxide nanowires for DNA sensory applications

R. Niepelt, U. C. Schröder, J. Sommerfeld, I. Slowik, B. Rudolph, R. Möller, B. Seise, A. Csaki, W. Fritzsche, and C. Ronning
NANOSCALE RESEARCH LETTERS 6, 511 (2011)

Other publications

Influence of metallic coatings on the photoluminescence properties of ZnO nanowires

J.-P. Richters, A. Dev, S. Müller, **R. Niepelt**, C. Borschel, C. Ronning, and T. Voss
PHYSICA STATUS SOLIDI (RRL) 3, 166-168 (2009)

Alignment of semiconductor nanowires using ion beams

C. Borschel, R. Niepelt, S. Geburt, C. Gutsche, I. Regolin, W. Prost, F.-J. Tegude,
D. Stichtenoth, D. Schwen, and C. Ronning
SMALL 5, 2576 (2009)

Ion beam doping of semiconductor nanowires

C. Ronning, C. Borschel, S. Geburt, and **R. Niepelt**
MATERIALS SCIENCE AND ENGINEERING: R: REPORTS 70, 30-43 (2010)

DNA hybridization assay at individual, biofunctionalized zinc oxide nanowires

C. Leiterer, B. Seise, I. Slowik, G. Brönstrup, **R. Niepelt**, K. Weber, C. Ronning, S.
Christiansen, and W. Fritzsche
submitted to JOURNAL OF BIOPHOTONICS (2012)

Ehrenwörtliche Erklärung

Ich erkläre hiermit ehrenwörtlich, dass ich die vorliegende Arbeit selbstständig, ohne unzulässige Hilfe Dritter und ohne Benutzung anderer als der angegebenen Hilfsmittel und Literatur angefertigt habe. Die aus anderen Quellen direkt oder indirekt übernommenen Daten und Konzepte sind unter Angabe der Quelle gekennzeichnet.

Bei der Auswahl und Auswertung folgenden Materials haben mir die nachstehend aufgeführten Personen in der jeweils beschriebenen Weise unentgeltlich geholfen:

1. Die Herstellung und die Kontaktierung der GaAs-Nanodrähte wurden von Christoph Gutsche, Uni Duisburg, durchgeführt.
2. Einige der EBIC-Messungen wurden zusammen mit Christoph Gutsche und Martin Gnauck durchgeführt.
3. Die Photolumineszenzmessungen an ZnO-Drähten wurden von Apurba Dev durchgeführt.
4. Einige Implantationsexperimente und elektrische Messungen an ZnO-Nanodrähten wurden in Zusammenarbeit mit oder von Henry Holland-Moritz durchgeführt.
5. In-situ-Messungen während der Ionenstrahlimplantation wurden in Zusammenarbeit mit Andreas Johannes durchgeführt.
6. Versuche zum Vergleich von PIC und PPC wurden von Andreas Johannes durchgeführt.
7. Die Biofunktionalisierung von Nanodrähten und die anschließenden fluoreszenzmiroskopischen Untersuchungen wurden teilweise von Ulrich Christian Schröder und Irma Slowik durchgeführt.
8. XPS-Messungen an biofunktionalisierten Nanodrähten wurden in Zusammenarbeit mit Marc Brötzmann, Uni Göttingen, durchgeführt.
9. Im Übrigen waren jeweils die Koautoren der angeführten Veröffentlichungen (siehe Anhang A) an der Interpretation der Ergebnisse beteiligt.

Weitere Personen waren an der inhaltlich-materiellen Erstellung der vorliegenden Arbeit nicht beteiligt. Insbesondere habe ich hierfür nicht die entgeltliche Hilfe von Vermittlungs- bzw. Beratungsdiensten (Promotionsberater oder andere Personen) in Anspruch genommen. Niemand hat von mir unmittelbar oder mittelbar geldwerte Leistungen für Arbeiten erhalten, die im Zusammenhang mit dem Inhalt der vorgelegten Dissertation stehen. Die Arbeit wurde bisher weder im In- noch im Ausland in gleicher oder ähnlicher Form einer anderen Prüfungsbehörde vorgelegt. Die geltende Promotionsordnung der Physikalisch-Astronomischen Fakultät ist mir bekannt.

Ich versichere ehrenwörtlich, dass ich nach bestem Wissen die reine Wahrheit gesagt und nichts verschwiegen habe.

Curriculum vitae

Niepelt, Raphael

- *03.03.1982 geboren in Hildesheim
- 1988-1992 Besuch der katholischen Grundschule in Hameln
- 1992-1994 Besuch der Orientierungsstufe Nord in Hameln
- 1994-2001 Besuch des Schiller-Gymnasiums in Hameln, abgeschlossen mit Abitur
- 2001-2002 Zivildienstleistender im Krankentransport beim DRK Hameln
- 2002-2008 Studium der Physik an der Georg-August-Universität Göttingen
- 2008 Abschluss des Studiums an der Georg-August-Universität Göttingen als Diplom-Physiker
- 2008-2012 Wissenschaftlicher Mitarbeiter an der Friedrich-Schiller-Universität Jena mit dem Ziel der Promotion

Jena, 10. Februar 2012

Raphael Niepelt

Zusammenfassung der Arbeit

Halbleiternanodrähte werden oft als vielversprechende Kandidaten für die Integration in zukünftige elektronische und photonische Bauelemente genannt, wodurch sie eine besondere Rolle unter der großen Vielfalt von bottom-up-modellierten Nanostrukturen einnehmen. Daher ist es notwendig, die Eigenschaften der Nanodrähte zu kennen und zu verstehen. Für die Entwicklung neuartiger, funktionaler Elemente ist auch die gezielte Modifizierung dieser Eigenschaften, die durch eine Änderung der chemischen Zusammensetzung oder der Nanodrahtoberfläche erfolgen kann, von besonderem Interesse. Die vorliegende Arbeit beschäftigt sich mit beidem, der Charakterisierung und der gezielten Modifizierung der Eigenschaften von Halbleiternanodrähten.

Mit Hilfe rasterelektronenmikroskopischer Methoden wurden die Ladungsträgerdiffusionslängen in GaAs- und ZnO-Nanodrähten untersucht, die in beiden Fällen im Vergleich zum Festkörper stark reduziert sind. Durchmesserabhängige EBIC-Messungen an axialen pn-Übergängen in GaAs-Nanodrähten ermöglichen die Bestimmung der Oberflächenrekombinationsgeschwindigkeit. Im n-dotierten Teil der Drähte ergab sich ein niedrigerer Wert als erwartet, was auf eine niedrigere Dotierung im Bereich des pn-Übergangs, bedingt durch den Wachstumsprozess, zurückzuführen ist. Bei CL-Messungen an identisch präparierten ZnO-Nanodrähten konnten stark unterschiedliche Emissionseigenschaften beobachtet werden. Die Bestimmung der Exzitondiffusionslängen erfolgte an Nanodraht-Schottky-Übergängen.

Als Beispiel für die gezielte Modifikation von Nanodrähten wurde die Änderung der Eigenschaften von ZnO-Nanodrähten durch Wasserstoffionenimplantation untersucht. Die Nanodrähte zeigten eine Verstärkung der bandkantennahen Lumineszenz - bei gleichzeitigem Rückgang der Defektlumineszenz - und eine stark erhöhte Leitfähigkeit, die nach einigen Tagen etwas zurückging. Das Verhalten konnte mit dem parallelen Auftreten von stabilem, substitutionell implantierten und instabilem, interstitiellem Wasserstoff erklärt werden. Bei der Implantation von ZnO-Nanodrähten zeigte sich auch eine über Stunden persistente ionenstrahlinduzierte Leitfähigkeitserhöhung. Der Effekt basiert auf den selben Ursachen wie eine ebenfalls vorhandene persistente Photoleitfähigkeit. Die Wechselwirkung zwischen Ion und Nanodraht ermöglicht auch die Detektion von einzelnen Ionen mit ZnO-Nanodrähten, was ebenfalls gezeigt wurde.

Die Biofunktionalisierung von ZnO-Nanodrähten ist ein Beispiel für eine gezielte Veränderung der Nanodrahtoberfläche für den Einsatz des Drahtes als funktionales Element in einem Biosensor. Fluoreszenzmikroskopische Untersuchungen zeigten die erfolgreiche Immobilisierung von DNA auf der Nanodrahtoberfläche.

Die in dieser Arbeit erzielten Ergebnisse bilden wichtige Grundlagen für die weitere Forschung an Halbleiternanodrähten.

Danke...

...möchte ich allen sagen, die mich auf meinem Weg zur Promotion begleitet und unterstützt haben. Es war eine schöne Zeit, die ich nicht missen möchte.

Ich bedanke mich bei Carsten Ronning für die Möglichkeit, in seiner Arbeitsgruppe zu promovieren und die Betreuung meiner Doktorarbeit; außerdem für die stetige Unterstützung und das mir entgegengebrachte Vertrauen im wissenschaftlichen Tun, überlassene Freiräume bei der Gestaltung meiner Arbeit, die vielen Möglichkeiten, ins Ausland zu fahren um meinen physikalischen Horizont zu erweitern und an diversen Konferenzen teilzunehmen, die fachlichen Diskussionen über Physik und Fußball und nicht zuletzt die Möglichkeit, diese Promotion in Ruhe fertigstellen zu können.

Danke auch an "meine" Arbeitsgruppe, es hat sehr viel Spaß gemacht, mit Euch zusammenarbeiten in dieser Zeit, und ich freue mich, dies auch noch ein halbes Jahr weiter tun zu können. Insbesondere vielen Dank für die Zusammenarbeit auf dem Gebiet der elektrischen Charakterisierung und Modifikation von Nanodrähten an Martin Gnauck, Steffen Milz, Ulrich Christian Schröder, Andreas Johannes, Yaser Haj Hmeidi, Henry Holland-Moritz und Irma Slowik. Vielen Dank auch an meine Bürokollegen Christian Borschel, Jana Sommerfeld und Sebastian Geburt für die gemeinsame Zeit und die meist gute Büroatmosphäre. Weiterhin vielen Dank für eine tolle Zusammenarbeit und eine schöne Zeit an Michael Kozlik, Maria Fravventura, Jessica Richter, Stefanie Kosan, Falk Wyrwa, Gabriele Bulgarini, Julian Kühnel, Susann Spindler, Christian Müller, Stefan Weidner, Andreas Thielmann, Franziska Riedel, Jura Rensberg, Davide Cammi und Robert Röder.

Auch allen anderen Kollegen am Institut für Festkörperphysik gebührt ein herzlicher Dank: Danke für Frühstücksrunden und Institutsausflüge, aber auch für viele fachliche und interessante Diskussionen und die vielen guten Beiträge im Institutsseminar.

Ganz besonders bedanken möchte ich mich auch bei Anja Mittelstedt, Uta Bornkessel, Carmen Voigt, Gerald Lenk, Frank Jehn, Uli Barth und Petra Richter für die Hilfe bei vielen verwaltungs- und nichtverwaltungstechnischen Problemen.

Ich bedanke mich bei Herrn Marius Grundmann aus Leipzig für die Übernahme des Korreferats dieser Arbeit.

Außerdem herzlich Dank an Herrn Alois Lugstein aus Wien und Frau Silke Christiansen aus Erlangen für die Bereitschaft, diese Arbeit ebenfalls zu begutachten.

Vielen Dank an alle, die beim Korrekturlesen der Arbeit geholfen haben: Danke Christian, Andreas, Daniel, Jana, Henry und Irma!

Ganz herzlich möchte ich nicht bei meinen Kooperationspartnern aus anderen Arbeitsgruppen bedanken. Ein besonderer Dank gilt Christoph Gutsche und Werner Prost aus Duisburg für eine tolle Kollaboration und auch einige lustige Abende in Jena und in Duis-

burg. Vielen Dank auch an Tobias Voss und Apurba Dev aus Bremen, Rainer Adelong aus Kiel, Alan Colli aus Cambridge, Mariano Zimmerler und Federico Capasso aus Boston, Martin Otto aus Halle, Daniel Stichtenoth aus Erfurt, Marc Brötzmann, Kun Zhang und Hans Hofsäss aus Göttingen, Sven Müller aus Nordenham, Bettina Rudolph, Barbara Seise, Christian Leiterer und Wolfgang Fritzsche aus Jena sowie ganz besonders auch Frank Schmidl aus Jena.

Bei den alten und neuen Freunden, mit denen ich in den letzten drei Jahren viel erleben durfte möchte ich mich ebenfalls bedanken, für viele schöne Abende, teils aufmunternde Worte, wenn es mal nötig war und Hilfe in allen Lebenslagen, von A wie Auto leihen bis Z wie umZug. Danke Paul, Kohle, Tratschi, Andreas, Tobbser, Muffe, Daniel, Frank, Robert und Jule und der Rest von Rugbyjena, danke Thomas, Fabi, Christian und Elli, Felix, Daniel, Anna, Hajo, danke Matthias, Tobi, Jan, Sebastian² und Jens, danke Jochen, Jobo und ::mark. Vielen Dank auch an Thomas für das einzigartige Erlebnis beim Scooter Stadium Techno Inferno.

Schließlich möchte ich mich bei meiner Familie, den Großeltern und Schwiegereltern und insbesondere meinen Eltern und Geschwistern bedanken. Vielen Dank für Eure Unterstützung in den letzten Jahren!

Und last but not least: Anne, vielen Dank für Deine Unterstützung, ich freue mich auf die nächsten Jahre mit Dir!